Aus dem Neurowissenschaftlichen Forschungszentrum

der Medizinischen Fakultät Charité – Universitätsmedizin Berlin

DISSERTATION

The Role of RIM1α in Synaptic Plasticity at the Cerebellar Parallel Fiber

zur Erlangung des akademischen Grades

Doctor of Philosophy (PhD)

im Rahmen des

International Graduate Program Medical Neurosciences

vorgelegt der Medizinischen Fakultät

Charité – Universitätsmedizin Berlin

von

Michael Kintscher

aus Braunschweig

Datum der Promotion: 22.06.2014

Synopsis

Synaptic plasticity is a core feature of neuronal communication. It describes the activity-dependent change of the strength of synaptic transmission. Dependent on the duration of the transmission alteration synaptic plasticity is commonly divided into short-term and long-term plasticity. Whereas long-term plasticity is based on molecular changes at the presynaptic and/or postsynaptic site, factors influencing short-term plasticity are predominantly located at the presynapse. There, basic synaptic transmission and activity-dependent plasticity are governed at the active zone. This is a presynaptic plasma membrane patch with a complex protein network where vesicles are docked and primed, meaning that the required release machinery is assembled together with the vesicle and voltage-dependent Ca^{2+}-channels. This protein network ensures the spatiotemporally highly regulated process of action potential triggered Ca^{2+}-influx and the subsequent exocytosis of neurotransmitter filled vesicles.

In this work we focused on the presynaptic protein RIM1α, a core component of the multiprotein complex at the active zone. Dependent on the type of synapse tested, previous studies have shown RIM1α to either alter short-term plasticity or to be an essential mediator of presynaptic long-term plasticity or both.

Combining electrophysiological analysis of release properties and synaptic plasticity with two-photon calcium imaging at the cerebellar granule cell synapse we could show that the loss of the single isoform RIM1α already leads to a significant reduction in action potential triggered Ca^{2+}-influx at axonal boutons. As a consequence the release probability is reduced and short-term plasticity is enhanced. In contrast we could not find any difference in the expression of presynaptic long-term plasticity. To further test this finding, we mimicked the reduction of Ca^{2+}-influx found in RIM1α KO mice by reducing the external Ca^{2+}-concentration. The resulting lower intracellular Ca^{2+}-concentration does not fall below but comes close to the threshold of inducibility of long-term plasticity. Our results argue against an indispensable role of RIM1α in the expression of long-term plasticity but indicate a rather universal role of the protein in interacting with voltage-dependent Ca^{2+}-channels to enable proper synaptic neurotransmitter release.

In addition, we found a significant difference between the Ca^{2+}-influx in boutons of the ascending compared to the parallel fiber segment of granule cell axons, which adds additional information to previous studies that showed differential synaptic properties of these two axonal segments as well.

Key words: parallel fiber long-term potentiation, short-term plasticity, RIM1α, cerebellum, calcium imaging

Zusammenfassung

Synaptische Plastizität beschreibt die aktivitätsabhängige Änderung der Stärke synaptischer Transmission und stellt ein Hauptmerkmal neuronaler Kommunikation dar. Abhängig von der Dauer der Transmissionsänderungen wird sie in Kurzzeit- und Langzeitplastizität unterteilt. Während Langzeitplastizität auf molekularen Änderungen der prä- und/oder postsynaptischen Seite basiert, sind die beeinflussenden Faktoren für Kurzzeitplastizität hauptsächlich präsynaptisch. Dort werden synaptische Transmission und aktivitätsabhängige Plastizität an der aktiven Zone reguliert. Diese Zone ist ein präsynaptischer Abschnitt der Plasmamembran welcher mit einem komplexen Proteinnetzwerk versehen ist. Sie dient dem Andocken und der Vorbereitung von synaptischen Vesikeln zur Neurotransmitterfreisetzung, welches die Zusammenführung der Vesikel mit dem Freisetzungsapparat und dem Ca^{2+}-Kanal beinhaltet. Das Proteinnetzwerk stellt dabei den räumlich und zeitlich sehr genau regulierten Prozess des durch ein Aktionspotential ausgelösten Ca^{2+}-Einstroms, mit anschließender Exozytose des neurotransmittergefüllten Vesikels sicher.

Der Fokus dieser Arbeit liegt auf dem präsynaptischen Protein RIM1α, welches eine Hauptkomponente des Proteinkomplexes der aktiven Zone darstellt. Vorherige Studien konnten zeigen, dass RIM1α abhängig von der getesteten Synapse entweder Kurzeitplastizität verändert oder präsynaptische Langzeitplastizität vermittelt oder beides.

Durch die Kombination von elektrophysiologischen Analysen der synaptischen Transmission und Freisetzungswahrscheinlichkeit zusammen mit 2-Photonen Ca^{2+}-Messungen an der zerebellaren Körnerzellsynapse konnten wir zeigen, dass bereits das Fehlen der Isoform RIM1α zu einer signifikanten Reduktion des Ca^{2+}-Einstroms in axonalen Boutons führt. Infolgedessen ist die Freisetzungswahrscheinlichkeit reduziert und die Kurzeitplastizität erhöht. Dahingegen konnten wir keine Unterschiede in der Expression von präsynaptischer Langzeitplastizität feststellen. Zur weiteren Überprüfung der Befunde wurde der reduzierte Ca^{2+}-Einstrom durch eine Reduktion der extrazellulären Ca^{2+}-Konzentration nachgeahmt. Die daraus resultierende, niedrigerer intrazelluläre Ca^{2+}-Konzentration unterschritt die Grenze der Induzierbarkeit von Langzeitplastizität nicht, kam ihr jedoch nahe. Unsere Ergebnisse sprechen gegen eine unabdingbare Rolle von RIM1α in der Expression von präsynaptischer Plastizität. Stattdessen weisen sie auf eine universellere Rolle des Proteins in der Interaktion mit spannungsabhängigen Ca^{2+}-Kanälen hin, welche gewährleistet, dass die synaptische Freisetzung von Neurotransmittern exakt erfolgt.

Des weiteren wurde ein bedeutender Unterschied im Ca^{2+}-Einstrom in den Boutons zwischen dem aufsteigenden Astes und denen des Parallelfasersegments von Körnerzellaxonen festgestellt. Dies ist eine zusätzliche Information ergänzend zu vorherigen Studien, welche bereits unterschiedliche synaptische Eigenschaften der beiden axonalen Segmente zeigen konnten.

1 Introduction

The brain is an organ that enables organisms to interact with the environment in a directed fashion. It does so by receiving sensory information, performing information processing and generating output like motor commands (Reichert, 1992). Neurons are thought to be the functional modules of this process. They are interconnected and integrated in complex networks, and differ in morphology and physiology to perform a variety of computational tasks (Shepherd, 2010).

The first described neuron in the human brain, although the term did not exist at that time, was the Purkinje cell (PC). It was named after its discoverer Jan Evangelista Purkinje in 1837 (Figure 1). A systematic description of neurons and their organization in the brain started with the contribution of Camillo Golgi and his *reazione nera* (Golgi staining) in 1873 (Golgi, 1873). The technique was utilized by Santiago Ramón y Cajal and enabled him to perform detailed morphological studies of the microorganization of almost every region of the central nervous system (CNS), e.g. the cerebellum (Figure 2). His work and that of others finally led to the "Neuron Doctrine" (1889) which proposed that the interaction between two (separate) neurons is made up by axons contacting dendrites or the soma (Glickstein et al., 2009). Cajal suggested that the contact between neurons is the point where information flows from one cell to another and he is therefore considered the founder of modern neuroscience (DeFelipe, 2002). The theory formed the counterpart to the "Reticular Theory" which was supported by Camillo Golgi in the then-current

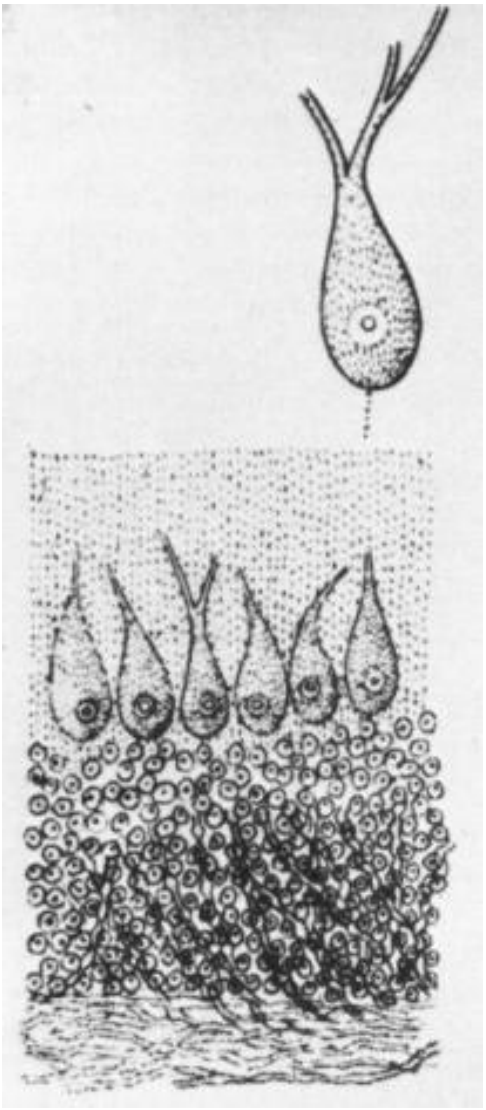

Figure 1: Purkinje cells drawn by Purkinje. The large neurons in the cerebellar cortex were described as "a great number of similar corpuscles, which surround the yellow substance (granular layer)", Purkinje, 1837 from Glickstein et al., 2009.

debate. Golgi assumed that neuronal networks consist of a continuous reticulum formed in the axonal plexus.

The term "synapse" was first introduced by Sherrington and Michael Foster in the 1897 edition of the *Text-book of physiology* and described these zones of contact (that had been suggested by Cajal) between neurons or neuron and effector cell. Their concept was based on findings from physiological experiments demonstrating, amongst others, a longer latency of conduction in reflex arcs as compared to the conduction velocity in nerve fibers (Burke, 2006). He therefore proposed a "nexus between neuron and neuron", termed synapse, and thereby highlighted one of the key structures in the CNS. Since then, neurons and their synaptic connections were one of the major targets of neuroscientific research (Ito, 2011).

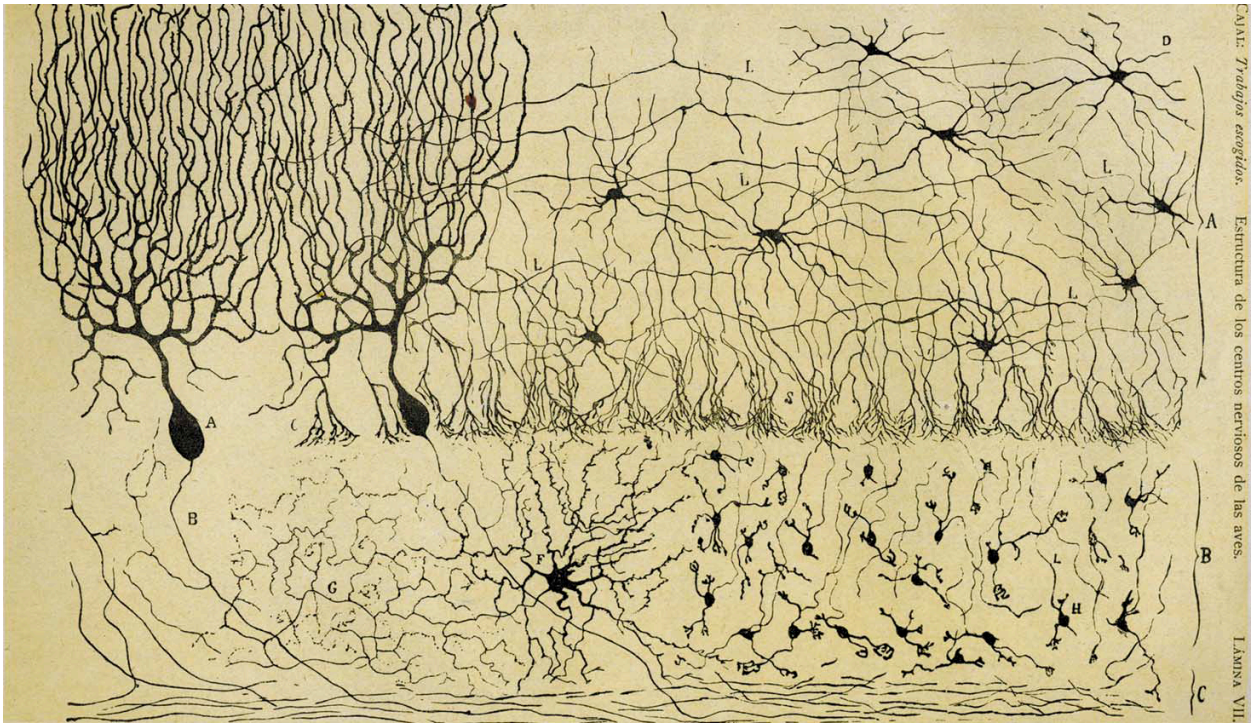

Figure 2: Drawing of the cerebellar cortex of a hen by Santiago Ramón y Cajal. Different layers are shown (labeling on the right hand site): the molecular zone (A), the granular layer (B) and the 'white matter' (C) (not labeled is the Purkinje cell layer between A and B). Illustrated are five different cell types: Purkinje cells (A), stellate cells (D), Golgi cells (F), granule cells (H) and basket cell axons (S). Taken from DeFelipe, 2002, originally from Cajal, S.R. (1888) 'Estructura de los centros nerviosos de las aves.`Rev. Trim Histol. Norm. Patol. 1, 1-10.

1.1 Neuronal communication

Neuronal communication describes the transduction of chemical or electrical signals from one neuron to another. Three principle mechanisms of fast signaling in the CNS are known so far: Electrical coupling, ephaptic coupling and communication via chemical synapses.

Electrical coupling is mediated by gap junctions. They are composed of six protein subunits, connexins, which form a hemichannel. The docking of two hemichannels forms a aqueous channel between the cytoplasm of two cells that mediates direct electrical and metabolic coupling (Bennett and Goodenough, 1978; Harris et al., 1983; Giaume et al., 2010). Recently, a new family of gap junction proteins, called pannexins, has been discovered, which are also involved in electrical coupling (Bruzzone et al., 2003). Gap junctions are thought to play a role in astroglial networks (Pannasch and Rouach, 2013), fast neuronal communication (Schmitz et al., 2001) and network oscillations (Draguhn et al., 1998). Furthermore, they have been shown to compensate for sublinear dendritic integration in Golgi cells of the cerebellum by spreading excitatory inputs to neighboring interneurons (Vervaeke et al., 2012).

Ephaptic coupling describes the interaction of two closely spaced neurons. The activity of one neurons creates a local electric field by the ion flow through its membrane and thereby potentially influences the activity of its neighboring neurons (Jefferys, 1995; Anastassiou et al., 2011).

It is worth noting that information transfer in the CNS is not only a neuron-specific performance. There is growing evidence that glia cells, especially astrocytes, are capable of regulating synaptic transmission and plasticity. They have been shown to sense neuronal activity and respond via calcium signaling, so that their function seems to exceed mere metabolic support (Oliet et al., 2001; Pannasch et al., 2011).

However, electrical coupling, ephaptic interaction and astrocytic contribution to neuronal communication have been shown to be of significant function in special cases or in an indirect fashion. The vast majority of neural communication is attributed to chemical synaptic transmission via neurotransmitters.

1.1.1 Chemical synaptic transmission

Evoked synaptic transmission is preceded by the initiation of an action potential (AP) in the soma of a neuron. The temporal and/or spatial summation of depolarizing events eventually leads to the opening of sodium channels at the axon initial segment, thereby triggering an AP. The AP is then transferred along the axon by active conductances of sodium and potassium

channels and finally leads to a depolarization of the presynaptic membrane, which in turn opens voltage-dependent Ca^{2+}-channels. The rise in presynaptic calcium triggers - with a certain probability - the fusion of a vesicle with the presynaptic membrane and thereby the release of neurotransmitter into the synaptic cleft (1.1.3). Neurotransmitter then binds to postsynaptic receptors that transduce a receptor-dependent signal to the cytosol (Zucker and Regehr, 2002; Shepherd, 2003).

The impact of neurotransmitter binding to a synaptic receptor depends on the specific receptor type. Broadly speaking, they can be divided into ionotropic (ligand-gated ion channels) and metabotropic (G-protein coupled) receptors that mediate fast and slow synaptic transmission, respectively (Hammond, 2012).

The process of fast synaptic transmission includes the release of neurotransmitter from the presynaptic element and its subsequent binding to postsynaptic receptors. The binding leads to a temporally and spatially limited increase in the membrane ionic conductance through the opening of ligand-gated ion channels. Dependent on the ion selectivity and the electrochemical gradient between the extracellular and intracellular milieu of these ions the conductance change leads to a (relative to the intracellular potential), more positive, excitatory postsynaptic potential (EPSP), or more negative, inhibitory postsynaptic potential (IPSP) (Shepherd, 2003). In voltage clamp experiments, where the intracellular potential is kept constant at a given holding potential by current injections, these changes are thus detected as excitatory postsynaptic currents (EPSCs) or inhibitory postsynaptic currents (IPSCs).

At glutamatergic synapses, there are three ionotropic receptors that are classified according to their specific agonists: α-amino-3-hydroxy-5-methyl-4-isoxazole propionic acid receptors (AMPARs) are composed of four subunits (GluA1-4) forming a tetramer. AMPARs are Na^+ and K^+ permeable and, depending on their subunit composition, also able to conduct Ca^{2+}-ions. Even though they can exhibit a wide range of different biophysical properties, AMPARs usually have rapid kinetics. N-methyl-D-aspartate receptors (NMDARs) have slower kinetics and their channel pore is blocked by Mg^{2+} at negative membrane potentials. The opening of the receptor channel depends on the depolarization of the postsynapse and the subsequent release of the Mg^{2+}-block. The conductivity of NMDARs is much higher for Ca^{2+}-ions compared to AMPARs. The function of kainate receptors (KARs), compared to AMPA and NMDA receptors, is less well understood due to a lack of selective pharmacology until recently but they also play a role in synaptic transmission and plasticity. KARs are permeable to Na^+ and K^+ and possess slower kinetics than AMPARs (Castillo et al., 1997b; Vignes and Collingridge, 1997; Bortolotto et al., 1999; Lerma, 2006; Pinheiro and Mulle, 2008).

The kinetic properties of ionotropic glutamate receptors are not only regulated by their subunit composition, but also by transmembrane auxiliary subunits that form an integral part of the receptor complex. They are able to modulate receptor trafficking, gating and pharmacology and are thus crucially involved in the regulation of glutamatergic transmission. Their function has been first described for transmembrane AMPAR regulatory proteins (TARPs) but recent studies suggest similar interactions for NMDARs and KARs (Chen et al., 1999; Hashimoto et al., 1999; Ng et al., 2009; Jackson and Nicoll, 2011; Straub et al., 2011).

Slow synaptic transmission involves the activation of metabotropic receptors. Their signal transduction is mediated by intracellular cascades via guanine nucleotide-binding proteins (G-proteins), which can activate multiple downstream effectors (Hammond, 2012). In the inactive state, G-protein coupled receptors loosely bind a G-protein complex consisting of the α-, β- and γ-subunit and GDP. After activation by an agonist a transient high-affinity complex is formed, GDP is replaced by GTP and the G-protein complex dissociates into α-subunit and a βγ-dimer, both able to activate several effectors (Pierce et al., 2002). A common example is the presynaptic $GABA_B$ receptor. Upon activation it decreases calcium influx by modulating voltage-dependent calcium channels (VDCCs), reduces cyclic adenosine monophophate (cAMP) levels and increases the energy barrier for vesicle fusion (Takahashi et al., 1998; Rost et al., 2011).

Although synaptic transmission is normally described as a feedforward process from the pre- to the postsynapse, other important signaling mechanisms operate at the synapse as well. After the release of neurotransmitter and its diffusion into the synaptic cleft, it not only binds to receptors on the post- but also on the presynaptic side. These so-called autoreceptors are mostly metabotropic and act as a feedback loop in signal transduction by leading either to an increase or decrease of the release probability (Thompson and Gähwiler, 1989; Scanziani et al., 1997). Synaptic feedback communication can also occur by means of retrograde messengers. A prominent example is the release of endogenous cannabinoids triggered by postsynaptic depolarization that subsequently suppresses presynaptic transmitter release. The endocannabinoid system is thought to act as a feedback loop that regulates presynaptic inputs according to postsynaptic firing rates (Kreitzer and Regehr, 2001; Ohno-Shosaku et al., 2001; Wilson and Nicoll, 2001). Additionally, release of neurotransmitter has been shown to act in a non-synaptic manner. Depending on the spatial separation of synapses by glia cells and the type of neurotransmitter uptake mechanism, released neurotransmitter can diffuse out of the synapse and activate distant receptors, a process that is called volume transmission (Barbour and Häusser, 1997; Oláh et al., 2009).

1.1.2 Structure and function of the presynaptic active zone

Neurotransmitter is released into the synaptic cleft by vesicle exocytosis. The process is exclusively restricted to the active zone, a small part of the presynaptic membrane with an electron dense appearance in electron micrographs (Figure 3A,B). It is the site of information transfer from an electrical signal (action potential) to a chemical signal (vesicular exocytosis of chemical messenger).

The active zone performs several crucial steps in synaptic transmission: (1) It docks and primes synaptic vesicles, (2) recruits Ca^{2+}-channels and brings them into close vicinity of the release trigger, (3) brings together the pre- and postsynapse opposite to each other and (4) mediates long-term and short-term plasticity as a synapse specific characteristic. It thereby ensures synaptic transmission with the requisite speed and accuracy (Südhof, 2012).

A key component of the active zone is a multiprotein core complex that brings together the vesicle and its release machinery with the VDCC (Figure 3C). In vertebrates, it associates with cell adhesion molecules (CAMs) like neurexin, piccolo and bassoon (Ziv and Garner, 2004), or SYD-1 in invertebrates (Owald et al., 2012), to ensure proper positioning of the active zone opposite to postsynaptic specializations. The exocytosis itself is mediated by the fusion machinery, which is formed by the SNARE (SNAP (soluble NSF attachment protein) receptor) proteins SNAP-25, synaptobrevin (v-SNARE) and syntaxin (t-SNARE). The complex, together with Munc18, performs the fusion process that is controlled by Ca^{2+} via synaptotagmin and complexin (Südhof and Rizo, 2011).

The core complex consists of five evolutionary conserved proteins: RIM (Rab3-interacting molecule) (Wang et al., 1997), RIM-BP (RIM binding protein), Munc13 (mammalian unc-13), α-liprin and ELKS (Figure 3C). In this complex α-liprin and ELKS are the only proteins which do not possess multiple, functionally different modules. α-liprin is involved in the active zone formation and vesicle recruitment. The function of ELKS in vertebrates is largely unclear but experiments in *Drosophila* have shown that it is part of the fusion protein bruchpilot and important for vesicles recruitment (Hallermann et al., 2010).

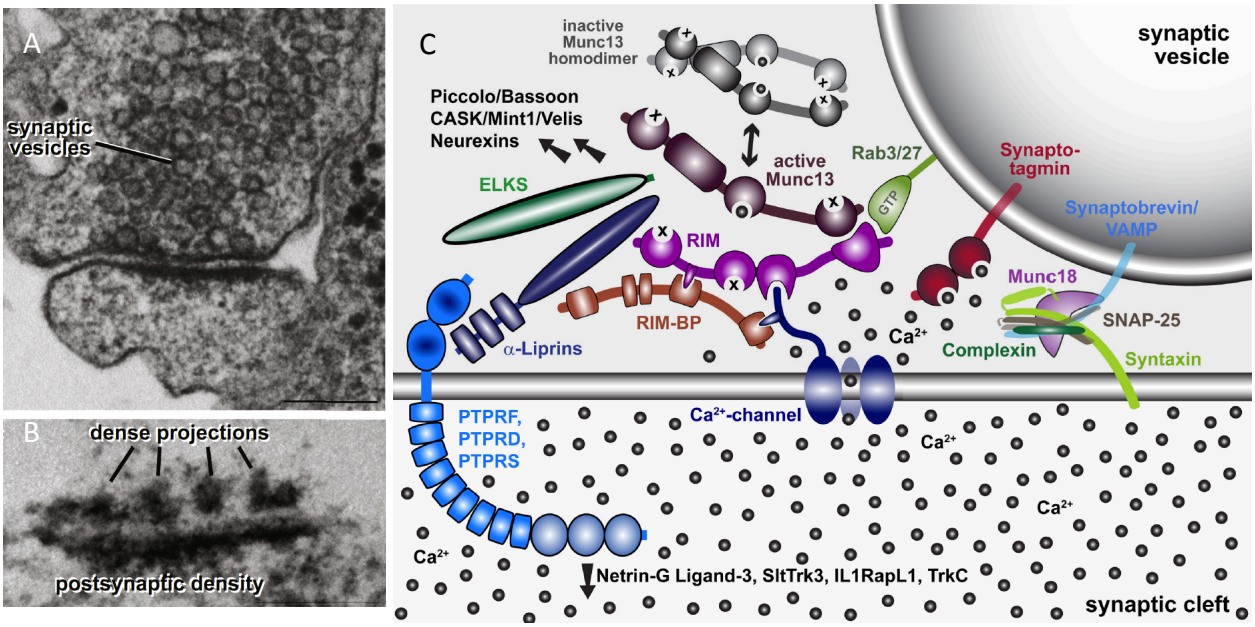

Figure 3: Electron micrographs and molecular scheme of the presynaptic active zone. (A) Electron micrograph of a hippocampal synapse. (B) Detailed electron micrograph of a synapse with the presynaptic dense projections and the opposing postsynaptic density. (C) Scheme of the presynaptic molecular components. ELKS – glutamine/leucine/lysine/serine-rich protein, Munc13/18 – mammalien unc13/18, CASK - Ca2+/calmodulin associated serine kinase, RIM - Rab3-interacting molecule, RIM-BP – RIM binding protein, VAMP - vesicle associated membrane protein, SNAP-25 - soluble NSF attachment protein 25, PTPR - LAR-type receptor phosphotyrosine phosphatases. All pictures taken from Südhof, 2012.

Much more information has been gathered for the functional significance of the three multidomain proteins: RIM plays a central role in the organization of the molecular presynaptic scaffold. The RIM protein family consists of 7 members of which five are encoded by the RIM1/2 genes and two shorter C-terminal isoforms (γ-RIMs) by RIM3 and RIM4 respectively (Figure 4). There are only two full-length isoforms, RIM1α and 2α, that comprise all RIM domains and two β-RIMs that lack either a Rab-3 binding N-terminal part (RIM1β) or the whole zinc finger domain (RIM2β) (Mittelstaedt et al., 2010). Recent studies with RIM1/2 conditional KO mice have demonstrated that RIM is involved in a number processes: it assists in the recruitment and targeting of VDCCs to the active zone, the coupling of vesicles to VDCCs, the priming and establishment of the readily releasable pool (RRP) and it furthermore inhibits the homodimerization of Munc13 (Deng et al., 2011; Han et al., 2011; Kaeser et al., 2011). Earlier, it has been shown that the binding of RIM1 to VDCCs alters gating properties and vesicle docking (Kiyonaka et al., 2007). RIM performs these tasks by interacting with other proteins via its five different functional domains (Figure 4): The N-terminal zinc-finger, which is surrounded by α-helices, binds to Munc13 (Deng et al., 2011) and to the vesicular proteins Rab3 and Rab27 in a GTP-dependent manner (Fukuda, 2003). This tripartite complex is thought to be responsible for

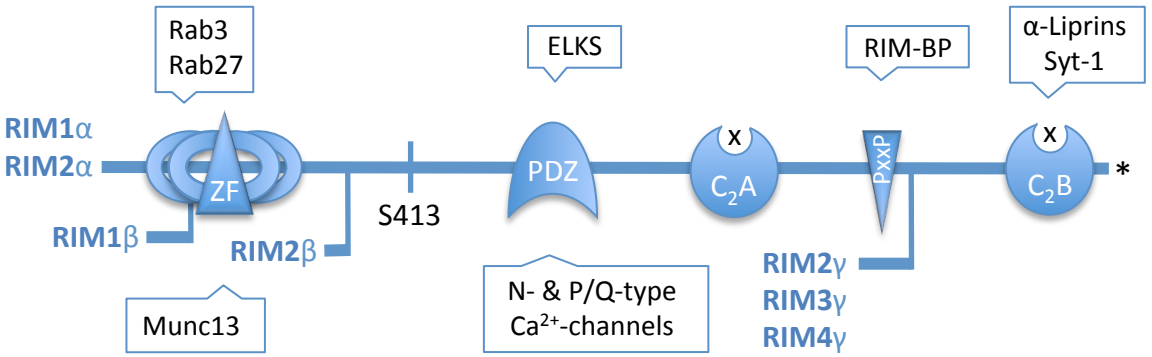

Figure 4: Domain structure of the RIM protein. Shown are the domains (white label) and RIM isoforms (blue label). ZF – zinc finger, surrounded by α-helices; PDZ – protein domain first described in PSD-95, Discs-large and ZO-1; C_2A, C_2B – C2 domains without Ca^{2+}-binding capacity; PxxP – proline-rich sequence, Munc13–mammalien unc13, RIM - Rab3-interacting molecule, ELKS – glutamine/leucine/lysine/serine-rich protein, RIM-BP – RIM binding protein, Syt1 – Synaptotagmin 1. Boxes indicate interaction sites with other proteins. * indicates the position of the C-terminus. Adapted from Südhof, 2012.

the priming of vesicles (Dulubova et al., 2005). The PDZ domain can bind to ELKS and P/Q- and N-type calcium channels and is thus important for the recruitment of VDCCs to the active zone (Han et al., 2011). In contrast, the physiological relevance of the two C2 domains of RIM, that interact with α-liprin, synaptotagmin-1 and SNARE proteins, is unclear. In addition to the just mentioned proteins, they have been shown to bind to the α1B subunit of N-type Ca^{2+}-channels and with lower affinities to the α1C subunit of L-type Ca^{2+}-channels (Coppola et al., 2001). Yet, the functional significance of this is also indistinct. A proline rich region (PxxP) between the two C2 domains binds to RIM-BP, which performs additional functions in targeting Ca^{2+}-channels to the active zone (see below). Of note is also the phosphorylation site at serine-413. It was thought to mediate plastic long-term changes but has recently been shown to be dispensable for this process (Kaeser et al., 2008a).

RIM-BP has been shown to possess three Src homology 3 (SH3) domains that bind to PxxP motifs in α_1-subunits of L-type, P/Q-type and N-type Ca-channels and to RIM (Hibino et al., 2002). It thereby acts as a linker of VDCCs to RIM and the priming machinery. Experiments in *Drosophila* revealed that RIM-BP mutants have reduced Ca^{2+}-influx and VDCC clustering is impaired. As a consequence release probability and evoked neurotransmitter release are reduced (Liu et al., 2011).

The current view of the role of Munc13 (Brose et al., 1995) in synaptic transmission is that it is essential for vesicle priming. By an interaction of the MUN domain with the closed form of the SNARE protein-complex syntaxin-1/Munc18, it catalysis the transition to the open conformation

in a stable SNARE complex (Basu et al., 2005; Gerber et al., 2008; Ma et al., 2011). Recent studies revealed that the priming function of Munc13 is regulated. It forms homodimers via the binding of the N-terminal C2A domains and is thereby inactivated. After binding of the RIM zinc-finger to the C2A domain, the homodimer is disrupted and the priming function is activated (Deng et al., 2011; Südhof, 2012). Additionally, Munc13-mediated priming can be altered in an activity-dependent manner by the central signaling domain which consists of a calmodulin binding sequence and a C1 and C2B domain. The two domains are activated by Ca^{2+}/calmodulin, diacylglycerol or phosphatidylinositol phosphate/phosphatidylinositol bisphosphate (Shin et al., 2010).

1.1.3 The role of calcium in neurotransmitter release

The signaling of intracellular Ca^{2+}-ions has a multitude of different functions and implications. One of the most prominent is the regulation of neurotransmitter release at the active zone of nerve terminals. The influence of calcium concentration ($[Ca^{2+}]$) on neurotransmitter release has been described earlier by del Castillo and Katz, 1954a assuming a interaction of Ca^{2+}-ions and a reactive site. Later it has been shown directly that increasing $[Ca^{2+}]$ also leads to an increase in the postsynaptic potentials and that this enhancement is not due to changes in action potential conduction (Katz and Miledi, 1965). Based on these findings Dodge and Rahamimoff, 1967 developed a first quantitative description of the relationship between the extracellular $[Ca^{2+}]$ and neurotransmitter release. For low $[Ca^{2+}]$, they demonstrated a supralinear dependency of the postsynaptic potential on extracellular $[Ca^{2+}]$ that pointed to a cooperative involvement of Ca^{2+}-ions in the release of a vesicle. For higher extracellular $[Ca^{2+}]$ the relationship becomes sublinear which is due to the saturation of Ca^{2+}-influx. This is taken into account when data is plotted against the intracellular $[Ca^{2+}]$ and fitted with a power function, which evidently demonstrates the supralinear relationship between $[Ca^{2+}]$ and transmitter release (Mintz et al., 1995; Reid et al., 1998).

Extensive research has provided a detailed picture of the many mechanistic steps involved in neurotransmitter release. After the steep rise of the presynaptic $[Ca^{2+}]$ by the opening of VDCCs, exocytosis of neurotransmitter-filled vesicles is triggered by the Ca^{2+}-sensor synaptotagmin (Neher and Sakaba, 2008). The process of Ca^{2+}-influx and neurotransmitter release is highly regulated by the active zone scaffold proteins (1.1.2), the release trigger and release machinery, VDCC function and fast Ca^{2+}-buffering (Kiyonaka et al., 2007; Neher and Sakaba, 2008; Kochubey et al., 2011; Schneggenburger et al., 2012).

Stimulus evoked release can be distinguished into fast synchronous release (< 2 ms after the AP) and a slower asynchronous release (> 2 ms after the AP). The mechanistic principles underlying these differential release kinetics are not completely solved. One possibility is the presence of a profoundly different [Ca^{2+}] profile during high frequency stimulation and the resulting [Ca^{2+}] at distant sites of vesicle fusion (Neher and Sakaba, 2008). Alternatively, the existence of two different Ca^{2+}-sensors with distinct affinities (Sun et al., 2007) or possibly different Ca^{2+}-cooperativities, leading to differential reactions at different [Ca^{2+}] (Lou et al., 2005), has been hypothesized . A combination of all the afore mentioned cases is possible as well (Kochubey et al., 2011).

In vertebrate brains Synaptotagmin 1, 2 and 9 are the mediators of fast synchronous release (Xu et al., 2007). The affinity of these Ca^{2+}-sensors is relatively low, they react to a brief (< 1 ms) and local (< 100 nm) [Ca^{2+}] signal of tens of μM in amplitude. Thus, Ca^{2+}-triggered release is only possibly within a small area in the vicinity of VDCCs, so called nano- or microdomains. Earlier modeling studies have shown that the temporal and spatial profile of the [Ca^{2+}] "depends on the distance to the VDCC, the single channel Ca^{2+}-current, and the on-rate, concentration and mobility of the cellular Ca^{2+}-buffers" (Schneggenburger et al., 2012). Hence, the relatively high [Ca^{2+}] at the pore of the VDCC upon opening rapidly decreases by the diffusion into the intracellular space and binding to fast Ca^{2+}-buffers. Unfortunately, up to now, it has not been possible to measure this process directly. Because of its local restriction, which is below the optical resolution limit, it cannot be determined with conventional optical methods. However, early modeling studies predict that a single Ca^{2+}-current of a P/Q-type channel with 2 mM extracellular [Ca^{2+}] would have a Ca^{2+}-transient of about 20 μM at 10-20 nm distance (Neher, 1998). In fact, experiments have demonstrated the tight coupling of Ca^{2+}-source and Ca^{2+}-sensor that ranges between 10-20 nm in GABAergic basket cells of the hippocampus (Bucurenciu et al., 2008) and is < 30 nm at the PF – PC synapse in the cerebellum (Schmidt et al., 2012).

Taken together, it is generally accepted that the release probability of a docked and primed vesicle strongly depends on the number of and distance to neighboring VDCCs. However, the exact interaction of VDCCs at the active zone to achieve sufficient [Ca^{2+}] for triggering release remains elusive. There are two possibilities of VDCCs collocation that would yield a [Ca^{2+}] sufficient to trigger release: (1) A more or less equal distribution of several VDCCs at the active zone that provide a "pooled" [Ca^{2+}] signal or (2) few VDCCs that are tightly anchored to a particular vesicle. The above mentioned studies show that the latter seems to be the more likely scenario at cortical synapses (Bucurenciu et al., 2008; Schmidt et al., 2012) but an intermediate VDCC grouping has been described in younger animals (Kochubey et al., 2009).

Ca^{2+}-influx trough VDCCs at the active zone is normally mediated by different VDCC-subtypes. Synaptic transmission is mainly controlled by P/Q- and/or N-type channels but L- and R-type channels are also involved. They are classified according to their α_1-subunit, which contains the voltage sensor, the conduction pore and the gating apparatus. The α_1-subunit associates with four distinct auxiliary subunits and also contains most of the target sites for channel regulation by second messengers, drugs and toxins (Catterall and Few, 2008). VDCCs are regulated, amongst others, by Gβγ (e.g. via mGluRs, adenosine receptors or $GABA_b$), PKC, SNARES, CaMKII and nCaS/CaM (Catterall and Few, 2008) or by binding to RIM (Kiyonaka et al., 2007).

In conclusion, Ca^{2+}-influx and intracellular Ca^{2+}-handling constitutes a main regulatory element of presynapse physiology.

1.2 The Cerebellum

To further examine the above mentioned mechanisms of synaptic transmission we chose the granule cell – Purkinje cell synapse in the cerebellum. This synapse is very well suited to probe synaptic plasticity because of three reasons: (1) The cerebellar structure permits good experimental accessibility for electrophysiological as well as fluorometric experiments (2.2). (2) It displays a pronounced short-term plasticity and possesses a presynaptic form of long-term plasticity (1.3, 1.4). (3) A long history of cerebellar research has yielded an extensive knowledge basis of its physiology which will be outlined in the following, and on which one can fall back when planning and interpreting experimental results.

Early descriptions of the cerebellum connected a low number of cerebellar folia with cretinism and suggested that it may function as an organ for sexual drive (Combe and Combe, 1838). However, experimental evidence for these conclusions was sparse and none of them turned out to be true. Pierre Flourens was the first who, in 1824, made the fundamental observation that after cerebellar ablation in animals movements are not completely lost but coordination was missing. He therefore concluded that the production and the coordination of movement results from separate mechanisms (Glickstein et al., 2009). More than a 100 years later cerebellar research made great progress on the cellular connectivity with a detailed description of the cerebellar circuitry by John Eccles, Masao Ito and Janos Szentägothai (Eccles et al., 1967). It finally led to the comprehensive theories of cerebellar function in motor learning and control from David Marr (Marr, 1969) and James S. Albus (Albus, 1971).

1.2.1 Function and organization

The modern view of the cerebellum holds that it acts as a sensorimotor control system where it receives a variety of sensory inputs and calculates, according to internal computational rules, an adequate motor output (Apps and Garwicz, 2005). It is involved in coordination as well as motor learning, reflex adaptation and locomotion conditioning (De Zeeuw et al., 2011). How these complex behaviors are produced by the cerebellum is not completely solved but motor prediction, which will be explained in the following, seems to be a crucial part of it. The concept of motor prediction deals with the problem that the CNS is not capable of determining the exact peripheral state during ongoing movement which is due to the time delays in conduction from the periphery to the CNS (Miall et al., 2007). An initial idea as to how this might be solved has been put forward by Hermann von Helmholtz who suggested an internal signal copy of the motor command, termed efference copy. The idea gave rise to several theories of cerebellar

function in which motor prediction is implemented in sensorimotor loops to control motor coordination (Ito, 1984; Wolpert et al., 1995; Wolpert and Flanagan, 2001) and which could also be strengthened experimentally (Miall et al., 2007).

Recent work suggests that it might also play a role in emotional and cognitive processing and autism (Schmahmann, 2010; Timmann et al., 2010; Tsai et al., 2012) but it is unclear if this is a general feature of the mammalian cerebellum or specific to humans (Galliano et al., 2013b). A theory combining different aspects of information processing interprets the cerebellum as a "general-purpose co-processor" (i.e. the expansion of the concept of motor prediction to non-motor functions) whose action depends on the connection of individual modules to specific brain regions. It generalizes the concept of the cerebellum being a forward controller of the motor system to an "anticipatory" processing. The latter encompasses the alignment of neural activity representing a virtual reality (because of the temporal delay of sensory input) and the actual sensory stimuli (real world perception) (D'Angelo and Casali, 2012).

Despite the ongoing debate on cerebellar function, the concept of the structural organization of the cerebellum is less controversial. It can be divided anatomically into a cortical part and subcortical part (Figure 5). The functional organization of the cerebellum consists of parasagittal zones or microzones, which consist of several PCs having the same somatotopic receptive field. They are sagitally oriented and synchronously modulated by climbing fibers arising from a particular subnucleus of the inferior olive (D'Angelo and Casali, 2012). The PCs in turn project to particular cerebellar nuclei that project back to the same subnucleus of the inferior olive and thus represent cerebellar microcircuits (De Zeeuw et al., 2011) (Figure 5).

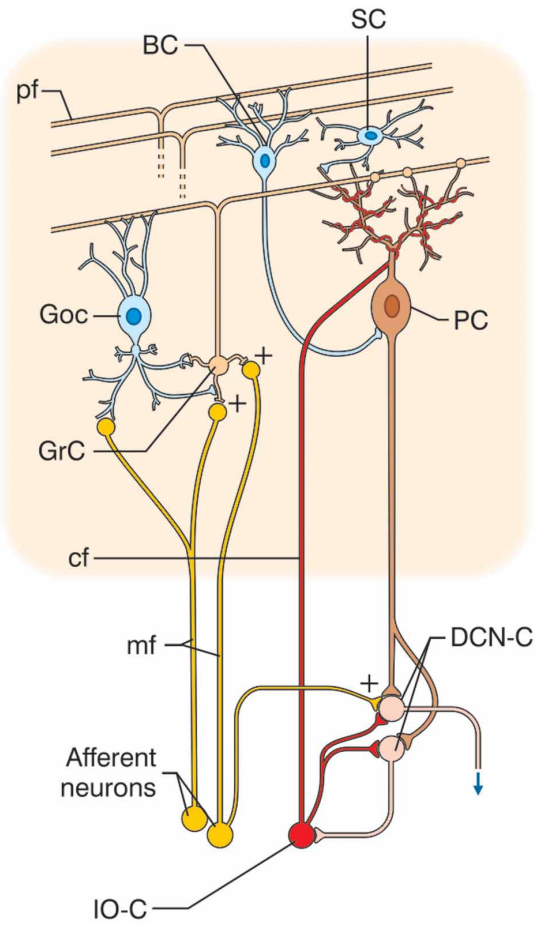

Figure 5: The cerebellar microcircuit consists of a cortical (orange) and subcortical section. Shown are (from top to bottom): parallel fibers (pf), basket cells (BC), stellate cells (SC), Golgi cells (Goc), Purkinje cells (PC), granule cells (GrC), climbing fiber (cf), mossy fiber (mf), deep cerebellar nuclei (DCN) and inferior olive (IO). Taken from D'Angelo and Casali, 2012.

1.2.2 The cerebellar cortex

The cerebellar cortex is a three-layered structure consisting of the molecular layer, Purkinje cell layer and granular cell layer (Figure 2). It is part of the cerebellar microcircuit that also comprises subcortical sections (Figure 5). The circuit gets external input from mossy fibers and climbing fibers (Figure 6). Mossy fibers arise in various regions in the brain stem and spinal cord nuclei and diverge to the deep cerebellar nuclei and innervate the granular cell layer. There they make contacts with granule cells and Golgi cells. Golgi cells functionally regulate the degree of mossy fiber-granule cell divergence. They get excitatory input from mossy fibers and granule cell ascending axon and thereby inhibit granule cells in a feedforward and feedback manner (Cesana et al., 2013). Each granule cell gives rise to an ascending axon, which bifurcates in the molecular layer to form the parallel fibers. They run orthogonally to the dendritic tree of the PC through the molecular layer and form about 2000 contacts with individual PCs. Besides receiving parallel fiber input, each PC is innervated by one climbing fiber that makes thousands of synaptic contacts with the dendritic tree of the PC resulting in a powerful connection.

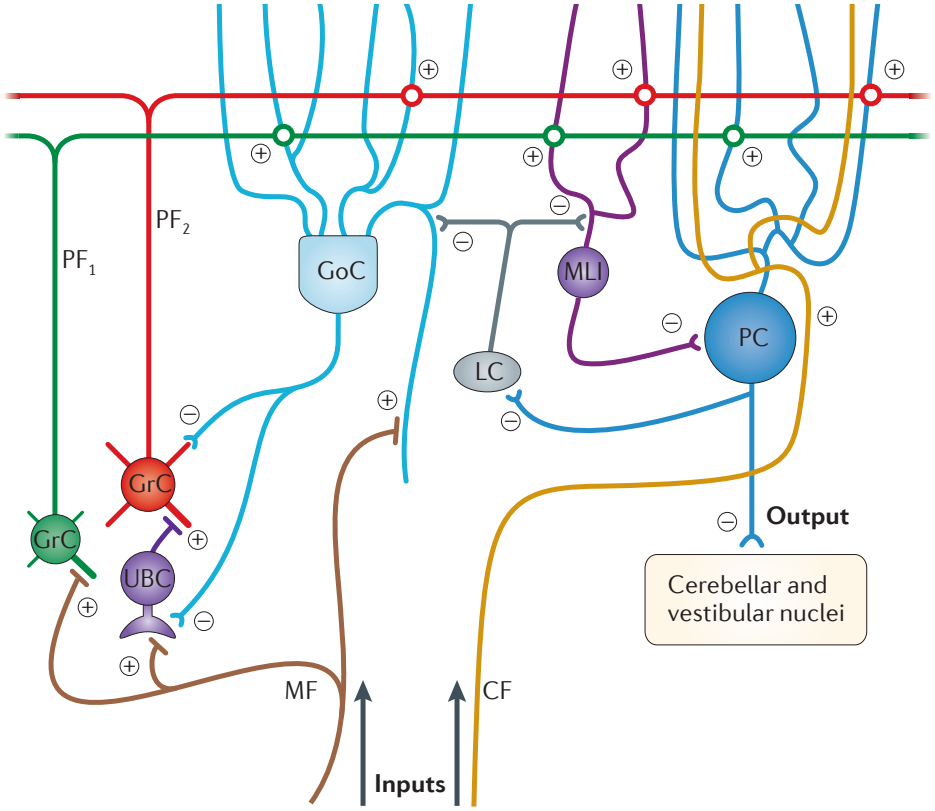

Figure 6: Wiring diagram of the cerebellar cortex. (+) and (-) denote excitatory and inhibitory connections, respectively. GoC – Golgi cell, MLI – molecular layer interneuron, PC – Purkinje cell, LC – Lugaro cell, GrC – granule cell, UBC – unipolar brush cell, MF – mossy fiber and CF – climbing fiber. From Gao et al., 2012.

Inhibitory input onto PCs is provided by stellate cells at the dendritic level and by basket cell axons that form a "pinceau" structure at the axon initial segment. Together, they are called molecular layer interneurons and mediate feedforward inhibition from PFs to PCs. The PC itself is GABAergic too and targets neurons in the deep cerebellar nuclei, which are the output of the cerebellum (Ito, 2006; Shepherd, 2010). The deep cerebellar nuclei also give rise to inhibitory connections that project back to the inferior olive (Figure 5). Recently, it has been shown that this olivo-cortico-nuclear network is capable of controlling olivary afferents to PCs, and thus by activating this particular set of PCs forming a closed signalling loop (Chaumonta et al., 2013).
A less well-described type of interneuron is the Lugaro cell that is located in the granular cell layer. They make contact with Golgi cells and provide mixed glycinergic/GABAergic input. They are silent under normal conditions but discharge at 5 - 15 Hz in the presence of serotonin (Dumoulin et al., 2001; Hull and Regehr, 2012). Unipolar brush cells are exclusively present in the granular cell layer of the vestibulocerebellum. They are innervated by mossy fibers and synapse onto granule cells and other unipolar brush cells. They are thought to amplify mossy fiber input (Shepherd, 2010).

1.2.3 Properties of the granule cell – Purkinje cells synapse

PCs get excitatory input from climbing fibers and from parallel fibers. Interestingly, both types of input are exclusively mediated by non-NMDA receptors (Perkel et al., 1990). At the PF – PC synapse transmission is mediated by AMPARs whereas at the CF – PC synapse AMPARs and kainate receptors are involved (Huang, 2004). The PF – PC synapse displays a prominent paired pulse potentiation (Perkel et al., 1990) and a low release probability (Dittman et al., 2000). Ultrastructural analysis revealed that they are ensheathed by astrocytic processes to a greater extent (67 %) than e.g. Schaffer collateral - CA1 pyramidal cell synapses (43 %) making them less sensitive to synaptic cross-talk (Ventura and Harris, 1999; Xu-Friedman et al., 2001). PF synapses possess around eight anatomically docked vesicles per release site and normally one release site per synapse (Xu-Friedman et al., 2001). An extensive 2-photon laser scanning Ca^{2+}-imaging study demonstrated that Ca^{2+}-influx at PF synapses varies considerably between boutons (peak volume average Ca^{2+}-transients: 400 – 900 nM) but is highly reliable at single boutons. The authors calculated the number of VDCCs to range between 20 – 125 (dependent on the single channel conductance) per synapse (Brenowitz and Regehr, 2007). Another group performed paired recordings of unitary PF – PC connections together with a multi-probability fluctuation analysis and Ca^{2+}-imaging. The data enabled them to model the coupling between the

Ca^{2+}-source and the sensor and estimated it to be < 30 nm, thus clearly in the nanodomain range (Schmidt et al., 2012).

It is noteworthy that synaptic properties of granule cell synapses are seemingly not homogenously distributed along the axon. Two studies described electrophysiological differences between the ascending axon (AA) and the PF segments. They could show that the paired-pulse ratio is decreased and release probability is increased in AA compared to PF (Sims and Hartell, 2005). Furthermore, it was demonstrated that several forms of long-term plasticity are strongly limited in the AA whereas the PF segments exhibits postsynaptic long-term depression (LTD) and potentiation (LTP) and presynaptic LTP (Sims and Hartell, 2006).

Transmitter release from granule cells boutons is regulated, amongst others, by presynaptic G-protein coupled receptors (e.g. adenosine receptors, metabotropic glutamate receptors and cannabinoid receptors), which attenuate AP-triggered Ca^{2+}-influx. The neuromodulatory action of these receptors has been shown to be heterogeneous and depends on the bouton size and the AP triggered Ca^{2+}-transient amplitude (Zhang and Linden, 2009).

Under *in vivo* conditions granule cells exhibit a low spontaneous firing rate of 0.5 Hz and are inhibited by tonically activated $GABA_AR$. Upon mossy fiber input they fire in bursts of activity around 75 Hz and up to 250 Hz (Chadderton et al., 2004).

1.3 Short-term synaptic plasticity

Synapses are activated at a variety of frequencies ranging from less than once a second to several hundred Hertz (Catterall and Few, 2008). However, the synaptic output in dependency of the firing frequency varies widely among different types of synapses. This activity-dependent change in the strength of synaptic transmission is called synaptic plasticity (Figure 7). Short-term plasticity comprises activity-dependent changes that range from millisecond intervals (short-term potentiation and depression), to several seconds (augmentation) or minutes (post-tetanic potentiation, PTP). The direction of plasticity, i.e. facilitation or depression, is specific for a particular synapse and an intrinsic feature of synaptic transmission (Abbott and Regehr, 2004). The underlying processes are numerous and usually it is not possible to completely disentangle all of the ones involved (Zucker and Regehr, 2002; Fioravante and Regehr, 2011). Except for postsynaptic receptor desensitization (Jones and Westbrook, 1996), short-term plasticity represents a change in presynaptic neurotransmitter release (Catterall and Few, 2008). It provides synaptic transmission with a powerful computational property because it integrates current activity with the recent history of synaptic activity (Fioravante and Regehr, 2011).

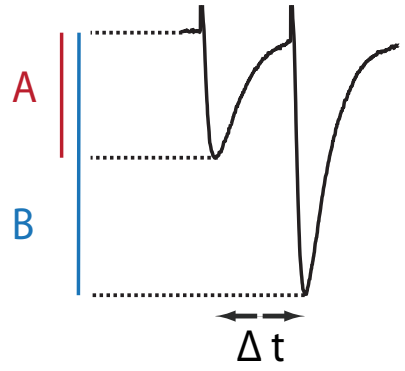

Figure 7: Example for short-term facilitation upon paired stimulation. A and B is the amplitude of the first and second EPSC (excitatory postsynaptic current), respectively. Δt denotes the temporal delay (inter stimulus interval) between the stimulation pulses. The paired pulse ratio is normally expressed as B/A and is >1 for facilitating and <1 for depressing synapses.

1.3.1 Mechanisms of short-term facilitation

Several mechanisms have been proposed for short-term facilitation. Initially it had been assumed that residual Ca^{2+}, remaining at the synapse after an action potential triggered Ca^{2+}-influx, contributes to the increase in release probability during subsequent stimuli (Katz and Miledi, 1968). This led to the proposal of a high affinity Ca^{2+}-sensor, distinct from synaptotagmin, that increases release probability on a slower time course (Atluri and Regehr, 1998). To date, no such Ca^{2+}-sensor has been identified (Fioravante and Regehr, 2011). Instead, two recent studies could show that (1) the increase of residual Ca^{2+} is not sufficient to account for the facilitation and that

Ca^{2+}-sensitivity does not change (Felmy et al., 2003) and that (2) the wash-out of endogenous Ca^{2+}-buffer leads to a decreased paired-pulse facilitation (Blatow et al., 2003). These results suggest that stimulus triggered Ca^{2+}-influx leads to a local saturation of fast, endogenous Ca^{2+}-buffers, like calbindin, so that more Ca^{2+}-ions will reach the nearby release trigger in response to a second stimulus (Catterall and Few, 2008; Fioravante and Regehr, 2011).

Additionally, it became evident that Ca^{2+}-influx can be altered in an activity-dependent manner (1.1.3) (Catterall and Few, 2008). Ca^{2+} binds to neuronal Ca^{2+}-senor proteins (CaS) that modulate Ca^{2+}-influx trough $Ca_v2.1$ channels (P/Q-type) and thereby increase Ca^{2+}-influx, leading to an increase in release probability (Mochida et al., 2008). Taking into account not only the local saturation of Ca^{2+}-buffers and modulation of Ca^{2+}-influx, but also the sensitivity of transmitter release to $[Ca^{2+}]$ (1.1.3), leads to the fact that already small changes in $[Ca^{2+}]$ can cause significant changes in synaptic output.

It has been shown that also subthreshold depolarization in the soma or axon can alter neurotransmitter release and thereby short-term plasticity. At the hippocampal mossy fiber – CA3 pyramidal cell synapse and in cortical layer 5 pyramidal cells it has been shown that subthreshold somatic depolarization increases the probability of transmitter release (Alle and Geiger, 2006; Shu et al., 2006). In cerebellar molecular layer interneuron pairs it has been shown that the electronic spread of subthreshold somatic depolarization facilitates axonal Ca^{2+}-entry and thereby release (Christie et al., 2011). Complementary work on CA3 pyramidal cells of hippocampal slice cultures has shown that not only somatic subthreshold depolarization but also AP width during axonal conduction is modulated by glutamate application and able to increase synaptic release (Sasaki et al., 2011). All the aforementioned mechanisms are very well suited to contribute to short-term plasticity in the sense that previous activity is capable of altering ongoing output.

Augmentation and PTP are similar forms of facilitation and probably share parts of their mechanistic principles. Both are induced by high-frequency stimulation and their duration depends on the train length of the stimulation protocol. The accumulation of free presynaptic Ca^{2+} during tetanic stimulation elevates residual $[Ca^{2+}]$ to several hundred nanomolar. Because residual $[Ca^{2+}]$ and PTP decay with a similar time courses they seem to be interconnected but residual $[Ca^{2+}]$ itself is not sufficient to cause an increase in synaptic transmission (Korogod et al., 2007). Among the proposed mediators are PKC, Munc13, CaMKII and synapsin (Fioravante and Regehr, 2011) of which the role of PKC is described best. Recent studies demonstrated the differential action of the PKC isoforms at different synapses. At the calyx of Held, PKCα and especially PKCβ are crucial for PTP (Fioravante et al., 2011). At the cerebellar PF – PC synapse

the loss of both PKC isoforms is being compensated by other regulatory mechanisms that are PKA inhibitor sensitive suggesting a compensatory action of PKA (Fioravante et al., 2012).

1.3.2 Mechanisms of short-term depression

Repetitive synaptic stimuli do not always lead to a facilitation of transmission. At many synapses, transmission is depressed when stimulation paradigms with shorter time intervals are used. Also a combination, first facilitation and later depression, is possible during train stimulation (Dittman et al., 2000).

Although the total number of presynaptic vesicles is much higher, the number of release-ready vesicles at a given active zone is limited to only a few (Xu-Friedman et al., 2001). The overall number of vesicles being released by an AP depends on the number of vesicles in the readily releasable pool and their release probability. If an AP triggers the release of a large number of vesicles from the readily releasable pool, then a subsequent stimulus will release fewer vesicles because of the reduced pool size (Zucker and Regehr, 2002). This model predicts synapses with high release probabilities to exhibit short-term depression and low P_r synapses to have short-term facilitation which indeed holds true for many synapses in the CNS (Fioravante and Regehr, 2011). Short-term depression by depletion of the readily releasable pool is likely to occur due to multi-vesicular release (MVR) (Zucker and Regehr, 2002), which is the simultaneous release of more than one vesicle upon AP-triggered Ca^{2+}-influx. The principle possibility of MVR at artificially high release probabilities has been shown earlier (Heuser et al., 1979). On the contrary, early physiological and morphological studies led to the “one site – one vesicle” hypothesis. It postulates the release of only vesicle per release site and trigger (univesicular release) and the existence of a mechanism that prevents the fusion of multiple vesicles at these sites (Triller and Korn, 1982; Redman, 1990). Today though, MVR has been shown to be regulated in an activity–dependent manner (Bender et al., 2009) and to be present both at high and low P_r synapses (Wadiche and Jahr, 2001; Foster et al., 2005).

Besides the depletion of the readily releasable pool, inactivation of release sites is also thought to contribute to synaptic depression. If a vesicle is exocytosed, its membrane and the vesicular proteins are fused with the presynaptic membrane and block parts of the active zone. It thereby inhibits subsequent fusion events until the vesicular membrane proteins are cleared away endocytotically (Hosoi et al., 2009).

Similar to short-term facilitation, short-term depression seems to be regulated by calcium channel modulation as well. It has been shown that Ca^{2+}-influx can induce inactivation of

VDCCs. This is due to the fact that the control of Ca^{2+}-channels by calcium-sensing proteins (CaS), like calmodulin, calcium binding protein 1 (CaBP1) and neuronal calcium sensor 1 (NCS-1), modulates VDCCs in a bidirectional fashion (Catterall and Few, 2008). The particular activity pattern that induces Ca^{2+}-channels activation or inactivation varies between different types of synapses so that the contribution of Ca^{2+}-influx reduction depends on the experimental conditions (Fioravante and Regehr, 2011).

It is important to mention that both, mechanisms of facilitation and depression, exist in parallel and are not mutually exclusive. Their relative contribution depends on the previous activity pattern and the particular synapse.

1.3.3 Computational consequences of short-term plasticity

The aforementioned mechanisms demonstrate that short-term plasticity is a variable but tightly regulated process of synaptic transmission. It is therefore thought to represent an essential feature of neuronal computation. So far, short-term plasticity has been shown to be of functional importance in many processes like e.g. synaptic filtering. It describes the dependency of the strength of synaptic transmission on its frequency and is interpreted as a low-, band- or high-pass filter that shows high, moderate or low release probability characteristics accordingly. The importance of STP has further been demonstrated for burst detection, dynamic input compression and sensory adaptation (Abbott and Regehr, 2004).

Synapses from the same neuron can vary widely in their transmission properties and are differentially regulated dependent on their target neuron (Pelkey et al., 2006). They may even vary in synaptic properties when targeting the same postsynaptic cell (Sims and Hartell, 2005). Furthermore, if the synaptic connection consists of a single release site, then information transmission is a digital event that depends on the release probability of the synapse. Because the actual output (i.e. the pattern of synaptic transmission at individual synapses) of a cell varies profoundly from trial to trial compared to its firing pattern, the pattern of transmitting synapses might contain different information than the somatic activity. It is therefore conceivable to consider the synapse as the computational unit of information processing rather than the somatic action potential (Abbott and Regehr, 2004).

Although, the notion of synaptic transmission as a probabilistic process was known for quite some time (Fatt and Katz, 1952) it was proposed only recently that probabilistic representation and computation might be implemented in neuronal circuits as an intrinsic property of synaptic coding (Pouget et al., 2013).

1.4 Long-term synaptic plasticity

The discovery of LTP at the perforant path synapse of rabbits *in vivo* (Bliss and Gardner-Medwin, 1973; Bliss and Lomo, 1973) formed the experimental and cellular analog to the learning and memory theory of Donald Hebb (1949). Hebb proposed a coincidence-detection rule in which the simultaneous activity of two connected neurons would lead to the strengthening of this specific synaptic connection. The properties of NMDAR-dependent LTP (i.e. associativity, with the NMDAR functioning as molecular coincidence detector, input specificity and persistence over time) resemble those features formulated by Hebb.

In the following, further advances led to a set of more specific concepts. It could be shown that other features of synaptic plasticity, namely depression and facilitation underlie behavioral habituation and sensitization during reflex learning in *Aplysia californica* and that these changes are based on cAMP-dependent protein phosphorylation (Kandel and Schwartz, 1982). For vertebrates a neuronal model derived of how LTP could act on a cellular level to form memory traces representing information storage. It is based on the connections and functional properties of the hippocampus, a brain area known to be crucial for associative memory (McNaughton and Morris, 1987). These and other studies shared the idea that synaptic long-term plasticity forms the neuronal basis for learning and memory processes occurring at the behavioral level and was summarized as the synaptic plasticity memory hypothesis:

"Activity-dependent synaptic plasticity is induced at appropriate synapses during memory formation, and is both necessary and sufficient for the information storage underlying the type of memory mediated by the brain area in which that plasticity is observed" (Martin et al., 2000).

In order to be able to assess the validity of the synaptic plasticity memory hypothesis four criteria have been formulated: (1) The detectability of a change of synaptic efficacy (memory engram) congruent with a learning event. (2) The artificial induction or mimicry of a memory by changing the pattern of synaptic weight. The (3) anterograde and (4) retrograde alteration of learning and memory (i.e. the blockade of learning by preventing LTP (anterograde) or deletion of an existing memory (retrograde)). Although not all of the above mentioned criteria have been undoubtedly met, there is good evidence for every single one. For example detectability and mimicry have been shown by the identification of contextual memory engrams in the dentate gyrus and subsequent manipulation with optogenetics (Ramirez et al., 2013). Anterograde alteration has been shown by the *in vivo* application of the NMDAR antagonist AP-5, which leads to a selective impairment of learning (Morris et al., 1986)). Today, long-term plasticity is

considered to be a cellular substrate for learning and memory (Bliss and Collingridge, 1993; Martin et al., 2000; Ho et al., 2011; Nicoll and Roche, 2013).

On the cellular level long-term synaptic plasticity is an activity-depend change in the strength of transmission (Bliss and Lomo, 1973). Unlike short-term plasticity it can last for several minutes (>30 min), hours or even days and comprises depression as well as potentiation (Malenka and Bear, 2004). The most prominent and extensively studied form is the long-term potentiation at the Schaffer collateral-CA1 synapse. It could be shown that the activation of NMDARs is required for the induction of this form of LTP (Collingridge et al., 1983) and that postsynaptic AMPARs mediate the increase in synaptic strength (Nicoll and Malenka, 1995). The Ca^{2+}-influx through NMDARs activates CaMKII and finally leads to a translocation and increased number of AMPARs in the postsynaptic membrane (Malenka and Bear, 2004; Nicoll and Roche, 2013).

Besides the well described postsynaptic form of LTP long lasting alterations at the presynaptic site have been shown as well. Whether presynaptic long-term plasticity contributes to learning and memory is under debate. However, recent studies have shown that presynaptic plasticity may underlie behavioral adaptation *in vivo* (Powell et al., 2004; Blundell et al., 2010).

1.4.1 Presynaptic long-term plasticity

Activity induced long-term plasticity at the presynapse is expressed as an enduring increase (LTP) or decrease (LTD) in neurotransmitter release. Currently, presynaptic LTP and LTD has been described for many excitatory and inhibitory connections (Castillo, 2012). Several mechanisms of induction and expression have been discovered that differ from the initially described form of presynaptic plasticity present at mossy fiber – CA3 and PF – PC synapses. But also mechanistically similar forms were found in other brain regions, including subiculum (Wozny et al., 2008) and amygdala (Fourcaudot et al., 2008) (Figure 8).

As mentioned, the first description of a form of long-term potentiation that is independent of NMDARs was at the hippocampal mossy fiber-CA3 synapse and it could be shown that this form of LTP is fundamentally different from the earlier discovered ‘classical’ Schaffer collateral -CA1 LTP (Harris and Cotman, 1986).

Early studies already suggested that this form of LTP is of presynaptic origin because of a decrease in PPR, independency of postsynaptic intracellular calcium and the lack of cooperativity (Zalutsky and Nicoll, 1990; 1992). The presynaptic expression of mossy fiber LTP (mfLTP) could be demonstrated by imaging increased glia glutamate transporter currents due to an increase in synaptically released glutamate (Kawamura et al., 2004).

The question whether or not mfLTP is independent of postsynaptic Ca^{2+}-influx was under debate for some time with arguments for (Castillo et al., 1994; Weisskopf et al., 1994; Tong et al., 1996; Mellor and Nicoll, 2001) and against it (Williams and Johnston, 1989; Yeckel et al., 1999). An important study demonstrated that mfLTP is intact when synaptic transmission is transiently blocked during the induction phase. Furthermore, mfLTP can be induced without the specific contribution of L-type, N-type or P/Q-type channels showing that VDCC subtypes can compensate for each other but that presynaptic Ca^{2+}-influx is crucial for mfLTP induction (Castillo et al., 1994). In parallel it was established that forskolin (i.e. an activator of the adenylyl cyclase (Figure 8)) mimics mfLTP and occludes subsequent expression. Furthermore, it was confirmed that mfLTP is expressed through an enhancement of transmitter release (Weisskopf et al., 1994).

Despite earlier controversy, cumulative evidence gave rise to the proposal that Ca^{2+}-influx triggers a Ca^{2+}/calmodulin dependent activation of the adenylyl cyclase that transiently increases cAMP levels and PKA activity and finally leads to a persistent enhancement of evoked glutamate release (Figure 8).

Experiments in the cerebellum revealed that cAMP dependent LTP is not exclusively restricted to the mossy fiber synapse but also present at the PF – PC synapse (Salin et al., 1996). Analyses of parallel fiber long-term plasticity (pfLTP) led to a more detailed understanding of the mechanism. It could be shown that pfLTP is adenylyl cylase 1 and 8 (AC1, AC8) dependent

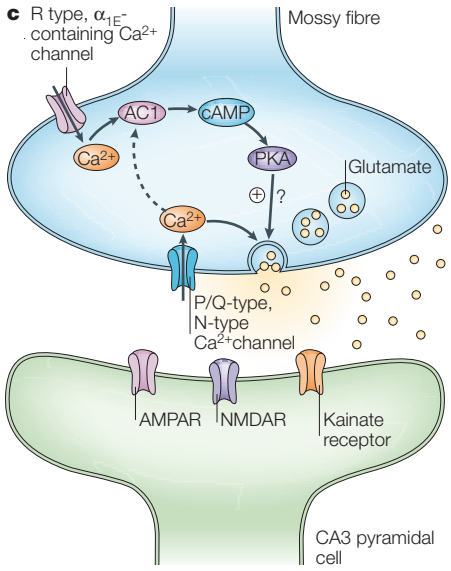

Figure 8: Prototypic signaling cascade in presynaptic long-term potentiaition. Example scheme is shown for the mossy fiber – CA3 synapse. AC - adenylyl cyclase, PKA - protein kinase A, cAMP - cyclic adenosine monophosphate, PKA – protein kinase A, AMPAR - α-amino-3-hydroxy-5-methyl-4-isoxazole propionic acid receptor, NMDAR – N-methyl-D-aspartate receptor. From Nicoll and Schmitz, 2005.

(Storm et al., 1998; Wang et al., 2003) and that presynaptic cAMP-PKA signaling but not postsynaptic PKA mediates potentiation (Linden and Ahn, 1999). As a result miniature EPSC frequency, release probability and multi vesicular release (MVR) is increased (Chen and Regehr, 1997; Bender et al., 2009).

For both synapses (mfLTP and pfLTP) it could be shown that the R-type VDCC is important for Ca^{2+}-influx triggering LTP. At mossy fiber terminals loss of R-type channels blocks LTP when induced with a mild stimulus protocol but can be rescued with stronger induction trains (Breustedt et al., 2003; Dietrich et al., 2003). At the PF – PC synapse R-type Ca^{2+}-channel antagonists block pfLTP completely (Myoga and Regehr, 2011). The current interpretation of these results is that at the mossy fiber synapse R-type channels contribute to a presynaptic [Ca^{2+}] increase and thereby shift the induction threshold to lower levels, whereas at the PF – PC synapse R-type channels seem to control LTP induction locally on a microdomain scale.

1.4.2 Expression of presynaptic long-term potentiation

There is wide agreement that an increase in release probability is causal for enhanced synaptic transmission and the expression of presynaptic LTP (Nicoll and Schmitz, 2005). Despite that consensus, there are still many open questions as to how the increase in neurotransmitter release is maintained on a molecular basis. A most critical element that remains to be determined in order to construct a coherent mechanistic description is the presynaptic substrate of the PKA.

An early study identified the vesicular GTP-binding protein Rab3A as an essential mediator of mfLTP. Genetic deletion of the protein led to a complete loss of LTP while short-term plasticity was unchanged (Castillo et al., 1997a). Because Rab3A contains no phosphorylation site the question of how it interacts with PKA arose. The Rab3-interacting molecule (RIM) was shown to be a crucial mediator in this process. RIM1α knockout mice displayed an altered short-term plasticity at the Schaffer collateral -CA1 synapse (Schoch et al., 2002) but impaired LTP at the mossy fiber-CA3 synapse (Castillo et al., 2002). Of note, in both studies, was the effect of forskolin that still elicited normal chemical LTP while tetanically evoked LTP was impaired. Detailed work in cerebellar cultured neurons could show that RIM1α is directly phosphorylated by PKA at serine 413 and thereby triggers pfLTP (Lonart et al., 2003). It was therefore thought that phosphorylation regulates release by altering protein-protein interaction between Rab3A and RIM1α. In the following, the findings of the experiments done in cultured neurons were tested under *in vivo* conditions. A knock-in mouse was generated with an amino acid exchange at serine 413 to alanine to prevent phosphorylation. Surprisingly, PKA-dependent presynaptic LTP

was completely normal in these mice (Kaeser et al., 2008a). The authors conclude that PKA targets other than RIM1α participate in the expression of LTP. The results have been confirmed by a second group that performed an acute rescue of RIM1α function by viral injection of RIM1α wildtype and RIM1α S413A constructs in RIM1α deficient mice (Yang and Calakos, 2010).

The latest target of cAMP-dependent PKA phosphorylation is synaptotagmin-12. It has been shown that the loss of the protein in KO mice leads to a reduced potentiation in mfLTP but not to changes in STP. Mice possessing a single amino acid exchange in synaptotagmin-12 that prevents phosphorylation at serine 97 (S97A) show reduced mfLTP as well and accordingly potentiation by FSK was also reduced in synaptotagmin-12 KO and S97A mice (Kaeser-Woo et al., 2013).

In conclusion, for mfLTP and pfLTP it has been convincingly shown that induction requires presynaptic Ca^{2+}-influx, preferentially through R-type VDCCs, the activation of adenylyl cyclases (AC1 and AC8) by Ca^{2+}/calmodulin and a subsequent rise in cAMP levels that activates PKA (Figure 8) (Nicoll and Schmitz, 2005). However, the precise downstream target of phosphorylation and the molecular mechanism that finally leads to an increased neurotransmitter release are still not fully understood yet. RIM1α and synaptotagmin-12 are potential candidates but their exact role in presynaptic long-term potentiation has to be further clarified.

1.5 Aims of this work

As outlined above synaptic transmission is a precisely regulated process but its strength is plastic and varies in an ever-changing manner dependent on neuronal activity and intrinsic synaptic properties (1.3, 1.4). Synaptic plasticity has been shown to be an imperative part of neuronal computation that affects behavior. In this work we focus on the presynaptic protein RIM1α, a protein that is part of the central protein complex of the active zone.

Based on its initial descriptions, RIM1α seemed to play a dichotomic role in synapse function: at connections where it mediates long-term plasticity it does not affect short-term plasticity, whereas at connections lacking presynaptic forms of long-term plasticity it alters short-term plasticity (Castillo et al., 2002; Schoch et al., 2002). Although it has been shown later at the cortico-amygdala synapse that both forms of plasticity can be affected by the loss of RIM1α (Fourcaudot et al., 2008) it remained puzzling how the functional specificity is realized at other connections.

Two recent studies in RIM1/2 double KO mice yielded a detailed description of the functional range of RIM proteins (Han et al., 2011; Kaeser et al., 2011). However, their role in long-term plasticity could not be tested in these studies. Therefore, important questions remain concerning the specific role of RIM1α:

- How does RIM1α affect short-term and long-term plasticity and is there a common mechanism?
- Is there a synapse specific function in short-term and long-term plasticity?
- Does the RIM1α isoform alone display the same complexity of interactions and functions as RIM1/2 proteins or does it serve a more specialized function?
- What is the role of RIM1α regarding voltage-dependent Ca^{2+}-channel trafficking and presynaptic Ca^{2+}-influx?
- What are the consequences of a lack of RIM1α for the induction and expression of presynaptic long-term potentiation?

To tackle these questions experimentally, we focused on the granule cell – Purkinje cell synapse because it offers the possibility to perform a detailed analysis of synaptic transmission by electrophysiological means and 2-photon laser scanning microscopy Ca^{2+}-measurements at single presynaptic boutons. Also, both forms of synaptic potentiation, short- and long-term, are robustly expressed at this synapse.

2 Methods and Materials

2.1 Animal handling and slice preparation

All experiments were carried out in accordance to local and national guidelines (Berlin state government, T0100/03).

For all experiment C57BL6/N or RIM1α KO mice and wild type littermates with C57BL6/N gentetic background of both sexes at the age of 3 – 6 weeks were used. The animals were anesthetized with isoflurane, either by applying it with a syringe or a tissue paper to the cage or an evaporator. Afterwards the animals were decapitated, the brain was quickly removed from the skull and cooled down in ice-cold preparation solution for 3 minutes.

For the preparation of sagittal cerebellar slices for Purkinje cell recordings a low [Ca^{2+}] ACSF was used (2.7). Prior to slicing a parasagittal cut was made through the right paravermis and the brain was glued onto the resulting plane. Vermal slices were cut with a Leica VT1200S microtome at 0.05 mm/s speed, 1.00 mm amplitude and 300 µm thicknesses. Most parts of the preparation as well as the cutting were performed submerged in ice-cold preparation solution. After slicing the tissue was stored in the above solutions for 30 min at 35°C. Subsequently, slices were stored in recording solution at room temperature and experiments were started after 30 min and no longer than 6 h. The procedure for horizontal slices was the same as for sagittal, except that a sucrose-based solution was used (2.7) and the brain was glued on the ventral side without prior cutting.

2.2 Cutting plane for cerebellar slices

Experiments were performed in either sagittal or horizontal slices (Figure 9). For electrophysiological recordings from Purkinje neurons, sagittal slices were chosen, because their large and plain dendritic tree in the sagittal plane it is best preserved in this cutting angle. Parallel fiber run orthogonally to the PC dendritic tree and are best preserved in horizontal slices. This plane was chosen for Ca^{2+}-imaging experiments and recording of the fiber volley.

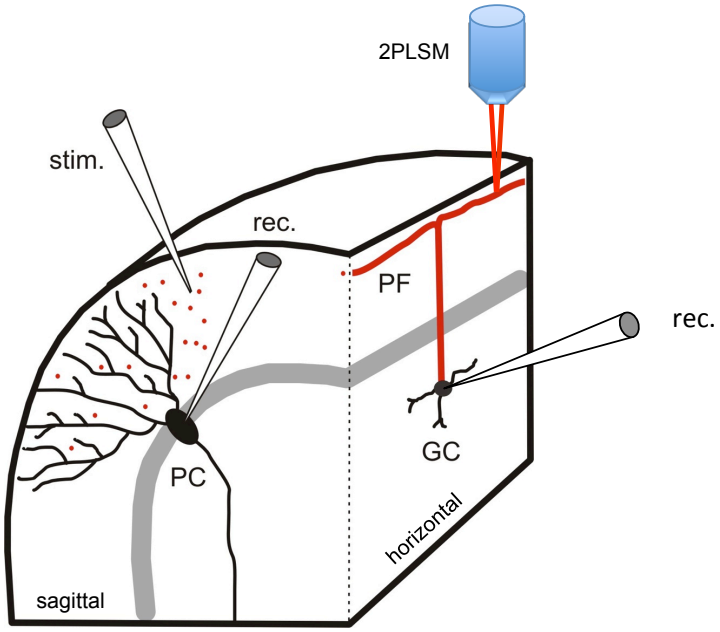

Figure 9: Scheme to illustrate the cutting planes for cerebellar slices. 2PLSM – 2-photon laser-scanning microscopy, stim. – stimulation electrode, rec. – recording electrode, PF – parallel fiber, PC – Purkinje cell and GC – granule cell. Shown are two experimental settings for both electrophysiological recordings (sagittal) and 2PLSM Ca^{2+}-imaging (horizontal). Not depicted are the settings for recording presynaptic fiber volleys.

2.3 Electrophysiology

Whole-cell recordings of Purkinje cells were done in sagittal slices with a MultiClamp 700B amplifier. Signals were filtered at 2 kHz and digitized (National Instruments, BNC-2090) at 5 kHz. Custom-made software in IGOR Pro was used for signal acquisition (WaveMetrics Inc., OR, USA). Experiments were performed in the presence of the $GABA_A$ receptor antagonist gabazine (1 μM) to block any contribution of fast inhibitory synaptic currents. For recordings, borosilicate glass electrodes (2-5 MΩ) were filled with a potassium-gluconate based intracellular solutions dependent on the celltype studied (2.7). Experiments were done in vermal slices between the lobules IV to VI. Purkinje cells could be easily identified by their large volume and their position between the granular cell layer and the molecular layer. After achieving the whole-cell patch clamp configuration, the membrane potential of the cell was determined and experiments were discarded if the membrane potential was less than -60 mV (without correction for liquid junction potential). Recordings were done in voltage clamp mode with a holding potential of – 60 mV. Series and input resistance (R_s, R_i) were constantly monitored by applying a 4 mV hyperpolarizing voltage step for 50 ms. Experiments were discarded if changes in the R_s were > 15%. No series resistance compensation was applied. Recordings were carried out at room temperature.

For extracellular fiber stimulation a low resistance patch pipette was filled with ACSF and placed in the molecular layer of the cerebellum, almost perpendicular to the Purkinje cell layer and the patched neuron close to the pia mater. Stimulation frequency was 0.05 Hz or is mentioned in the text if otherwise.

Chemical LTP was induced by applying forskolin at a concentration of 50 μM for 3 minutes. The tetanic induction protocol for LTP consisted either of a 8 Hz train applied once for 25 seconds or a 10 Hz train applied for 10 seconds.

Extracellular recordings of the fiber volley were done in horizontal slices to record from a large number of intact parallel fiber bundles. For recording a low resistance patch pipette was filled with recording ACSF and placed in the middle third of the molecular layer. The stimulation was placed at the same height as the recording electrode and approximately 400 μm apart.

Analysis of current and voltage traces was done offline after the experiment using the Igor plugin NeuroMatics.

2.3.1 Variance-mean analysis

The strength of synaptic transmission can be quantitatively described by the synaptic parameters: probability of release (P_r), quantal content (Q) and number of independent release sites (N) (del Castillo and Katz, 1954b). Thus, a signal that is recorded for several trials under stable conditions shows a certain fluctuation with a characteristic variance and mean amplitude dependent on the parameters. If recorded under several release probability conditions the variance-mean ratios can be plotted and utilized to calculate the synaptic parameters.

To construct the variance-mean plot EPSCs were recorded at five different release probabilities by altering Ca^{2+}/Mg^{2+} ratio. The reliability of this method critically depends on the number of events per epoch and stable recording conditions. Because non-physiological mechanisms can cause an overestimation of the variance precautions were taken (Clements and Silver, 2000). (1) For every condition epochs of at least 30 sweeps were chosen and (2) controlled by a Spearman rank correlation test to fit stability criterion. After subtraction of baseline noise variance a simple parabola (equation (1)) was fitted to the resulting variance-mean plot, which in all cases passed through a maximum. For fitting, the least squares (ordinary) fit was used (using GraphPad, Prism). Experiments were excluded if the goodness of fit was $R^2 < 0.7$. Weighted basal synaptic parameters (P_r, Q_{av}) were determined (Reid and Clements, 1999; Clements and Silver, 2000) according to the following equation:

$$y = A * \bar{x} - B * \bar{x}^2 \quad (1)$$

with

$$Q_{av} = A/(1 + CV^2) \quad (2)$$

and

$$P_r = \bar{x} * (B / A) * (1 + CV^2) \quad (3)$$

y = variance; $\bar{x}$ = mean amplitude; CV (Coefficient of variation of EPSCs at individual release sites) = 0.3;

The plot also allows for calculating the minimal number of independent release sites N_{min} with

$$N_{min} = 1/B \quad (4)$$

Because the number of release sites depends on the amount of activated fibers which is in turn set by the stimulation strength and position N reflects a primarily artificial measure and was therefore not analyzed.

2.4 Calcium imaging with two photon laser scanning microscopy (2PLSM)

Calcium dynamics are a key regulator of physiological processes in neurons, which vary widely across subcellular compartments. 2PLSM is ideally suited to measure the properties of calcium influx at single presynaptic boutons because of its high spatiotemporal resolution. Because of the nonlinearity of the 2-photon effect it also offers the possibility to record from structures deep in the tissue without causing significant photodamage like phototoxicity and photobleaching (Svoboda and Yasuda, 2006).

2-photon Ca^{2+}-imaging was done in horizontal cerebellar slices at physiological temperature (34°C). Granule cells were patched with thick-walled borosilicate glass electrodes (6-10 MΩ) filled with granule cell intracellular solution (2.7) which was complemented with 30 µM Alexa-594 for neuronal tracing and 200 µM Fluo-4FF as intracellular Ca^{2+}-indicator. Pairs of action potentials for opening of VDCCs were evoked through current injection (250-600 pA) for 1 ms with an inter-stimulus interval of 20 ms. Experiments were started after 20 min of loading the cell with Alexa-594 and Fluo4FF to ensure a proper diffusion of the dyes and stable concentrations at the site of interest (Brenowitz and Regehr, 2007). Fluometric Ca^{2+} measurements were performed with a two photon laser-scanning system (Femto2D; Femtonics, Hungary) equipped with a femtosecond laser tuned to 805 or 810 nm. Epifluorescence was collected with an Olympus LUMPlanFL N (60x/1.0 NA) water-immersion objective and for transfluorescence an Olympus oil-immersion condenser (1.4 NA) was used. Fluorescence was divided by a dichroic mirror at ~590-600 nm and green and red signal was filtered using 525/50 and 650/50 bandpass filters, respectively. A diagram of the light path is shown in Figure 10 (adapted from Chiovini et al., 2010). Measurement control, data acquisition, and analysis were performed using the Matlab-based MES program package (Femtonics). Line scans for fluometric measurements were done with 500 Hz. In order to calculate $\Delta[Ca^{2+}]$ from the corresponding G/R values, $(G/R)_{min}$ and $(G/R)_{max}$ was determined under conditions of 0 $[Ca^{2+}]$ and saturating $[Ca^{2+}]$ by adding 2 mM EGTA or 2 mM $CaCl_2$ to the pipette. $(G/R)_{max}$ values under physiological conditions were validated by application of a 500 Hz train of APs for 1 s at the end of some experiments and similar $(G/R)_{max}$ ratios could be obtained (Figure 20). The procedure was repeated for all calcium-indicator stocks and wavelengths used. Because the expected $[Ca^{2+}]$ was assumed to be in the linear regime of the Ca^{2+}-indicator ($[Ca^{2+}] << K_d$) it could be calculated according to the following equation with a $K_d = 8.1$ µM (Grynkiewicz et al., 1985; Yasuda et al., 2004) :

$$\frac{[Ca^{2+}]}{K_d} = \frac{\left(\frac{G}{R}\right) - \left(\frac{G}{R}\right)_{min}}{\left(\frac{G}{R}\right)_{max} - \left(\frac{G}{R}\right)_{min}} \qquad (5)$$

$[Ca^{2+}]$ = calcium concentration; $\left(\frac{G}{R}\right)$ = ratio of the intensities of the green and the red signal; K_d = dissociation constant;

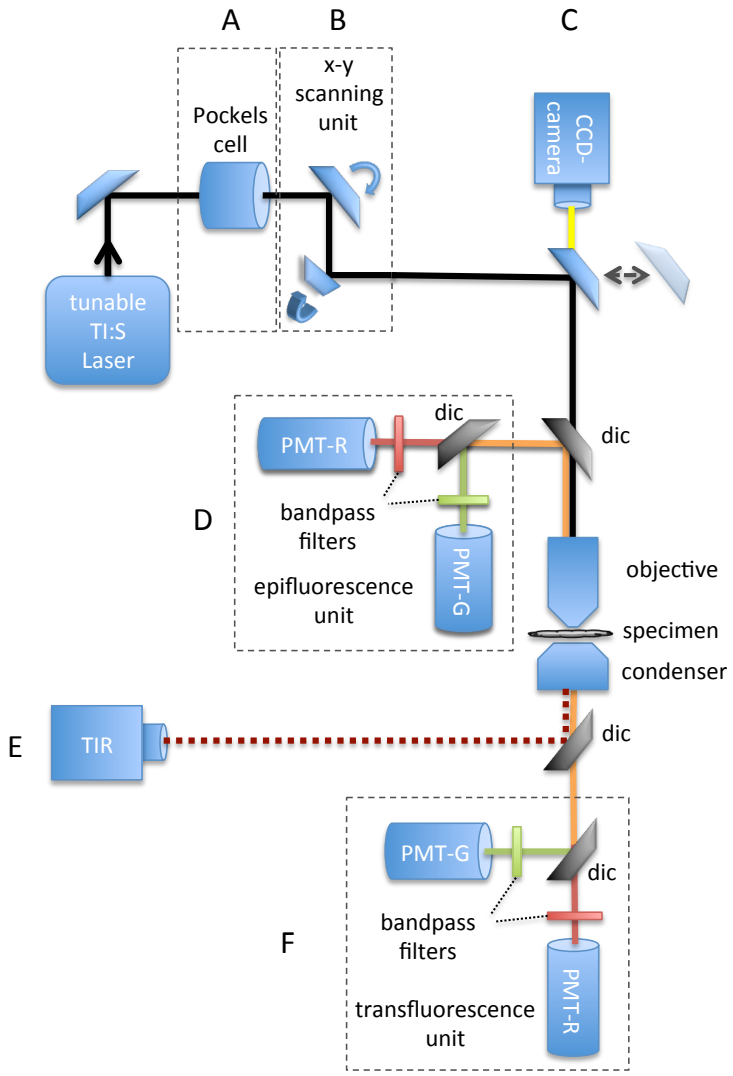

Figure 10: Light path of the two-photon laser scanning microscope. Lenses were left out for clarity; dic – dichroic mirror, TI:S laser – titanium-sapphire laser (A) Pockels cell for regulating laser intensity. (B) Scanning unit with two piezo driven scan mirrors. (C) CCD – charge-coupled device camera for working in light microscopy mode (light source left out). (D) Detection unit for the collection of epifluorescence emission (PMT - photomultiplier tube). (E) TIR – transmission infrared detector for microscopic images parallel to 2PLSM imaging. (F) Detection unit for the collection of transfluorescence emission.

2.5 Statistics

Statistical data analysis was performed using GraphPad Prism 5 (Graph Pad Software, La Jolla, USA). Results were considered significant if $p< 0.05$ (* , ** for $p< 0.01$ and *** for $p< 0.001$) using an unpaired t-test for two unmatched groups and paired t-test for two matched groups assuming Gaussian distribution. One-way ANOVA (Friedman test) was used for the comparison of more than two groups and the appropriate post-hoc test (Dunn's multiple comparison) according to non-Gaussian data distribution. All numerical values are given as mean ± SEM.

2.6 Technical Equipment

Preparation	
Microtome	VT1200S, Leica, Wetzlar, Germany
Glue	UHU dent Sekundenkleber, Germany
Electrophysiology	
Microscope	BX51WI, Olympus
Objectives	4x UPlanFL N, Olympus
	10 x UMPLFLN water immersion, Olympus
	60x LUMPLFLN water immersion, Olympus
Contrast microscopy	775 nm IR-DIC, WI-DICT-2 prism, Olympus
Camera	Olympus XM10
Shifting table	380 FM, Luigs & Neumann, Ratingen, Germany
Micromanipulators	Mini 25, Luigs & Neumann, Ratingen, Germany
Controller	SM 7/SM-5, Luigs & Neumann, Ratingen, Germany
Pulse generator	Master 9, A.M.P.I., Jerusalem, Israel
Stimulation unit	A.M.P.I. Iso Flex, Jerusalem, Israel
Amplifier	Multi Clamp 700B, Axon Instruments, Union City, CA, USA
A/D-Board	National Instruments BNC-2090A, Germany
Data acquisition	National Instruments PCI-6036I, Germany
Oscilloscope	Hameg HM507, Mainhausen, Germany
Manometer	Greisinger electronic GDH 12 AN, Germany
Perfusion pump	Gilson Minipulse 3, Middleton, USA
Glass pipettes	GC150F-10 (granule cells), GC150TF-10 (Purkinje cells), Harvard Apparatus, Kent, UK
Glass pipette puller	DMZ universal puller, Zeitz Instruments, Germany
Bath and pipette Ag/AgCl electrodes	Science Products, Hofheim, Germany

2-photon laser scanning microscopy (additional to electrophysiological equipment)

Microscope	Femto2D, Femtonics, Hungary based on BX61, Olympus
Laser	Ti:Sapphire Laser, Chameleon, Coherent
Water bath	JB Aqua 2 Plus, Grant, Shepreth, UK

Software

Optical acquisition BX51WI	CellSense Dimension, Olympus
Data acquisition	Igor Pro 6.2.1, Wavemetrics, Custom procedures
Data analysis	NeuroMatics software package with Igor Pro neuromatic.thinkrandom.com/
2PLSM control, acquisition, analysis	MES, Femtonics, Hungary
Data storage	Excel 2011 for Mac, Microsoft
Statistics	Prism 5, GraphPad, La Jolla, USA

2.7 Solutions and drugs

Extracellular solutions (ACSF – artificial cerebrospinal fluid)

Low Ca^{2+}-ACSF for preparation of sagittal slices for electrophysiology

119 mM	NaCl
26 mM	$NaHCO_3$
10 mM	glucose
2.5 mM	KCl
1.0 mM	NaH_2PO_4
0.5 mM	$CaCl_2$
1.3 mM	$MgCl_2$

Sucrose-based ACSF for preparation of horizontal slices for 2PLSM Ca^{2+}-imaging

87 mM	NaCl
26 mM	$NaHCO_3$
50 mM	sucrose
10 mM	glucose
2.5 mM	KCl
1.25 mM	NaH_2PO_4
0.5 mM	$CaCl_2$
3.0 mM	MgCl

Recording ACSF

119 mM	NaCl
26 mM	$NaHCO_3$
10 mM	glucose
2.5 mM	KCl
1 mM	NaH_2PO_4
2.5 mM	$CaCl_2$
1.3 mM	$MgCl_2$

All extracellular solutions were constantly oxygenated with 5 % O_2/ 95 % CO_2.

Intracellular solutions

Purkinje cells	Granule cells
135 mM K-Gluconate	114 mM $KMeSO_4$
20 mM KCl	10 mM HEPES
2.0 mM MgATP	4.0 mM MgATP
0.5 mM EGTA	0.4 mM NaGTP
5 mM phosphocreatine	14 mM phosphocreatin
10 mM HEPES	

All salts and compounds were purchased from Roth (Karlsruhe, Germany).
Intracellular solutions were adjusted to pH 7.2 – 7.4 with KOH and osmolarity was controlled to be 300 ± 10 mosm.

Drugs

Name	Chemical name	Biological activity
SR 95531 hydrobromide (Gabzine)	6-Imino-3-(4-methoxyphenyl)-1(6H)-pyridazinebutanoic acid hydrobromide	Selective $GABA_A$ receptor antagonist
γDGG	γ-D-glutamylglycine	Low affinity, competitive AMPA receptor antagonist
Forskolin	[3R-3α,4aβ,5β,6β,6aα,10α,10aβ,10bα)]-5-(Acetyloxy)-3-ethenyldodecahydro-6,10,10b-trihydroxy-3,4a,7,7,10a-pentamethyl-1H-naphtho[2,1-b]pyran-1-one	Adenylyl cyclase activator
NBQX	2,3-Dioxo-6-nitro-1,2,3,4-tetrahydrobenzo[f]quinoxaline-7- sulfonamide	Selective AMPA receptor antagonist

All drugs were purchased from Tocris/Biozol (Eching, Germany). Aliquots were made according to technical data sheets and stored at -20°C. (Chemical names according to tocris.com)

Dyes

Alexa-594	Alexa Fluor® Hydrazide, Sodium Salt
Fluo4FF	Fluo-4FF, Pentapotassium Salt

Dyes were ordered from Invitrogen/Life Technologies (Darmstadt, Germany). Aliquots of the dyes were stored at -20°C and used within one month.

3 Results

To study the role of RIM1α in synaptic transmission and its impact on short- and long-term plasticity as well as calcium influx at the presynaptic bouton we chose the granule cell – Purkinje cell synapse. The preparation is perfectly suited for a careful analysis of synapse function because of its good accessibility of the pre- and postsynaptic neuron. It enabled us to perform electrophysiological recordings and 2PLSM calcium imaging experiments in order to get a better understanding of presynapse physiology.

Electrophysiological experiments were done in order to probe properties of synaptic transmission at the PF – PC synapse. Synaptic transmission was triggered by extracellular stimulation of granule cell axons in the molecular layer and signals were recorded as EPSCs in Purkinje cells or extracellularly as field potentials (2.3, 3.1, 3.2 and 3.4).

To probe Ca^{2+}-transients in ascending axon and parallel fiber boutons granule cells were patched and filled with a Ca^{2+}-indicator as mentioned before (2.4). AP induced Ca^{2+}-influx was monitored as fluorescence intensity changes with a 2-photon laser-scanning microscope (3.3).

3.1 Short-term plasticity

In a first set of experiments we chose to investigate the short-term plasticity of RIM1α KO mice and wildtype littermates. We therefore applied a paired-pulse protocol in which two stimulation pulses are applied with several distinct inter-stimulus intervals (ISIs) (Figure 11). Paired-pulse ratios were analyzed as the response size of the second pulse relative to the first one for an ISI of 50, 71, 100 and 125 ms in wt and KO. We found a significant enhancement of the paired-pulse ratio in RIM1α deletion mice for the ISIs 50 ms and 71 ms (Figure 11B, PPR for 50 ms ISI, WT: 1.76 ± 0.05, n =14 cells, 4 mice vs. KO 1.92 ± 0.05, n = 16 cells; 6 mice; p = 0.036; 71 ms ISI, WT: 1.63 ± 0.04, n = 10 cells, 4 mice vs. KO 1.80 ± 0.06, n = 12 cells, 3 mice; p = 0.033; 100 ms ISI, WT: 1.52 ± 0.04, n = 11, 6 mice vs. KO 1.61 ± 0.08, n = 11 cells, 4 mice, p = 0.291; 125 ms ISI, WT: 1.60 ± 0.08, 11 cells, 5 mice vs. KO 1.65 ± 0.054, 13 cells, 5 mice, p = 0.542; unpaired Student's t-test).

The differences in PPR hint to alterations in short-term plasticity in RIM1α KO animals. However, genotypic differences are only significant for shorter paired-pulse intervals whereas longer ISIs did not lead to significantly different PPRs. In order to receive a more robust readout of STP we applied a second stimulation protocol. In previous studies describing the function of RIM1α in the hippocampal CA1 region it has been shown that changes in the short-term behavior are more pronounced in response to a train of stimuli (Schoch et al., 2002). We therefore applied the same protocol consisting of 25 pulses delivered at 14 Hz (Figure 12).

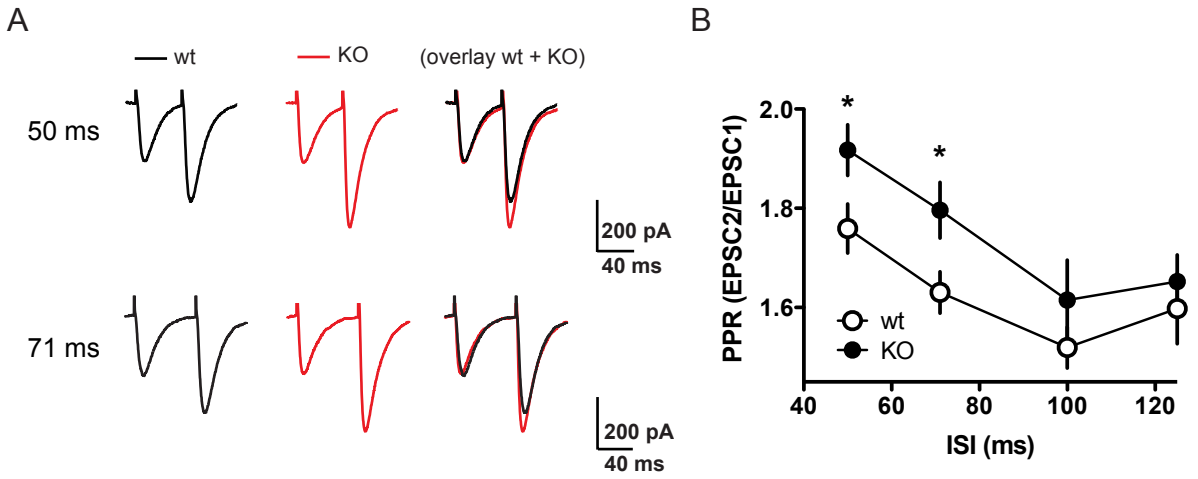

Figure 11: Paired-pulse ratio is enhanced in RIM1α KO mice. (A) Representative traces are shown for an ISI of 50 ms (top) and 71 ms (bottom). Wildtype traces are shown in black and knockout in red. (B) Summary graph for all ISIs, wildtype (open circles) and knockout (filled circles); * indicates $P < 0.05$, Student's t-test; ISI – inter-stimulus interval, PPR – paired-pulse ratio, EPSC – excitatory postsynaptic current.

When normalized to the first amplitude of the train we saw a constantly greater facilitation in the knockout mice during the complete time course of the train (Figure 12A-C). A statistical comparison of the average of the last five pulses revealed a significant difference in the potentiation of RIM1α KO mice (Figure 12D; WT: 1.4 ± 0.09, n = 10 cells, 4 mice vs. KO: 1.9 ± 0.1, n = 11 cells, 3 mice; p = 0.002).

Taken together the results of the paired-pulse experiments and train stimulation indicate differences in short-term plasticity. Among the factors influencing short-term plasticity many reside in the presynaptic element, such as Ca^{2+}-influx and buffering, or defects in the release machinery and other proteins of the active zone respectively (1.3) (Zucker and Regehr, 2002).

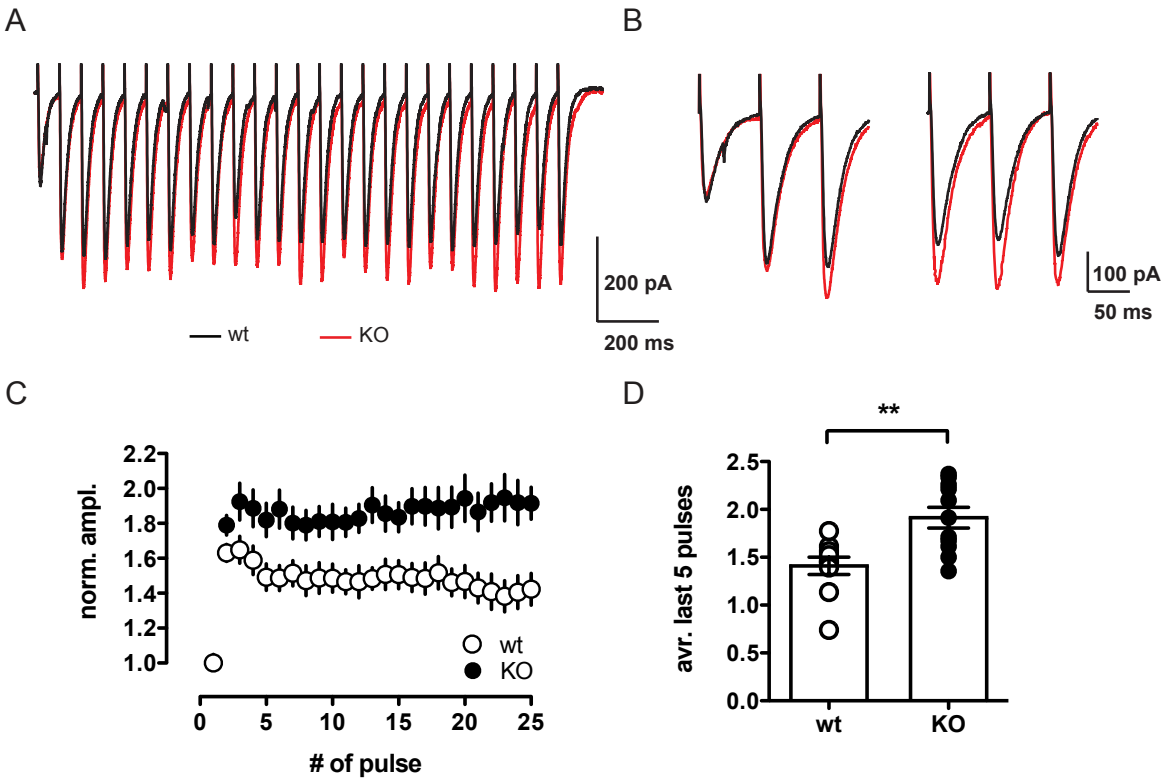

Figure 12: 14 Hz train shows enhanced potentiation in RIM1α deletion mice. (A) 14 Hz train was applied for 25 pulses. Example traces are shown for the whole train (A) and a magnification of the first and last 3 pulses of the train on an expanded time scale (B). Wildtype traces are shown in black and knockout in red. (C) Summary plot for wildtype (open circles) and knockout (filled circles). Data are normalized to the amplitude of the first pulse each. (D) Quantification of the last five pulse for wildtype and knockout shown as bar graph; open and closed circles represent single experiments for wildtype and knockout, respectively; ** indicates $P < 0.01$, Student's t-test.

3.2 Release probability

Next we wanted to test if changes in release probability underlie the increased short-term plasticity in RIM1α KO mice or if also postsynaptic mechanisms play an additional role. For the Schaffer collateral – CA1 synapse it has already been shown that RIM1α is essential for maintaining a normal probability of neurotransmitter release (Schoch et al., 2002) but STP at the PF – PC synapse has been reported to remain unchanged (Castillo et al., 2002). To further investigate this we performed additional sets of experiments to probe basic properties of synaptic transmission.

3.2.1 γDGG

In a first series we used the low affinity, competitive AMPAR antagonist γDGG. Its impact on synaptic transmission depends on the concentration of glutamate in the synaptic cleft (Clements et al., 1992). High glutamate concentrations are more efficient in displacing γDGG from a receptor, whereas low glutamate concentrations lead to a higher number of receptors being occupied by γDGG. The reduction of the amplitude by γDGG is thus inversely proportional to the amount of glutamate in the synaptic cleft. The latter also reflects the amount of released vesicles and is therefore sensitive to P_r and can be used to compare relative release probabilities between genotypes.

To control if the impact of γDGG depends on the glutamate concentration under our experimental conditions, we compared its impact with NBQX, a competitive and high affinity AMPAR antagonist, on paired-pulse stimulation. At the cerebellar parallel fiber synapse the release probability and thereby the glutamate release is enhanced on the second pulse (Atluri and Regehr, 1996). Consequently, the reduction by γDGG should be more efficient on the first pulse than on the second whereas NBQX should have the same impact on both pulses.

To test this, we recorded synaptic transmission with a paired-pulse protocol (ISI 50 ms) for 10 minutes each under conditions of normal recording solution (control), supplemented with 1 mM γDGG, washout with recording solution (wash) and 200 nM NBQX (Figure 13). The concentrations of the antagonists where chosen to reduce synaptic transmission approximately to the same amount. By analyzing the PPR we could detect a significant increase for 1 mM γDGG, which was not the case with 200 nM NBQX (Figure 13C, PPR: control 1.95 ± 0.10, γDGG 2.74 ± 0.13, wash 2.07 ± 0.06, NBQX 2.24 ± 0.09; control vs. γDGG; $p < 0.001$, wash

vs. NBQX $p > 0.05$, Friedman test with Dunn's multiple comparison test, $n = 5$). As expected, the experiment demonstrates that γDGG and NBQX have a differential impact on synaptic transmission at the PF – PC synapse and that reduction by γDGG seems to be sensitive to the glutamate concentration in the synaptic cleft.

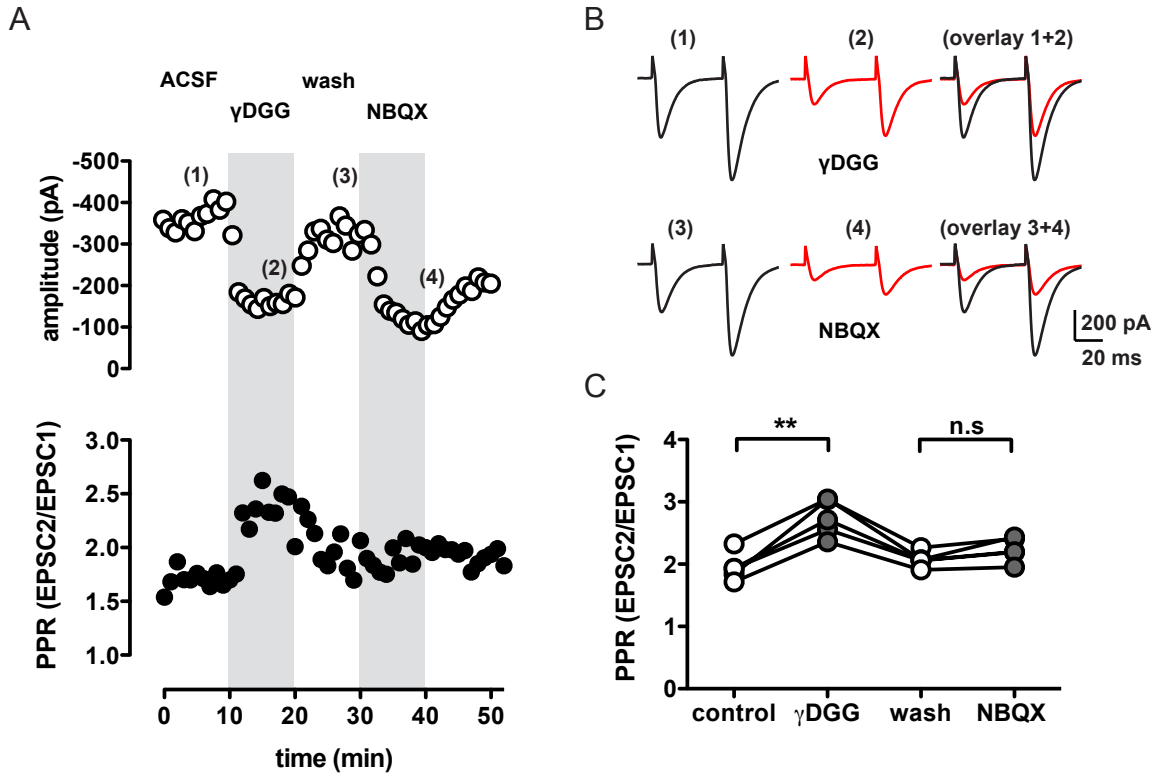

Figure 13: Differential effect of γDGG on PPR. Recordings were performed in the same cell each. (A) Top, time course of the amplitude and (bottom) paired-pulse ratio is plotted. Wash-in epochs of γDGG (1 mM) and NBQX (200 nM) are marked in grey. (B) Example traces are shown for γDGG (top) and NBQX (bottom) together with the respective previous baseline. (C) Summary plot of PPRs under each condition ** indicates $P < 0.01$ and n.s. not significant, Friedman test with Dunn's multiple comparison test. PPR – paired-pulse ratio, EPSC – excitatory postsynaptic current.

With respect to the univesicular release hypothesis, there are two likely mechanisms, amongst others, by which glutamate concentrations in the synaptic cleft are increased: (1) multi-vesicular release (MVR) and (2) glutamate polling and spillover from neighboring synapses (Carter and Regehr, 2000). The latter case is less likely to occur because the granule cell – PC synapse is to a great extend isolated from its neighboring synapses by glia enscheatment and virtually all synapses consist of only one release site (for more details see Xu-Friedman et al., 2001).

To test if MVR does occur in our preparation, we repeated the experiments under conditions that promote univesicular release. To this end the same concentration of γDGG is applied but extracellular [Ca^{2+}] is reduced to 1 mM to substantially lower release probability (Figure 14). Again, the PPR was used to monitor possible differential changes of the first and second amplitude. No difference could be detected in the PPR when comparing epochs before and after antagonist application (Figure 14, PPR: control 2.36 ± 0.07 vs. γDGG 2.16 ± 0.36, n= 5, p = 0.60, paired student's t-test). Taken together the results corroborate the assumption that in recording conditions with 2.5 mM extracellular [Ca^{2+}] MVR does indeed occur. Because changes in the glutamate concentration hence depend on the release probability, γDGG is a useful tool to test for differences in release probability.

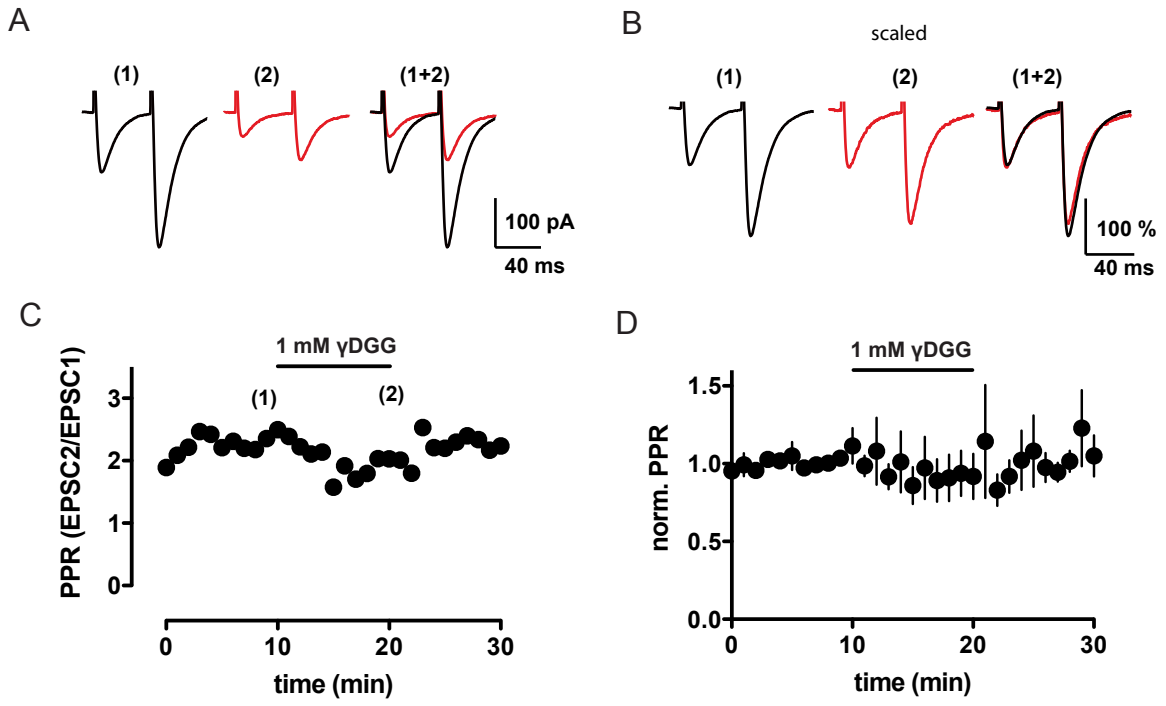

Figure 14: No changes in PPR after application of γDGG under univesicular release conditions. Recordings were done under low release probability conditions in 1mM extracellular calcium. (A) Paired-pulses were applied with an inter-stimulus interval (ISI) of 50 ms. Overlay of representative traces (1+2) is scaled to the first amplitude (100%). (B) Time course of the PPR of a single experiment. 1mM γDGG was applied after 10 min for 10 min. (C) Summary graph (n=5). Data are normalized to 10 min baseline. PPR – paired-pulse ratio, EPSC – excitatory postsynaptic current.

Knowing that the reduction by γDGG is sensitive to release probability changes we started to compare the impact of 1 mM γDGG on paired-pulse stimulation between RIM1α wildtype mice and knockout littermates (Figure 15). Similar to the experiments in Figure 13, baseline

transmission was recorded in 2.5 mM Ca^{2+} and 1mM γDGG was applied for 10 minutes. For the analysis, the reduction of the amplitude of the first and second pulse (EPSC1 and EPSC2) was calculated relative to the baseline amplitude. Indeed we found a stronger reduction in KO animals when compared to WT (Figure 15C, EPSC1 WT: 0.45 ± 0.02 vs. KO: 0.38 ± 002, p = 0.008 and EPSC2 WT: 0.59 ± 0.03 vs. KO: 0.46 ±0.021; p = 0.003, student's t-test, n = 7 cells and 3 mice each; parts of the results for WT are also shown in Figure 13). The results support the assumption that a loss of RIM1α changes short-term plasticity by reducing release probability. As a consequence the glutamate transient in the synaptic cleft is reduced. This is reflected by the reduced removal of γDGG from the AMPA receptors indicated by the stronger reduction of the EPSC amplitude in presence of the antagonist.

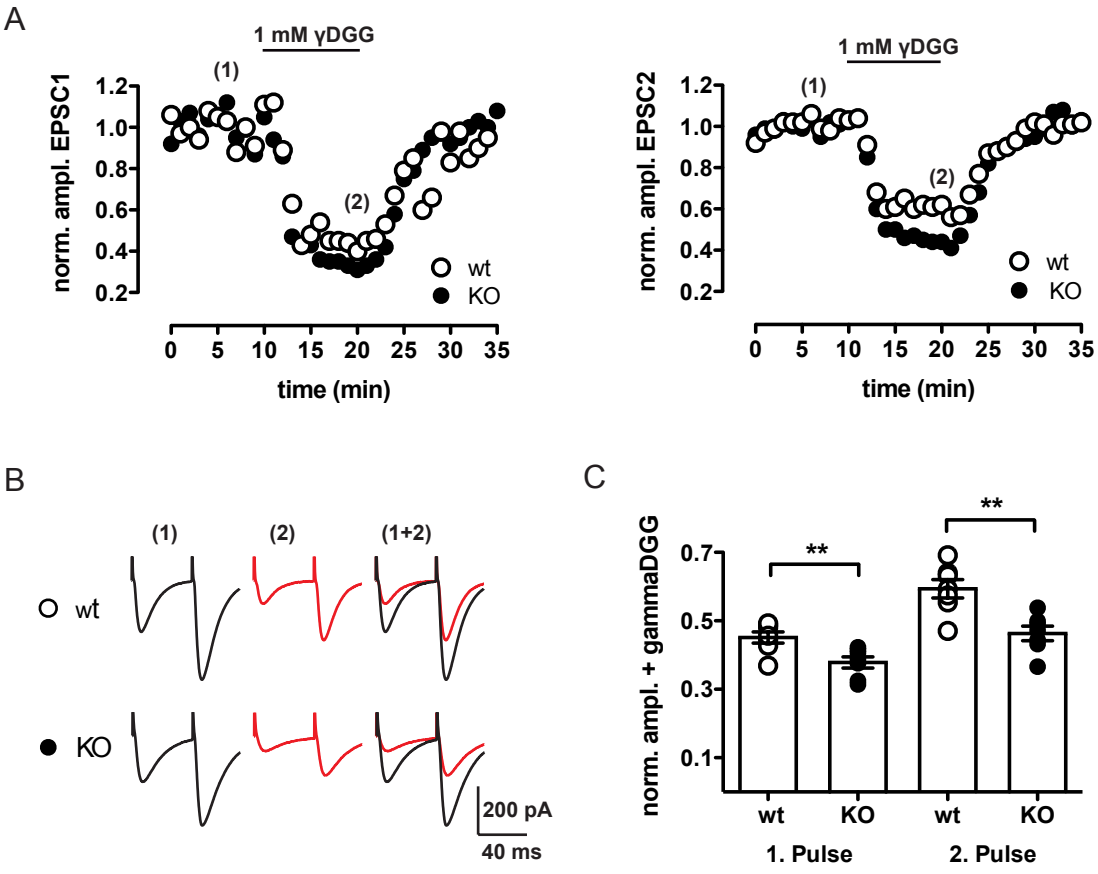

Figure 15: Decreased synaptic glutamate transients in RIM1α KO. 1mM γDGG was applied for 10 min in order to receive relative estimates of the glutamate transient in the synaptic cleft. (A) Normalized amplitude is plotted over time for the first (left) and second (right) pulse of a 50 ms paired-pulse. Data points shown are binned to 1 min. (B) Example current traces for both genotypes taken at the time points indicated. (C) Summary bar graph for all experiments for the fist and second pulse. Data points represent the average of the last 3 min before washout of γDGG; ** indicates P < 0.01, Student's t-test.

Interestingly, differences in γDGG sensitivity between the two genotypes already became apparent on the first pulse. This can be taken as evidence that MVR is already present under baseline conditions without potentiation by short-interval stimulation (4.2).

The action of γDGG and other fast dissociating antagonists relies on their low affinity and rapid kinetics which enable them to compete with glutamate for the receptor binding sites (Clements et al., 1992). It thereby relieves postsynaptic receptors at least partially from saturation (Foster et al., 2005). We made use of these qualities to test the extent to which AMPA receptor saturation contributes to changes in short-term plasticity in our conditions and thereby possibly affects our experimental interpretation .

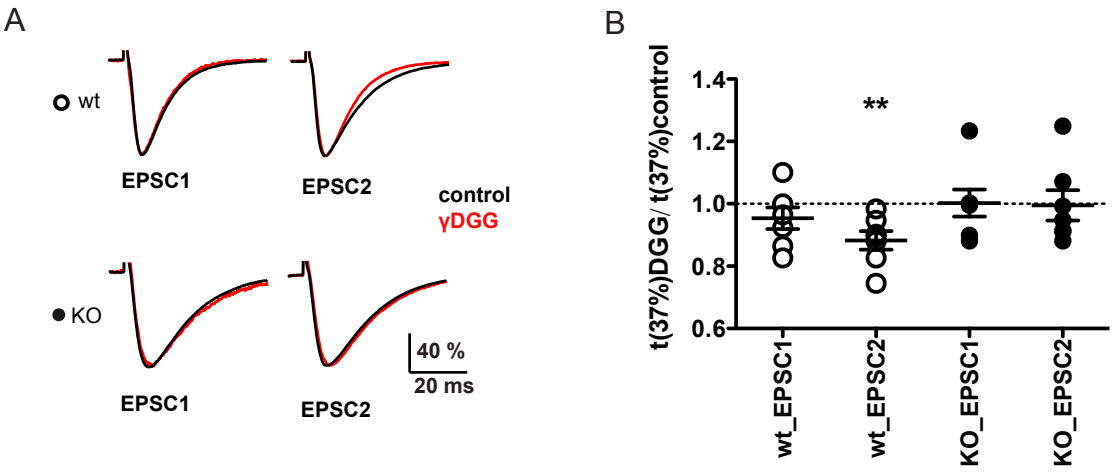

Figure 16: Analysis of decay time reveals slight receptor saturation in wt mice. Decay time at 37 % of the peak amplitude of a paired-pulse stimulation was determined under control conditions in 2.5 mM extracellular calcium and after application of 1mM γDGG. (A) Example traces are scaled to the peak amplitude (100 %) before drug application, respectively. (B) Summary plot; data are shown as ratio of t(γDGG)/t(control). A value < 1 indicates a fastening of the decay and therefore hints at receptor saturation; ** indicates P < 0.01, one-sample t-test; EPSC – excitatory postsynaptic current.

The dataset shown in Figure 15 was re-analyzed in regards to the EPSC decay times (Figure 16). In normal conditions, receptor saturation prolongs the decay time of the amplitude (Clements et al., 1992) whereas in the presence of γDGG saturation is reduced and the decay time thus faster (Foster et al., 2005). By comparing both conditions, one can get an estimate of the extent of receptor saturation. However, caution is warranted because decay times also depend on rise times, which can be affected by the position of the stimulation electrode and by the number of activated fibers. For that reason and to make data comparable between slices

and genotypes we decided to plot them as the ratio of the decay time after and before application of γDGG for each experiment. A value < 1 indicates fastening of the decay in the presents of γDGG. We could detect significant changes in the decay time under γDGG at the second EPSC in wild type mice whereas the first EPSC and both EPSCs in the KO were unaltered (Figure 16B): (time(37%)γDGG / time(37%)control WT: EPSC1 = 0.95 ± 0.03, p = 0.23, EPSC2 = 0.88 ±0.03, p = 0.008; KO: EPSC1 = 1.00 ± 0.04, p = 0.96, EPSC2 = 1.00 ± 0.05, p = 0.92; one-sample t-test). The data hint at moderate receptor saturation on the second pulse in WT mice under normal recording conditions. To which extent saturation alters short-term plasticity at this synapse is unclear but it has been shown that it contributes only partially to a decrease in facilitation (Foster et al., 2005). The differences in receptor saturation between RIM1α wildtype and KO animals are in line with our previous results that P_r might be reduced (4.2).

3.2.2 Variance-mean Analysis

An additional independent set of experiments was performed to further characterize the apparent defect in release probability in RIM1α KO mice by means of a variance-mean analysis. To this end, synaptic transmission was recorded under conditions of varying release probabilities. Experimentally, this can be achieved by altering the Ca^{2+}/Mg^{2+} ratio in the extracellular solution. More precisely, for every $[Ca^{2+}]$ alteration, the overall concentration of divalent ions is being kept constant by altering the Mg^{2+} concentration accordingly.

However, fiber excitability may be altered in response to changes in the composition of divalent ions. It is thus an important parameter to be controlled for, because the number of activated release sites directly depends on the number of activated fibers and their excitability (Sabatini and Regehr, 1997). To ensure that only the release probability and not the fiber excitability is affected by changed Ca^{2+}/Mg^{2+} ratios, we analyzed the extracellular presynaptic volley amplitude as a measure of the number of activated fibers (Figure 17). The experiment was performed in horizontal cerebellar slices to record from a large number of fibers simultaneously (1.1) and showed no significant alterations between conditions (Figure 17C: p = 0.85, one-way repeated measure ANOVA).

Next, synaptic transmission was recorded under conditions of (in mM) 1, 2.5, 3.5, 4.5 and 5.5 Ca^{2+} (Figure 18). A single stimulus was delivered every 10 seconds and the resulting EPSC

was recorded for several minutes and under each calcium condition when synaptic transmission was constant after altering the Ca^{2+}/Mg^{2+} ratio.

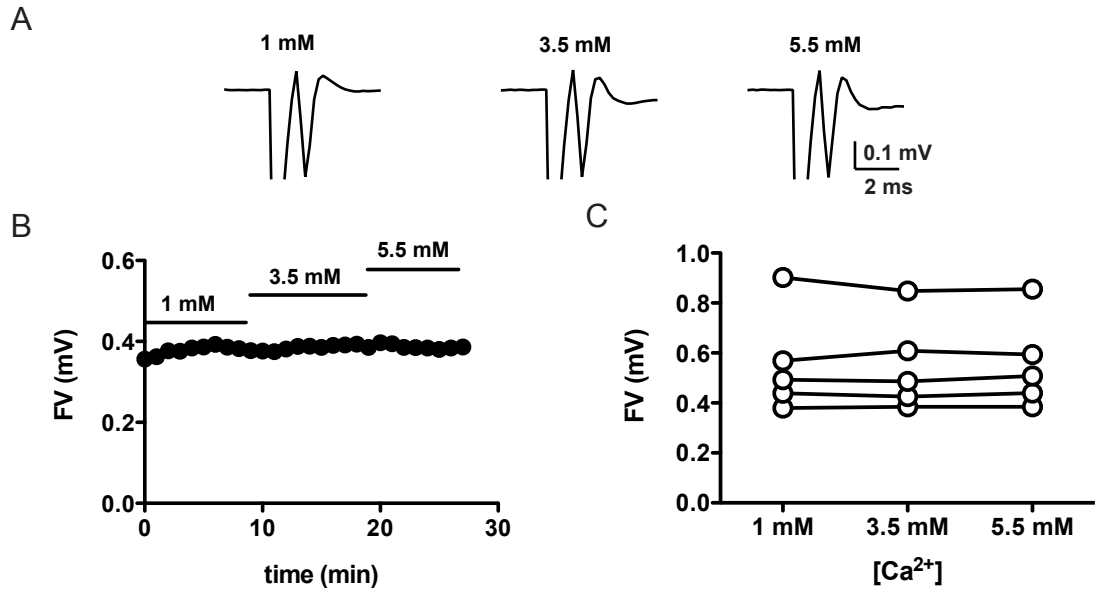

Figure 17: Number of stimulated fibers is not affected by changes of extracellular calcium concentration. [Ca^{2+}] was increased from 1 mM to 3.5 mM and 5.5 mM whereas the overall concentration of divalent cations was kept constant by adjusting [Mg^{2+}] accordingly. (A) Example traces of the fiber volley at different [Ca^{2+}]. (B) Representative experiment. Black bars indicate the respective [Ca^{2+}] in mM. (C) Summary graph (n=5). FV – fiber volley.

Stable epochs were identified after the experiment in an offline analysis according to described methods (2.3.1). Variance-mean plots were constructed from the resulting data, fitted with a parabola function (2.3.1 – Equation 1) and functional synaptic parameters were calculated according to described methods (2.3.1 – Equation 2 and 3). The statistical analysis revealed significant differences of the release probability in the moderate calcium range (Figure 18D, 2.5 mM Ca^{2+} Pr WT: 0.28 ± 0.03, n = 5 cells/4 mice vs. KO 0.14 ± 0.03, n = 5 cells/3 mice; p = 0.009 and 4.5 mM Ca^{2+} WT: 0.66 ± 0.04 vs. KO 0.45 ± 0.05; p = 0.011, student's t-test) whereas at the minimum (1 mM) and maximum end (5.5 mM) of concentrations tested no difference in release probability could be detected between the two genotypes (Figure 18D, 5.5 mM Ca^{2+}, Pr WT: 0.84 ± 0.05 vs. KO 0.77 ± 0.05; p = 0.36, student's t-test). The calculation of the quantal content (Q) yielded no differences between in WT and RIM1α KO mice (Figure 18E, Q_{av} WT: 3.5 ± 0.16 pA vs. KO: 3.9 ± 0.36 pA).

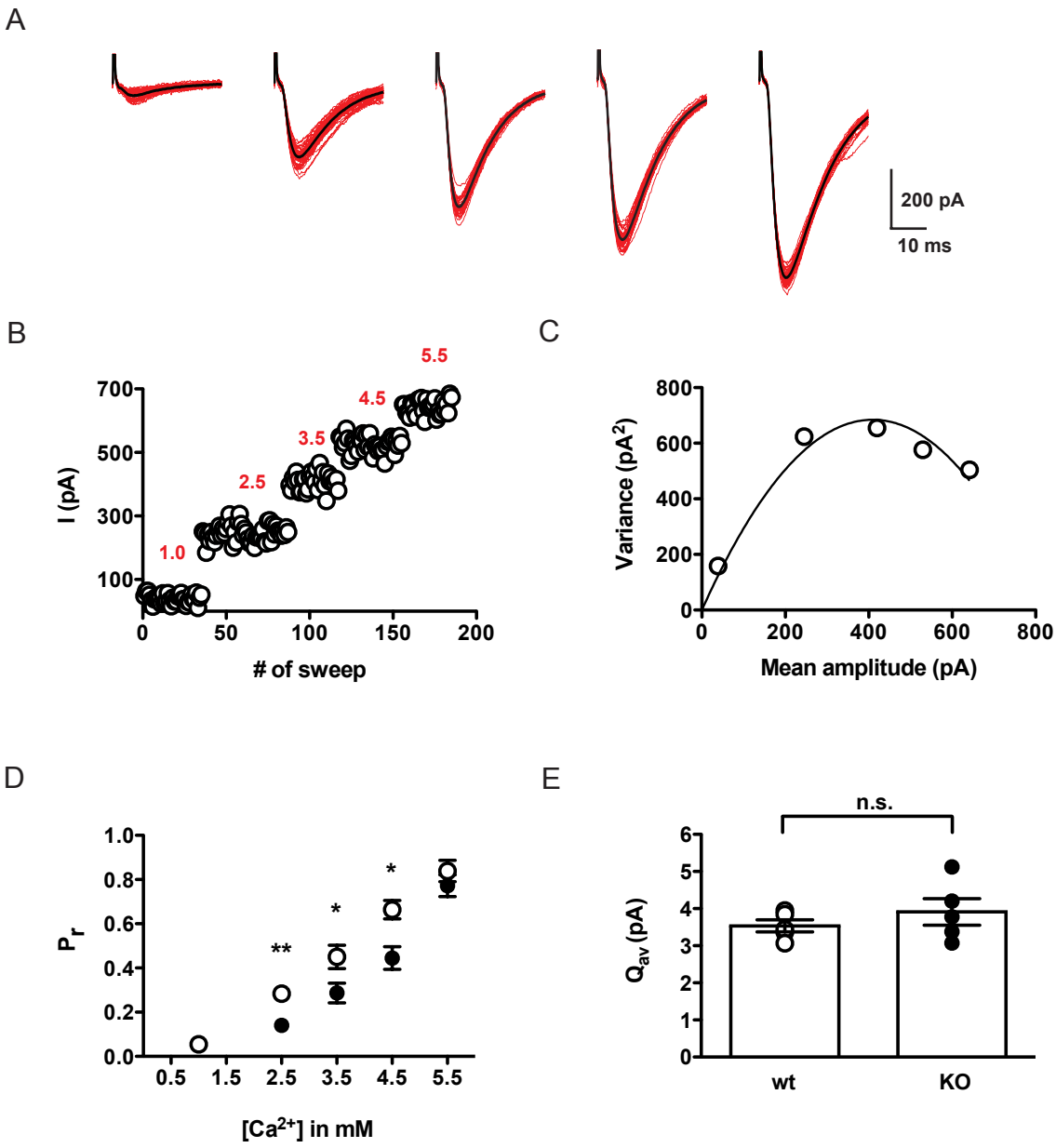

Figure 18: Reduced release probability in the absence of RIM1α. Variance-mean analysis was performed to quantify differences in the functional synaptic properties of the granule cell – Purkinje cell synapse. (A-C) Representative example from a wildtype slice. (A) EPSCs were recorded under several different release probability conditions by altering Ca^{2+} to Mg^{2+} ratio. Single traces (red) and average (black) are shown for (from left to right in mM) 1.0, 2.5, 3.5, 4.5 and 5.5 extracellular $[Ca^{2+}]$. (B) Plot of the analyzed epochs. Red numbers indicate corresponding $[Ca^{2+}]$ in mM. The non-analyzed intervals of the wash-in are left out for clarity. (C) Resulting variance-mean plot with respective data points (circles) and fitted parabola (black line). Based on these curves the release probability (P_r) (D) and averaged quantal content (Q_{av}) (E) was calculated for wild type (open circles) and RIM1α KO (filled circles); ** indicates $P < 0.01$ and n.s. not significant, Student's t-test.

The results represent a second set of evidence that the alteration in short-term plasticity can be attributed to a release defect in RIM1α KO mice, namely a reduced release probability. The fact that no difference in P_r is discernable at higher [Ca^{2+}] of 5.5 mM indicates that the reduction of this parameter can be overcome by increasing extracellular calcium.

3.3 Calcium imaging

Defects in neurotransmitter release can be caused by changes in the release machinery and/or alterations in VDCC function or number. It has been shown in hippocampal cell cultures and at the calyx of held that a loss of all RIM 1 and 2 isoforms leads to a reduced calcium current density and a smaller readily releasable pool due to inefficient priming (Han et al., 2011; Kaeser et al., 2011). In addition, increased extracellular [Ca^{2+}] seems to ameliorate release defects in RIM1α KO mice (3.2.2). An interesting question is whether RIM1α alone is capable of altering VDCC function or number. To elucidate the mechanism by which a single isoform, RIM1α, reduces release probability we investigated Ca^{2+}-influx in granule cell boutons.

Cerebellar granule cells were patched and filled with Alexa 594, for tracing the neuronal structure, and Fluo-4ff, a low affinity Ca^{2+}-indicator, to monitor Ca^{2+}-influx. By using both a Ca^{2+}-insensitive dye and a Ca^{2+}-indicator, data can be expressed as ΔG/R (2.4) and is therefore more stable because it is less sensitive to fluctuations in resting [Ca^{2+}]. The choice of the Ca^{2+}-indicator is critical and depends on the expected [Ca^{2+}] to be measured. On one hand its affinity has to be high enough to achieve a sufficient signal-to-noise ratio, on the other hand it is necessary to work in the linear regime of the dynamic range of the Ca^{2+}-indicator (Yasuda et al., 2004). The experiments were done in horizontal slices to preserve the axonal structure of the granule cells (2.2) and under the control of a 2-photon laser-scanning microscope (2.4) to achieve a sufficient spatiotemporal resolution and optical penetration depth (Figure 19). Within 20 minutes at most the axon became visible and could be trace to undoubtedly identify its structure with the ascending part and the two bifurcating parallel fiber segments (Figure 19A). With higher magnification faint swellings along the axon could be identified as putative ‘en passant’ boutons (Figure 19B, upper panel) (Pichitpornchai et al., 1994).

To probe these structures, two action potentials were elicited by suprathreshold current injection at the soma of the granule cell. In parallel, the intensity of the red and green channel was monitored by line-scanning the respective bouton (Figure 19B and C). An intensity increase in the green channel could be detected time-locked to the action potentials whereas the intensity of the red channel stayed unchanged. Hence, the identified boutons represent putative release sites of the axon (Brenowitz and Regehr, 2007) and the chosen calcium indicator is suitable to resolve single action potential triggered Ca^{2+}-influx with a sufficient signal-to-noise ratio (SNR).

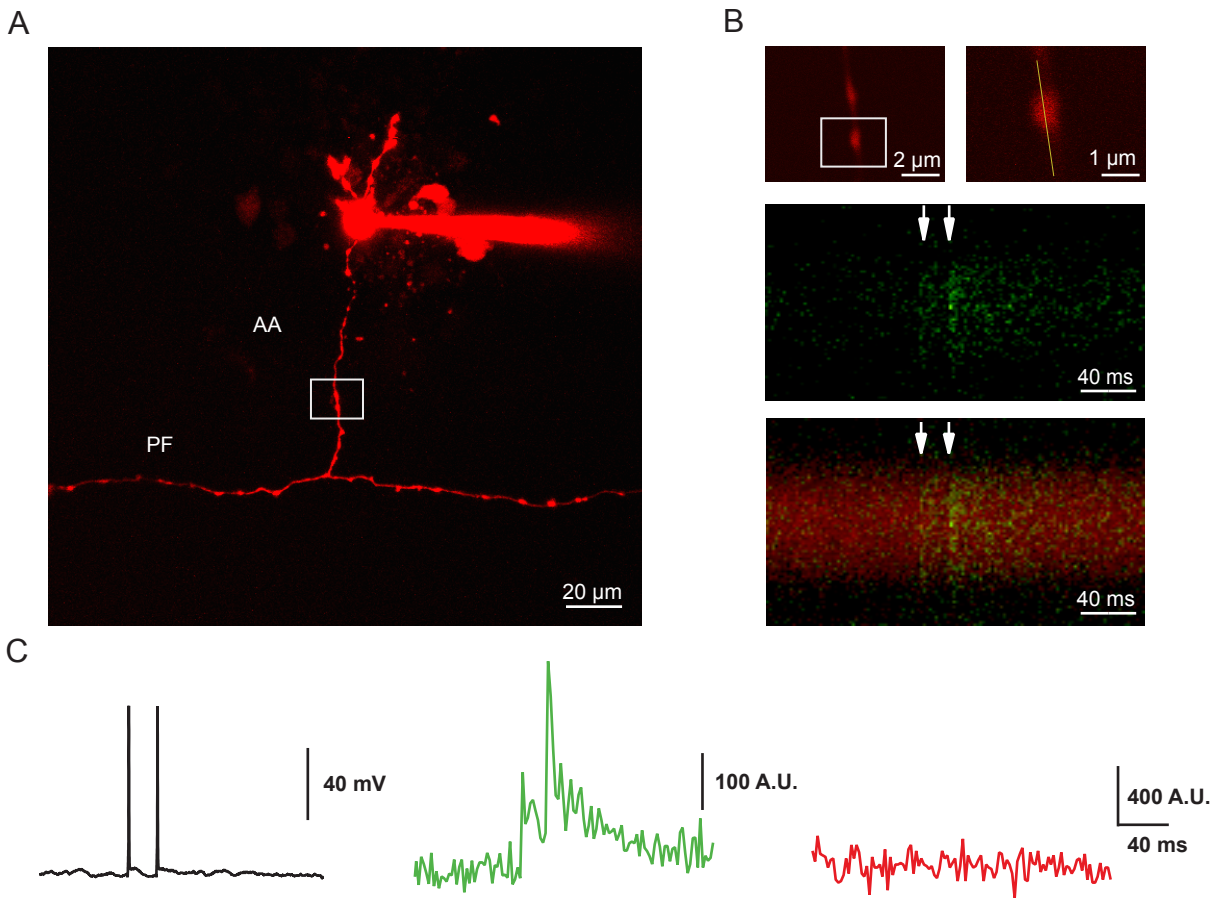

Figure 19: Single bouton Ca^{2+}-transients in cerebellar granule cells. Two-photon laser-scanning fluorescence microscopy was used to assess the Ca^{2+}-transient at single boutons of the granule cell ascending axon (AA) and the parallel fiber segment (PF). (A) 2-photon image of a cerebellar granule cell filled with Alexa-594 (30 µM) and fluo4FF (200 µM). (B) Medium (upper left) and high (upper right) magnification of a single ascending axon bouton. The yellow line indicates the orientation of the line scan (500 Hz) for the fluorescence measurement. Two action potentials (white arrows) with an inter-stimulus interval of 20 ms were elicited through current injection in the soma and the fluorescence intensity was recorded. The response to the paired action potentials is shown for the green channel (middle) and the green merged with the red channel (bottom). (C) Corresponding traces for the single trial shown in B of the somatic potential (top), the green channel (middle) and the red channel (bottom); A.U. – arbitrary unit.

Because the fluorescence intensity of a given Ca^{2+}-indicator is proportional to $[Ca^{2+}]$ changes, the actual Ca^{2+}-concentration can be calculated according to well-established methods (Grynkiewicz et al., 1985; Yasuda et al., 2004); 2.4 – Equation 5. For this purpose G_{min}/R and G_{max}/R were determined in the patch pipette (2.4) and G_{max} was validated by recording G/R ratios in boutons during a 500 Hz train of APs for 1 second (Figure 20). The train was applied in order to repetitively open presynaptic VDCCs for longer periods and to saturate the intracellularly applied calcium indicator. The results were similar in both cases (Figure 20D) showing that the calibration is valid and can be used to determine Ca^{2+}-influx as $\Delta[Ca^{2+}]$ in µM.

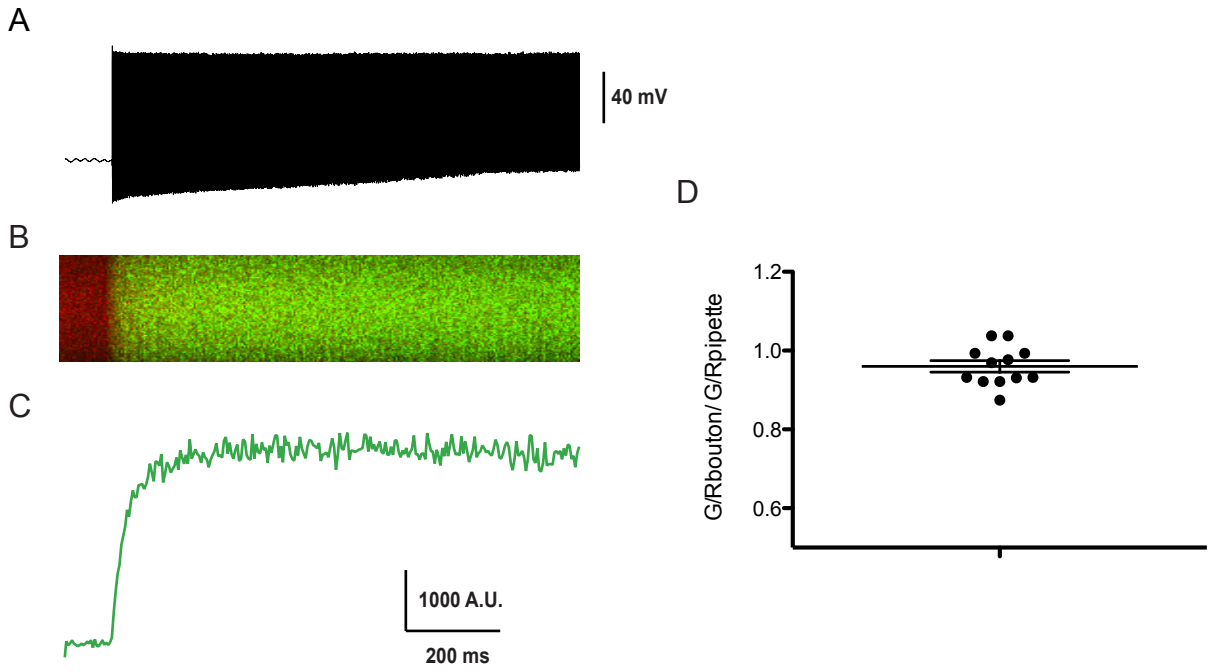

Figure 20: Comparison of G_{max} calibrations in the patch pipette and in axonal boutons. (A) A 500 Hz train of action potentials was delivered for 1 s to saturate the Ca^{2+}-indicator. (B) Fluorescence intensity was monitored in the bouton shown as G/R and quantified for G (C). (D) Comparison of Gmax/R values recorded in the pipette and in the bouton; A.U. – arbitrary unit.

3.3.1 RIM1α deficient boutons exhibit reduced Ca^{2+}-influx

A recent study by Brenowitz and Regehr, 2007 already used 2PLSM to describe Ca^{2+}-transients at the cerebellar parallel fiber. They could demonstrate that Ca^{2+}-influx at single boutons is very reliable but that the heterogeneity of Ca^{2+}-signals among boutons is substantial. Furthermore, earlier studies reported differences in the synaptic properties of the ascending axons and the parallel fiber segment (1.2.3) (Sims and Hartell, 2005; 2006).

Thus, two questions arose for the analysis of Ca^{2+}-transients in granule cell boutons: (1) Is the loss of the single isoform RIM1α sufficient to significantly reduce Ca^{2+}-influx and (2) are putative differences distributed homogeneously across the granule cell axon or are they segment specific? We therefore decided to perform two sets of experiments by investigating Ca^{2+}-influx in the ascending axon and the parallel fiber segment separately (Figure 21, Figure 22).

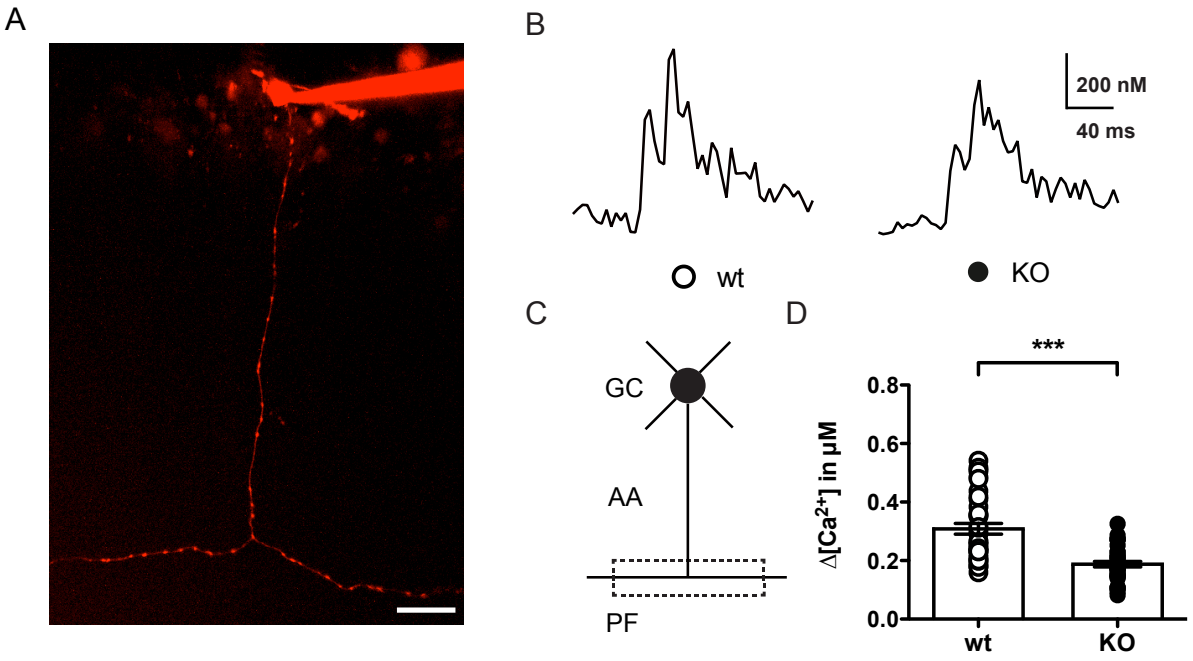

Figure 21: Parallel fiber Ca^{2+}-transients in RIM1α$^{+/+}$ and RIM1α$^{-/-}$ animals. (A) Image of a cerebellar granule cell in which PF Ca^{2+}-transients were analyzed; scale bar = 20 µm. (B) Representative calcium transients (average of 4 traces, binned to 250 Hz) for wildtype and knockout. (C) Illustration of the location of recorded boutons from granule cell (GC) axons; PF – parallel fiber, AA – ascending axon. (D) Summary graph for both genotypes recorded from parallel fiber boutons. [Ca2+] changes are calculated from the average of 16 ms (4 data points) from the first peak. Bar graph shows average values and data points for individual boutons (open circle corresponds to WT, closed circles to KO); *** indicates P < 0.001, Student's t-test.

The analysis of parallel fiber boutons revealed a considerably smaller calcium influx in RIM1α deficient animals compared to their wild type littermates (Figure 21D; WT = 0.31 ±0.02 µM, n = 38 boutons/3 mice vs. KO = 0.19 ± 0.01 µM, n = 35 boutons/3 mice; $p < 0.001$).

We then repeated the very same experiments at the ascending axon and could also detect a reduction in Ca^{2+}-influx in RIM1α KO mice (Figure 22D; WT = 0.42 ± 0.03 µM, n = 23 boutons/8 mice vs. KO = 0.31 ± 0.02 µM, n = 23 boutons/6 mice, p = 0.013, student's t-test).

Interestingly, loss of RIM1α impacts Ca^{2+}-influx differentially at the axonal segments. For parallel fiber boutons Ca^{2+}-influx in RIM1α$^{-/-}$ is reduced by about 40 % and in the ascending axon by 26 % on average.

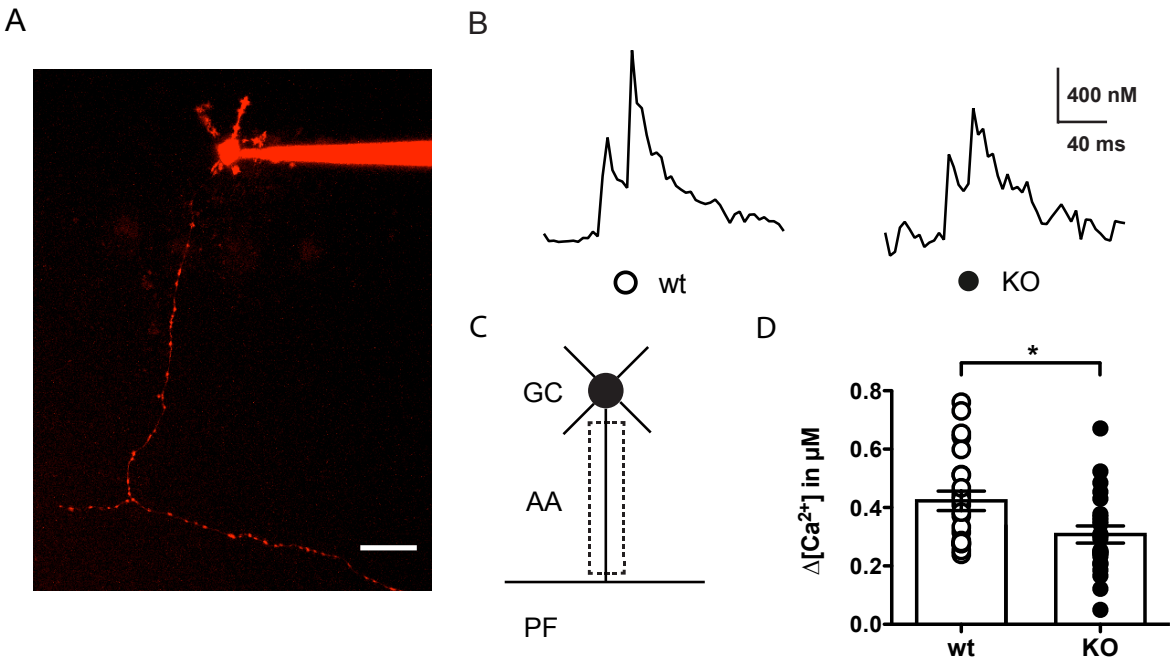

Figure 22: Ascending axon Ca^{2+}-transient in RIM1α$^{+/+}$ and RIM1α$^{-/-}$ animals. A, Image of a cerebellar granule cell in which AA Ca^{2+}-transients were analyzed; scale bar = 20µm. (B) Representative Ca^{2+}-transients (average of 4 traces, binned to 250 Hz) for wildtype and knockout. (C) Illustration of the location of recorded boutons from granule cell (GC) axons; PF – parallel fiber, AA – ascending axon. D, Summary graph for both genotypes recorded from ascending axon (AA) boutons. Bar graph shows average values and data points for individual boutons (open circle corresponds to WT, closed circles to KO); * indicates $P < 0.05$, Student's t-test.

Because release probability is strongly dependent on Ca^{2+}-influx the reduction of the latter one in RIM1α KO is a very likely causative factor underlying the reduced release probability and altered short-term plasticity. An additional side observation was that not only a difference between the two genotypes became apparent but also between the two axonal segments in wildtype mice (AA WT = 0.42 ± 0.03 µM vs. PF WT = 0.31 ±0.02 mM, p = 0.002, student's t-test). In the light of previous studies (Sims and Hartell, 2005; 2006) it seems that the already described synaptic differences are also reflected by differential Ca^{2+}-transients (4.4).

3.4 Presynaptic long-term potentiation

The influx of calcium is not only involved in transmitter release and short-term plasticity but also impacts long-term plasticity (see also 1.4.1 and Malenka and Bear, 2004). Additionally, even though it has been shown that RIM1α is not a direct target of phosphorylation, it is still assumed to be a essential mediator of presynaptic LTP (Kaeser et al., 2008a). We were therefore interested in whether the loss of RIM1α itself alters the expression of LTP at the parallel fiber – Purkinje cell synapse or if the reduction of the influx of calcium is perhaps strong enough to prevent LTP induction (Myoga and Regehr, 2011).
Both ideas could be tested separately. The role of RIM1α in the expression mechanism of LTP was probed by direct chemical activation of the intracellular signaling pathway, thus bypassing Ca^{2+}-signaling. The full sequence of induction and expression of LTP was tested by a set of experiments using different electrical induction protocols and extracellular Ca^{2+}-concentrations to determine the induction threshold.

3.4.1 Chemical induction of LTP by forskolin

To probe the intracellular signaling cascade downstream of presynaptic calcium influx, we applied the adenylyl cyclase activator forskolin which leads to a rise in cAMP that stimulates PKA activation (Salin et al., 1996) and finally increases presynaptic release probability (1.4.1). It has been shown that activation of PKA by AC/cAMP occurs exclusively at the presynaptic site (Linden and Ahn, 1999). This means that forskolin does not change the properties of postsynaptic transmission.
Forskolin bath application (3 minutes) led to a substantial increase in the amplitude of both genotypes with no discernable difference (Figure 23, WT 162.4 % ± 11.3 %, n = 9 slices, 5 mice vs. KO 165.5 % ± 10.6 %, n = 9 slices, 7 mice; p = 0.84, student's t-test, values taken from averages of min 26-30 after induction). The experiment demonstrates that the AC/PKA signaling cascade triggers an increase in transmitter release independent of RIM1α. This is in line with results from experiments in RIM1α KO mice at the mossy fiber synapse (Castillo et al., 2002) but contradictory to results from the lateral amygdala (Fourcaudot et al., 2008) and cultured cerebellar granule cells (Lonart et al., 2003).

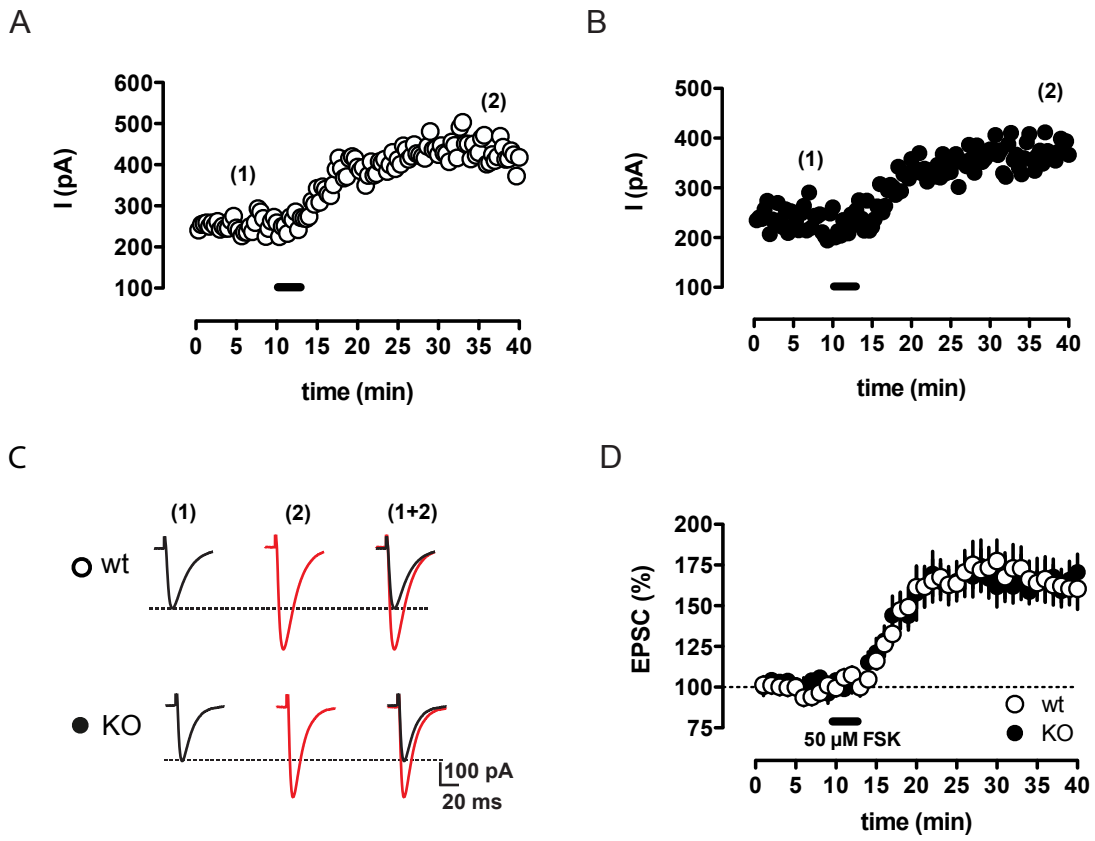

Figure 23: Forskolin induced long-term potentiation. LTP was chemically induced by applying 50 µM forskolin for 3 minutes (black bar). Time course for example experiments is shown for WT (A) and KO (B) as well as example traces (C) for the time points indicated by numbers in brackets. (D) Summary graph for all experiments; EPSC – excitatory postsynaptic current, FSK – Forskolin.

3.4.2 Tetanic induction of LTP

Next, we tested if the continuous process of induction and expression of long-term potentiation is disrupted by the loss of RIM1α when induced by tetanic stimulation. Two different sets of experiments were performed with induction protocols that differed in the frequency and number of stimuli delivered.

In a first approach we used a protocol consisting of 200 pulses with a frequency of 8 Hz (Figure 24). No significant difference in potentiation was detectable between the two genotypes (Figure 24D, WT 121.7 % ± 7.2 %, n = 8 slices, 4 mice vs. KO 123.7 % ± 4.4 %, n = 7 slices, 3 mice; p = 0.72, student's t-test, values taken from averages of min 26-30 after induction).

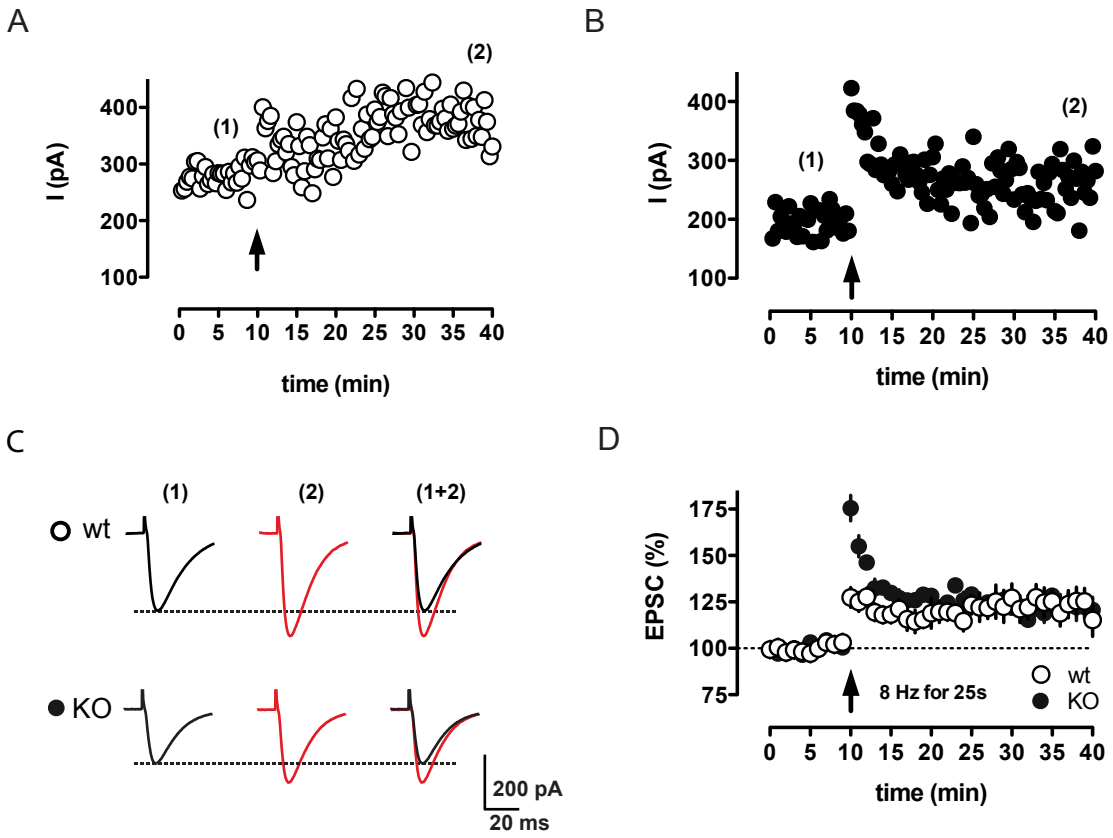

Figure 24: Long-term potentiation induced with 8 Hz for 25 s. A black arrow indicates the time point of induction. A, Representative experiment in RIM1α wild type and knockout (B) with respective example traces (C). The summary plot of all experiment is shown in D; EPSC – excitatory postsynaptic current.

In a second approach the experiments were repeated with a slightly different induction protocol consisting of 100 stimuli delivered at 10 Hz (Figure 25). Again, the level of potentiation did not differ between wildtype and knockout animals (Figure 25D, WT 119.2 ± 2.6, n = 7 cells, 5 mice vs. KO 118.6 ± 7.5, n = 8 cells, 5 mice, p = 0.94, student's t-test, values taken from averages of min 26-30 after induction).

Notably, although the level of potentiation remained unchanged, post-tetanic potentiation (PTP) is strongly enhanced in RIM1α KO mice in comparison to WT (Figure 28A, 8 Hz 25s (taken 25 s after induction train): WT = 123.6 ± 4.0 vs. KO = 183.8 ± 9.6, $p < 0.001$; Figure 28B, 10 Hz 10s (taken 10 s after induction train): WT = 131.3 ± 6.8 vs. KO = 218.2 ± 19.6, $p < 0.01$).

Taken together the results show that the loss of RIM1α is dispensable for the induction and expression of presynaptic parallel fiber long-term potentiation. Although calcium transients are strongly reduced in RIM1α deficient animals, the Ca^{2+}-influx during induction seems to exceed the threshold. Furthermore, the successful induction of presynaptic LTP with two different induction protocols supports the general validity of the results.

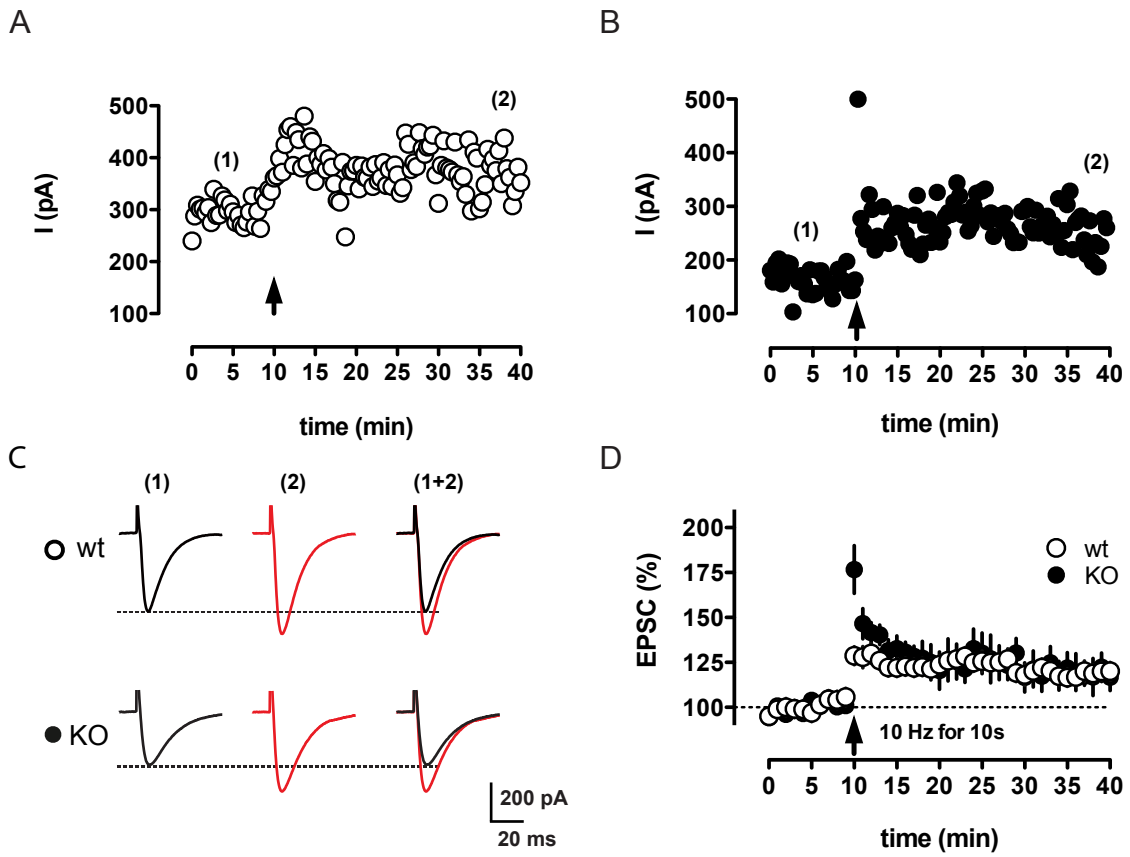

Figure 25: Long-term potentiation induced with 10 Hz for 10 s. Tetanic stimulus protocol consisting of 10 Hz for 10s (arrow). Time course of a single experiment for RIM1α WT (A) and RIM1α KO (B). (C) Shown are example traces for both genotypes, which represent the average of 5 min at the time points indicated in the graphs above. (D) Summary data for WT (open circles) and KO (closed circles); EPSC – excitatory postsynaptic current.

3.4.3 Calcium-dependence of induction

Ca^{2+}-influx into the presynaptic terminal is a crucial step for the induction of presynaptic LTP (see 1.4.1, Castillo et al., 1994 and Mellor and Nicoll, 2001) and its threshold is rather sharp. In a study by Myoga et al., 2011 normal parallel fiber LTP was inducible with concentrations of 1.5 mM Ca^{2+} but not with 1.25 mM extracellular [Ca^{2+}] using an 8 Hz stimulus. We therefore wanted to test if the induction threshold in our experimental setting with the 10 Hz/10s protocol was similarly sharp under conditions of reduced Ca^{2+}-influx.

Starting with 1.5 mM Ca^{2+}, LTP could readily be obtained (Figure 26, C57/Bl6n = 115.6 ± 5.7 %, n = 5 cells, 3 mice).

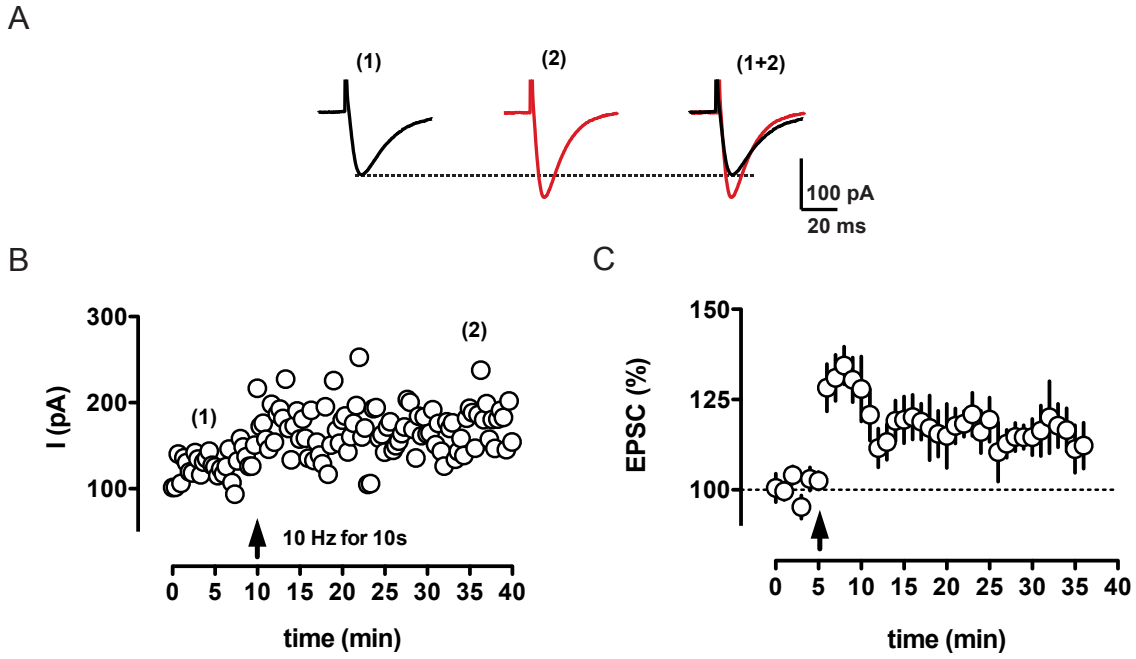

Figure 26: Successful LTP induction in 1.5 mM Ca^{2+}. LTP was induced with a 10 Hz stimulus for ten seconds (black arrow) under conditions of 1.5 mM extracellular calcium concentration. Example traces (A) and experiment (B) in 1.5 mM [Ca^{2+}]. Numbers in brackets indicate the time point for the example traces. (C) Summary of all experiments; EPSC – excitatory postsynaptic current.

Surprisingly, a further small reduction of 250 nM to 1.25 mM Ca^{2+} was effective to block the induction of LTP completely (Figure 27, C57/Bl6n = 98.7 ± 5.1 %, n = 4 cells, 3 mice), showing that the described threshold holds true for our preparation, too, even though a different induction protocol was used. The induction failure with low extracellular [Ca^{2+}] can most likely be attributed to a insufficient Ca^{2+}-influx through VDCCs (Myoga and Regehr, 2011).

A summary of the level of potentiation for all LTP experiments with the 10 Hz induction protocol is shown in Figure 28D. Of note is the differential distribution of successful potentiation and failures between RIM1α WT and KO mice compared to conditions of 1.5 mM and 1.25 mM Ca^{2+} (for discussion see 4.5).

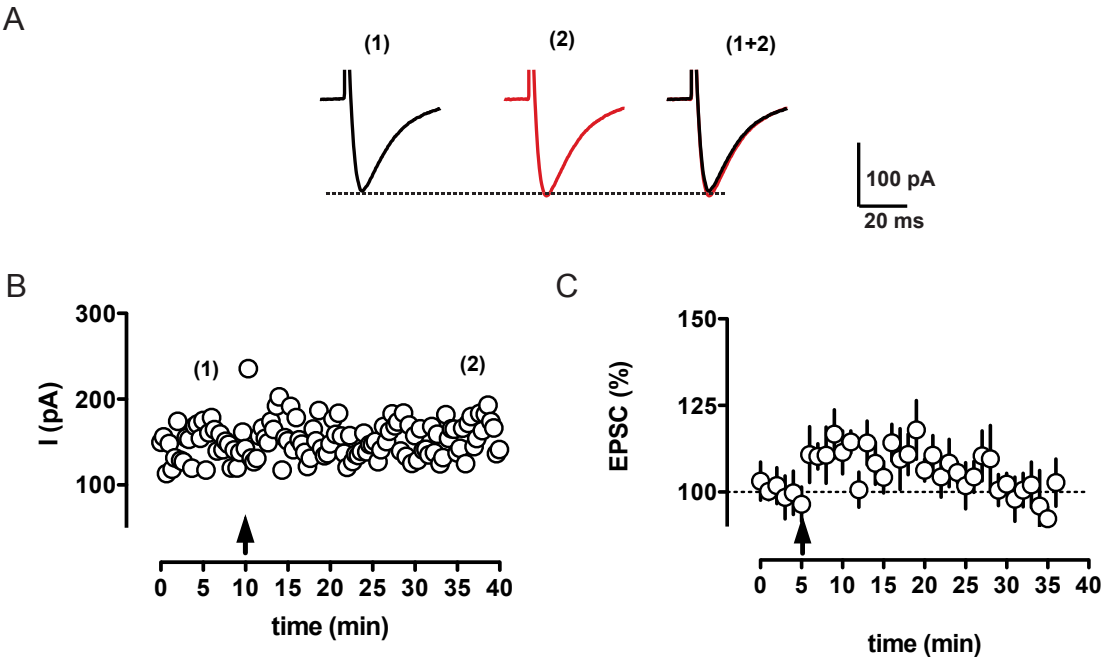

Figure 27: Unsuccessful LTP induction in 1.25 mM Ca^{2+}. LTP induction is sensitive to extracellular calcium concentration. LTP was induced with a 10 Hz stimulus for ten seconds (black arrow) under conditions of 1.25 mM extracellular calcium concentration. Example traces (A) and experiment (B) in 1.25 mM [Ca2+]. Numbers in brackets indicate the time point for example traces. (C) Summary of all experiments; EPSC – excitatory postsynaptic current.

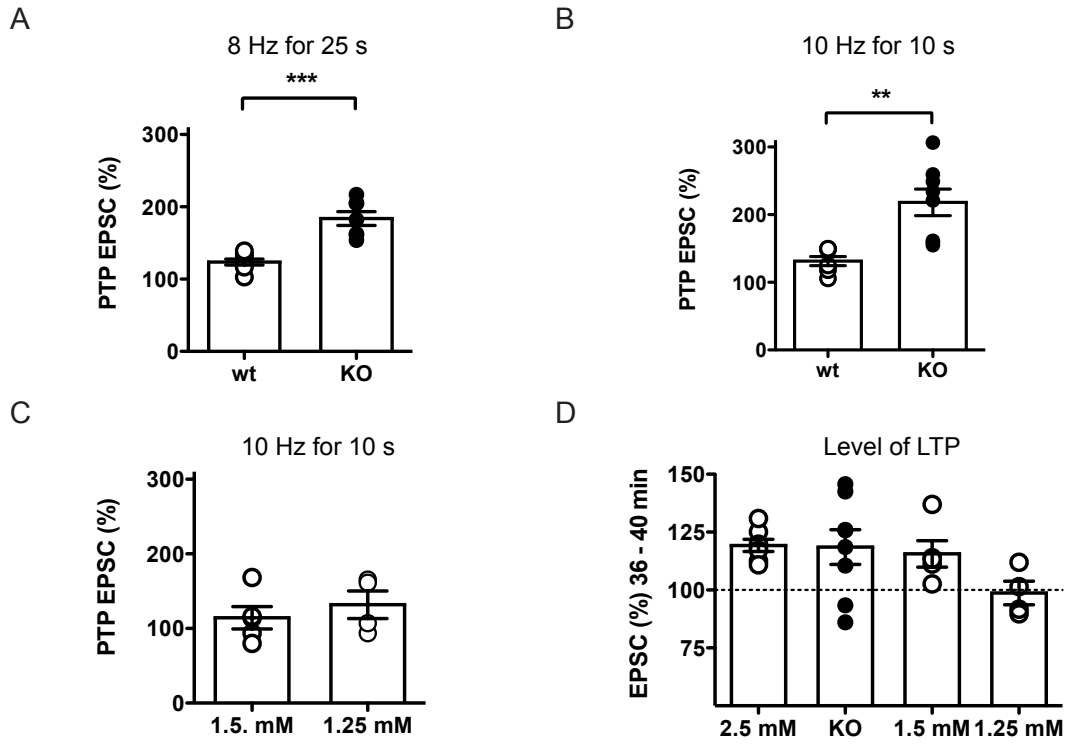

Figure 28: Summary post-tetanic potentiation and level of long-term potentiation. Summary of post-tetanic potentiation (PTP) for the 8 Hz tetanus for wild type and knockout (A) 10 Hz tetanus for both genotypes (B) and 10 Hz for C57/Bl6 under low Ca^{2+} conditions (C). (D) Summary graph of potentiation 26-30 min after induction with a 10 Hz train for 10 seconds for WT and KO and under reduced extracellular calcium; EPSC – excitatory postsynaptic current.

In summary, the experiments demonstrated that neither LTP induction nor expression is altered in RIM1α knockout mice (3.4.1 and 3.4.2). However, clear differences in the extent of the post-tetanic potentiation could be found between the two genotypes (Figure 28).

4 Discussion

In this work we studied the impact of the loss of the protein RIM1α on synaptic transmission at the granule cell – Purkinje cell synapse. For this purpose, synaptic properties were examined by electrophysiological and 2PLSM Ca^{2+}-imaging. We could show that RIM1α deficient mice exhibit reduced action potential induced Ca^{2+}-influx at presynaptic boutons. Consequently, the release probability is decreased and short-term plasticity is altered in these animals.

We furthermore examined if the loss of RIM1α or the reduced Ca^{2+}-influx has an influence on long-term plasticity. However, the characterization of the long-term plasticity behavior did not yield any differences in the induction or expression of presynaptic long-term potentiation but an increased post-tetanic potentiation in RIM1α knockout mice.

Additionally, our study revealed a difference in Ca^{2+}-influx between the two axonal segments of the granule cell, the ascending axon and the parallel fiber segment, which are also differentially affected by the loss of RIM1α.

In the next paragraphs I will discuss the results in the light of the current literature. I will present interpretations of the current work and discuss possible drawbacks and technical limitations. I will also identify questions that arise from this work and try to define aims of future research on this topic.

4.1 Loss of RIM1α reduces Ca^{2+}-influx and release probability

Different sets of experiments were performed to examine basic synaptic properties at the granule cell – Purkinje cell synapse that converged on the same result. We could demonstrate a reduced release probability in RIM1α deficient mice. Both, paired-pulse (Figure 11) and train stimulation experiments (Figure 12) showed an increased short-term potentiation (3.1) in RIM1α KO animals indicating changes of presynaptic properties (Zucker and Regehr, 2002). The use of γDGG as a relative measure of neurotransmitter concentration in the synaptic cleft revealed a reduced glutamate transient (Figure 15, 3.2.1) and a variance-mean analysis revealed a lower release probability in RIM1α KO mice (Figure 18, 3.2.2). Although neither of these results alone are sufficiently conclusive, together they constitute a strong piece of evidence arguing for a release defect caused by the loss of RIM1α. In search of a mechanistic cause for this release defect we identified a reduced Ca^{2+}-influx in boutons lacking the RIM1α protein (Figure 21, Figure 22, 3.3.1).

The influence of RIM1α on short-term plasticity has already been shown for the Schaffer collateral – CA1 synapse (Schoch et al., 2002) and at the cortico – lateral amygdala synapse where the authors also reported a reduced P_r (Fourcaudot et al., 2008). However, at the hippocampal mossy fiber synapse and most importantly at the parallel fiber synapse loss of RIM1α seemed to have no effect on STP (Castillo et al., 2002). Recently, two studies could show a reduced calcium current density or decreased Ca^{2+}-influx in RIM1/2 knockout animals and accordingly reduced P_r (Han et al., 2011; Kaeser et al., 2011) and an influence on calcium channel function of RIM (Kiyonaka et al., 2007). Both studies were made in either hippocampal cell cultures or at the calyx of held so the authors could not test LTP. Thus, our results are generally in line with most of the previous studies. Furthermore, we could show that the loss of one isoform, RIM1α - instead of all RIM1/2 isoforms - is already sufficient to cause a detectable reduction in Ca^{2+}-influx. The fact that calcium reduction is not as pronounced as in the RIM1/2 KO studies is presumably due to a partial compensation by the remaining RIM isoforms (see below). Nevertheless there is a discrepancy to the study of Castillo et al., 2002 in which experiments have been done at the very same synapse. The reason for this discrepancy remains elusive because the same experimental conditions were used in both studies. It is interesting that all the other studies detecting differences in short-term plasticity in RIM1α KO mice used additional techniques to strengthen their argument (variance-mean analysis in Fourcaudot et al., 2008 and an experiment using MK801 in Schoch et al., 2002). A possible explanation might be

that the PPR is not the most sensitive measure to detect changes in STP or P_r and subtle differences might be more prone to be overseen.

It remains unclear if the reduced Ca^{2+}-influx we find in the absence of RIM1α is due to a reduced calcium channel number or function. Furthermore, it is not know if the loss of RIM1α affects both P/Q- and N-type calcium channels to the same extent or if Ca^{2+}-influx is more attenuated at a certain channel type. However, a reduction of Ca^{2+}-influx of about 26 – 40 % is very likely to result in a reduced release probability. Three questions arise from these data: Is the reduced Ca^{2+}-influx sufficient to explain the increased short-term plasticity? Second, what can we deduce from the reduction caused by the single isoform in comparison to the RIM1/2 double KO? Thirdly, is the function of RIM1α the same in all synapses and is it homogenously distributed amongst them?

The first question deals with notion that RIM does not only assist in the recruitment and positioning of Ca^{2+}-channels at the active zone but also in priming and establishment of the readily releasable pool of vesicles as well as the modulation of the calcium sensitivity of neurotransmitter release (Han et al., 2011). Therefore, the observed release defect in RIM1α KO mice could in principle also be due to other effect besides a reduction of Ca^{2+}-influx. If one compares the Ca^{2+}-imaging data (Figure 21, Figure 22) with the variance-mean analysis (Figure 18) one can get an estimate of the relative contribution of the reduced Ca^{2+}-influx to the decrease in release probability in RIM1α KO mice. Ca^{2+}-imaging data show a 26 - 39 % reduction in the Ca^{2+}-transients in the KO animals (Figure 21, Figure 22). Assuming that Ca^{2+}-influx through VDCCs is only moderately saturated at our extracellular [Ca^{2+}], we find that a similar reduction of Ca^{2+} (from 3.5 mM to 2.5 mM, 28 %) leads to a 36 % decrease of Pr in wildtype mice (estimated again via variance-mean analysis). This value is close to the extent of Pr reduction we find in RIM1α KO animals (33 – 49 %, from 2.5 – 4.5 mM Ca^{2+}) suggesting that the reduced Ca^{2+}-influx already accounts for a large part of the decreased release probability in RIM1α deficient animals. However, recruitment of VDCCs and control of channel function are probably not the only functions of RIM1α so that other alterations might also contribute to the release defect we see.

If one compares the impact of the RIM1α KO with the RIM1/2 KO it is not surprising that the latter one has a much more pronounced phenotype than the animals deficient in only a single isoform. Assuming that γ-RIMs do not play a major role in priming and recruitment of VDCCs there are three RIM isoforms left in RIM1α deficient mice (one α-RIM and two β-RIMs) that could compensate for the loss of the protein (1.1.2). The absence of all RIM1/2 isoforms leads to a Ca^{2+}-current reduction of about 60 % in hippocampal cell cultures (Kaeser et al., 2011) and

50 % at the Calyx of Held (Han et al., 2011). Compared with the 26 - 40 % reduction in Ca^{2+}-influx that we find it seems that the loss of RIM1α already makes up a large part of the overall function of RIMs in setting Ca^{2+}-influx. Together with the prior notion that the reduced Ca^{2+}-influx is a major cause of the release defect in RIM1α KO mice it seems that the function of setting Ca^{2+}-influx is not compensated by the other RIM isoforms. This is in contrast with a recent study comparing the Ca^{2+}-dependence of neurotransmitter release at inhibitory synapses in RIM1, RIM2 or RIM1/2 deficient mice (Kaeser et al., 2012). The authors conclude from their data that RIM1 and RIM2 can fully compensate each others function in recruiting Ca^{2+}-channels to the active zone. The discrepancy might stem from the fact that Ca^{2+}-influx was not measured directly in this study but the dependency of neurotransmitter release on extracellular [Ca^{2+}]. Because this measure also includes processes like Ca^{2+}-sensor sensitivity and intracellular Ca^{2+}-dynamics the results might be difficult to interpret in terms of Ca^{2+}-channel recruitment to active zones.

The question remains if the function of RIM1α is the same at all synapses. It cannot be answered by solely looking at our data, but one may speculate based on our Ca^{2+}-imaging experiments at ascending axon and parallel fiber boutons. As mentioned before, both segments have been shown to posses different synaptic properties (1.2.3) (Sims and Hartell, 2005; 2006). The relative reduction in Ca^{2+}-influx is furthermore differentially affected by the loss of RIM1α with the ascending axon Ca^{2+}-transients being reduced by 26 % and the parallel fiber Ca^{2+}-transients by 39 %. A definite cause for the uneven impact of RIM1α deficiency remains elusive but there are at least three possible explanations: (1) Although RIM1α is expressed throughout the brain, its relative proportion with respect to other members of the RIM family might vary (Schoch et al., 2006). In this scenario, connections where RIM1α has a lower contribution to synaptic transmission under wildtype conditions might also be less affected by the loss of the protein. Thus, its function in setting Ca^{2+}-influx might also vary in a subcellular segment-specific manner. (2) Ca^{2+}-influx trough VDCCs for triggering vesicle fusion is mainly conducted by P/Q- and N-type channels at granule cell – PC synapses (Mintz et al., 1995). However, it is unclear if their relative contribution to neurotransmitter release is the same in both axonal segments. Both channels compete for the same binding domain at RIM1α so that the protein may preferentially recruit one channel type. Thus, if the relative contribution of P/Q- and N-type channels to transmitter release is not the same in both axonal segments, then a loss of RIM1α would differentially impact Ca^{2+}-transients at the ascending axon and the parallel fiber. (3) Although the disruption of the function of RIM1α seems to mainly affect Ca^{2+}-influx the overall function of RIM proteins in synapse function is much broader and it is very likely that different isoforms

have overlapping functions. Therefore it is conceivable that the function of a single isoform is partially compensated by the others. Again, as mentioned before, this process would depend on the amount of RIM isoforms still present at a certain synapse and might therefore vary between synapses.

In conclusion, all the above explanations lead to the assumption that not the function of RIM1α itself but its relative contribution to Ca^{2+}-influx and priming and accordingly neurotransmitter release is affected. Additionally, these explanations are not mutually exclusive and further research has to be done to clarify this question.

Besides RIM, the loss of other proteins of the presynaptic active zone or their mutation has been shown to alter release probability and/or short-term plasticity. Amongst them are: complexin, which has been shown to control the Ca^{2+} sensitivity of neurotransmitter release (Reim et al., 2001; Xue et al., 2008), SV2 assists in the priming of docked vesicles (Custer et al., 2006; Chang and Südhof, 2009), Munc13s, which are essential priming factors that also regulate the replenishment of the readily releasable pool during high-frequency stimulation (Rosenmund et al., 2002; Breustedt et al., 2010; Lipstein et al., 2013), Rab3 is thought to dock vesicles via interaction with α-RIMs and Munc13 to the priming machinery (Geppert et al., 1997; Dulubova et al., 2005), RIM-binding proteins assist in Ca^{2+}-channel clustering and RIM1α (Schoch et al., 2002). Although a disruption of either of these proteins eventually leads to a release defect, their individual function differs profoundly. Thus, every defect may also reveal an important function in the process of docking, priming and release. The role of Rab3a and RIM1α in this process is rather peculiar because their function is thought to be synapse specific. At some synapses that exhibit presynaptic LTP both proteins have been shown to be essential mediators for long-term changes but not to affect STP (Castillo et al., 1997a; 2002) whereas at other connections they do alter short-term plasticity (Geppert et al., 1997; Schoch et al., 2002). Our results instead give rise to the assumption that RIM1α is universally involved in setting short-term behavior in a non-synapse specific manner.

4.2 Impact of γDGG at the granule cell – Purkinje cell synapse

To probe for differences in the release probability between wildtype and RIM1α KO animals, we used the low affinity, competitive AMPAR antagonist γDGG (**Figure 15**). Because the impact of the drug is inversely proportional to the glutamate concentration in the synaptic cleft we could detect a reduced glutamate transient in RIM1α KO mice, from which we concluded a lower release probability in these animals. For the cerebellum, similar experiments have been carried out before showing that MVR is present at the CF – PC synapse (Wadiche and Jahr, 2001), the PF – PC synapse (Foster et al., 2005) and at the PF – molecular layer interneuron synapse (Bender et al., 2009). Additionally, the study of (Foster et al., 2005) showed that moderate receptor saturation is present at the PF – PC synapse.

The interpretation of the results of all studies is based on the assumption that an increase of the glutamate transient in the synaptic cleft stems mostly, if not completely, from the occurrence of multi-vesicular release (MVR). However, there are other possible mechanisms that could contribute to the glutamate concentration in the cleft. Glutamate pooling and spillover is one of them and has been shown to take place at the PF – molecular layer interneuron synapse during train stimulation (Carter and Regehr, 2000). The effect is less likely to occur at the PF – PC synapse because the spacing between synapses is wider and every connection is very well ensheathed by glia cells (Xu-Friedman et al., 2001). Experiments have shown that there is no difference in the impact of γDGG when neighboring synapses are either activated by axonal beams (i.e. many axon running in parallel) or disperse synaptic activation by stimulation in the granular cell layer, which makes the simultaneous release of glutamate at neighboring synapses less likely (Foster et al., 2005). Furthermore, testing spillover at the Schaffer collateral – CA1 synapse, which is less separated from neighboring synapses by glia (Ventura and Harris, 1999), the presence of the glutamate uptake blocker TBOA also did not show any significant contribution to peak amplitude (Christie and Jahr, 2006). Taken together, although glutamate spillover and pooling cannot be ruled out completely, their contribution to synaptic transmission at the PF – PC synapse seems to be of no significance. Another possibility that could affect glutamate concentration is either partial or compound fusion of synaptic vesicles. The former is less likely to occur because it has been shown that the quantal size does not change during paired-pulse facilitation and thus the released vesicular content remains constant independent of P_r (Chen et al., 2004). The latter has been tested at the PF – molecular layer interneuron synapse before and after LTP induction. Quantal size has been determined by analyzing the amplitude of asynchronous release and no difference was found between the two conditions (Bender et al.,

2009). Both findings suggest that the quantal size/content does not change dynamically during synaptic transmission. Systematic or rather phenotypic changes in the quantal content are discussed below (4.3). The remaining mechanism for differential glutamate transients in the synaptic cleft is multivesicular release. To test this directly, we probed the impact of γDGG under conditions of univesicular release (Figure 14). It has been shown earlier that MVR covaries with P_r and accordingly is more pronounced on the second pulse in an paired stimulation protocol (Foster et al., 2005; Bender et al., 2009). We therefore chose conditions of low extracellular calcium (1 mM) which have been shown to mimic mostly univesicular release on both pulses. Under these conditions no changes in the PPR during application of γDGG was detected (Figure 14). The result was reassuring because under conditions of univesicular release the concentration of glutamate in the synaptic cleft should not change and consequently the action of γDGG should be the same on both pulses. We concluded from these experiments that changes in the extent of inhibition of synaptic transmission by γDGG depends on the amount of MVR, which in turn depends on the release probability. This finding is also in line with previous studies (Wadiche and Jahr, 2001; Foster et al., 2005; Bender et al., 2009).

On that basis the increased inhibition of synaptic transmission in RIM1α KO animals can be interpreted as a reduced release probability (Figure 15). The difference was found at both pulses but more pronounced at the second. The differential impact of γDGG on the first pulse in RIM1α wt and KO mice demonstrates that MVR does already happen at the first stimulus (in 2.5 mM extracellular $[Ca^{2+}]$ and thus seems to be reduced in RIM1α KOs. This agrees well with a previous study showing a significant contribution of MVR starting at 2 mM extracellular $[Ca^{2+}]$ (Foster et al., 2005). If the release defect in RIM1α KOs is strong enough to prevent MVR on the first pulse then this might already explain the more pronounced difference between wt and KO on the second pulse. The effect of γDGG on univesicular release is the strongest because the concentration of glutamate is the lowest if only one vesicle is released. Therefore the impact of γDGG reaches a “threshold of inhibition”. For the second pulse, MVR is likely to happen in both genotypes and so differences in the extent of inhibition fully reflect changes in release probability and might therefore be more pronounced under these conditions.

Because of its fast dissociation kinetics and competitiveness, γDGG also has the ability to relieve AMPARs from saturation. This property was utilized to probe for saturation in RIM1α wt and KO animals and revealed a significant shortening of the decay time with γDGG on the second pulse of RIM1α wt mice (Figure 16). Changes in the decay time in the presence of γDGG hint at receptor saturation and confirm the finding of Foster et al., 2005 that demonstrates moderate receptor saturation at this synapse. The fact that saturation is not present in RIM1α KO slices is

in line with our argument that deletion of RIM1α leads to a reduction of release probability and reduced MVR and in turn results in smaller glutamate transients, which are less effective in saturating postsynaptic receptors.

4.3 Synaptic parameters probed by variance-mean analysis

The quantal nature of synaptic transmission leads to a certain fluctuation in the amplitude of postsynaptic signals. Because this fluctuation depends on the synaptic parameters it can be used to determine the properties of synaptic transmission defined as Q, quantal content, P_r, release probability and N, number of synapses (2.3.1). We used this approach in our study to distinguish differences in the synaptic transmission between wildtype and RIM1α deficient animals. It revealed a reduced release probability in RIM1α KO mice but no significant differences in the quantal content compared to wildtype mice (Figure 18). The results constitute a further piece of evidence that the loss of RIM1α alters transmitter release at presynaptic terminals.

The approach of using a variance-mean analysis to compare RIM1α wildtype and KO animals has been used before at the cortico – lateral amygdala synapse and could also show a reduced P_r in RIM1α deficient mice (Fourcaudot et al., 2008) which puts our result in line with the former study. Q and N however were not calculated in that study. As mentioned before, we too refrained from calculating the parameter N, because it mainly reflects the number of activated fibers by the stimulation electrode, which cannot be controlled with the required precision for a cross slice / cross genotype comparison. Still it is possible that the removal of RIM1α does not only lead to a reduced release probability but also to a complete shutdown of release sites and thereby a reduction of N.

The variance-mean analysis could also exclude a significant postsynaptic effect of the loss of RIM1α by showing no significant differences in the parameter Q (Figure 18E). It also strengthens the argument that the observed receptor saturation we find is only present at the second amplitude of paired-pulse stimulation. The variance-mean analysis has been performed with single pulses and therefore no differences in receptor saturation were detected. Yet, it cannot be excluded that the differences in receptor saturation between the genotypes might be more pronounced under *in vivo* conditions since it has been shown that granule cells tend to fire in high-frequency bursts (Chadderton et al., 2004). Thus, the accumulation of glutamate and saturation might be more pronounced in wildtype mice. An unexpected finding was the relatively low average value of the parameter Q being ~4 pA. This is at the lower end when compared with other studies also using a variance-mean analysis and computing Q = 6.3 pA (Sims and Hartell, 2005) or 8 pA in paired recordings from granule cells and Purkinje neurons (Schmidt et al., 2012). A possible explanation might be subtle differences in the position of the stimulation electrode and accordingly more or less contribution of dendritic filtering.

4.4 One axon, two outputs: Ascending axon and parallel fiber segment

Using 2PLSM Ca^{2+}-imaging we examined Ca^{2+}-influx at individual granule cell boutons (Figure 21, Figure 22). The results did not only demonstrate reduced Ca^{2+}-transients in RIM1α KO animals (4.1) but also a general difference in the amount of Ca^{2+}-influx between boutons from the ascending axon and the parallel fiber segment in wildtype mice. It became apparent that Ca^{2+}-influx in ascending axon boutons is larger by about 35 % on average than in parallel fiber boutons.

Differences in the synaptic properties of ascending axon and parallel fiber boutons have been described earlier (Sims and Hartell, 2005). In good agreement with the current work, the authors showed that paired-pulse ratio is decreased and release probability is increased in the ascending axon. Our Ca^{2+}-imaging data are complementary to these results in such a way that they provide a possible explanation for the differences in P_r. It seems that a higher Ca^{2+}-influx correlates directly with the strength of synaptic transmission. It also highlights the ambiguous output mode of the granule cell axon also present at the anatomical level. Mossy fibers and climbing fibers with similar receptive fields terminate in overlapping microzones (1.2.1) (Garwicz et al., 1998; Ekerot and Jörntell, 2008). Additionally, these mossy fibers innervate granule cells that give rise to an ascending axon, presumably making many contacts with one above lying PC and, after it bifurcated, spanning multiple sagittal zones with its parallel fiber making only 1-2 synapses with each of about 2000 PCs (Huang et al., 2006). In summary, it seems that there is an inverse relationship between the total number of synapses and their relative contribution to the input of a single Purkinje cell. Therefore, it has been suggested that the ascending axon – PC connection forms the hard wired input from the cortical sensory circuit, acting as an event detector, whereas the parallel fiber connection has a dynamic role in modulating cerebellar processing (Sims and Hartell, 2005). Accordingly, it has been shown that long-term synaptic plasticity is restricted to the parallel fiber segment (Sims and Hartell, 2006). It is an intriguing thought that the same axon making contacts with the same kind of postsynaptic target cell forms two sorts of functionally different connections, both in an anatomical and biophysical respect. Our result adds further evidence to the concept of differential information processing between the ascending axon and the parallel fiber segment.

Although electrophysiological experiments have been performed before to distinguish between synaptic properties of AA and PF (Sims and Hartell, 2005; 2006) (Figure 29) we refrained from applying this techniques in our study. Because the extracellular stimulation activates a bundle of fibers and AA are bifurcating to PF within the whole molecular layer is difficult to achieve a "pure" AA input to PCs. Settings to record inputs exclusively coming from PF are easier to

achieve if the stimulation is placed distally to the PC in the granular cell layer (for details see Sims and Hartell, 2005; 2006 and Figure 29). In the current study electrophysiological recordings have been performed by placing the stimulation electrode at the outer border of the molecular layer in sagittal slices (2.2). In this configuration the stimulation is not segment specific but likely to activate mainly PF – PC synapses because of the large percentage of PF synapses (95 %, (Huang et al., 2006)) in comparison to AA synapses.

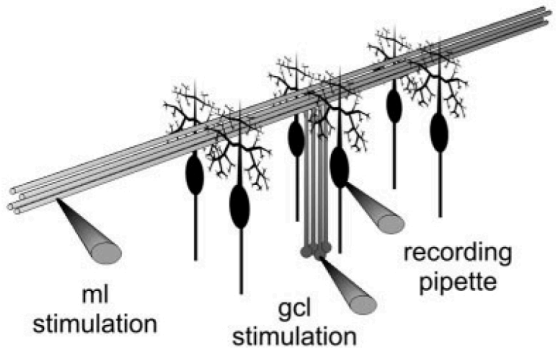

Figure 29: Positioning of the stimulation electrodes probing AA and PF synaptic properties. ml – molecular layer, gcl – granule cell layer; ml stimulation was done for activating the parallel fiber inputs and gcl stimulation for the ascending axon input. Taken from Sims and Hartell, 2005.

4.5 RIM1α is dispensable for presynaptic long-term potentiation

Activity dependent long-term changes in the strength of synaptic transmission (LTP) can be divided mechanistically into an induction and a later expression phase. RIM1α has been implicated in being essential for the expression of presynaptic LTP (Castillo et al., 2002). We tested the induction and expression of presynaptic parallel fiber – Purkinje cell LTP and found both to be normal in RIM1α deficient mice (Figure 23, Figure 24 and Figure 25). Thus, we conclude that RIM1α is dispensable for presynaptic LTP. We furthermore tested the threshold of extracellular [Ca^{2+}] for the induction of LTP and found it to be the similar to earlier studies (Myoga and Regehr, 2011), despite the use of a different induction stimulus.

The current view holds that RIM1α is an essential mediator of presynaptic LTP (Malenka and Bear, 2004; Kaeser and Südhof, 2005; Le Guen and De Zeeuw, 2010; Ho et al., 2011; Castillo, 2012; Yang and Calakos, 2013). In addition to the initial description (Castillo et al., 2002) other studies have tested the role of RIM1α in presynaptic plasticity. These studies have demonstrated a loss of presynaptic LTP in the absence of RIM1α and concluded a presynaptic pathway to be involved (Fourcaudot et al., 2008; Bocklisch et al., 2013). On the other hand it has been shown that direct phosphorylation of RIM1α by PKA is not an essential requirement (Kaeser et al., 2008a; Yang and Calakos, 2010) and has therefore cast some doubt on the mechanism involving RIM1α. The obvious question is where the apparent discrepancy of our data and previous studies stems from? To probe the expression of presynaptic LTP independent of induction by Ca^{2+}-influx we performed experiments with the adenylyl cyclase activator forskolin to bypass the step of enhanced Ca^{2+}-influx during the induction stimulus, and both genotypes displayed a robust potentiation (Figure 23). The same experiment has been performed before at the mossy fiber synapse and showed the same result, namely an intact potentiation (Castillo et al., 2002). It was therefore argued that the rise in cAMP levels might increase transmitter release by an additional RIM1α-independent pathway. This conclusion was called into question by later work done at the cerebellar parallel fiber and at cortico-amygdala synapse showing no potentiation by increasing cAMP levels in the absence of RIM1α by either applying a cAMP analog or the adenylyl cyclase activator forskolin (Lonart et al., 2003; Fourcaudot et al., 2008). The question whether or not RIM1α is an essential mediator of cAMP dependent increase in transmitter release might only be answered in a synapse specific way. In our hand, the expression of presynaptic LTP by a persistent increase of transmitter release triggered by a transient rise in cAMP levels is independent of RIM1α.

As the expression of LTP seems to be normal we next wanted to test the complete process of induction and expression by inducing LTP by synaptic stimulation. Two different induction protocols were tested and both showed normal levels of LTP in RIM1α KO mice (Figure 24, Figure 25). This is in direct contrast to the study of (Castillo et al., 2002) where the same induction protocol has been used. It has been shown in RIM1/2 KO mice that Ca^{2+}-influx is strongly reduced (Han et al., 2011; Kaeser et al., 2011) and also this study presented here demonstrates that a substantial fraction of this reduction is also present in RIM1α KO mice. It is therefore a reasonable idea that the reduction of Ca^{2+}-influx by the loss of RIM1α brings presynaptic LTP near to a threshold of induction. Slight differences in Ca^{2+}-influx or membrane potential might therefore be the pivotal parameters controlling whether or not LTP is induced in RIM1α KO mice.

The threshold for inducing presynaptic LTP has been tested earlier and it has been shown that LTP can be induced in conditions of reduced calcium (Castillo et al., 1994; Myoga and Regehr, 2011). For the parallel fiber it was shown that LTP can be induced without the contribution of P/Q- or N-type Ca^{2+}-channels but reducing extracellular [Ca^{2+}] to 1.25 mM or blocking R-type Ca^{2+}-channels is sufficient to abolish LTP (Myoga and Regehr, 2011). We repeated experiments with reduced extracellular [Ca^{2+}] and find the very same threshold using a 10 Hz induction protocol (Figure 26, Figure 27, Figure 28D). The expression of LTP at the granule cells axon is presumably restricted to the parallel fiber segment (Sims and Hartell, 2006) where we find a reduction of Ca^{2+}-influx by about 39 %. Because Ca^{2+}-influx at higher extracellular [Ca^{2+}] is partially saturated a reduction from 2.5 mM to 1.25 mM [Ca^{2+}] is close to mimic the reduction of Ca^{2+}-influx by 39 %. In this case, the induction of parallel fiber LTP in RIM1α KO mice would be at its limit. Another indicator that the loss of RIM1α shifts the threshold of induction is the distribution of failures and successes in LTP experiments (Figure 28D). Although the average level of potentiation is the same for both genotypes there is a substantial difference in the variance between wildtype and KO mice with two examples in KO animals where there is no successful induction. The data suggest that there is a rather sharp threshold for the LTP induction and that the loss of RIM1α shifts it to the brink of inducibility. A reduction of extracellular [Ca^{2+}] affects Ca^{2+}-influx through VDCCs at all channel types to the same fraction. In contrast, RIM1α binds to P/Q- and N-type calcium channels and a loss of this protein would therefore presumably only impact Ca^{2+}-influx through these channels. Thus it seems that, although LTP is readily inducible while separately blocking P/Q- or N-type channels, a reduction of Ca^{2+}-influx involving both channel types is sufficient to disturb the intracellular Ca^{2+}-profile in such a way that LTP is no longer induced. In summary, we conclude that presynaptic LTP can be induced

and expressed despite the loss of RIM1α. An explanation for the discrepancy with other studies might be the reduction of Ca^{2+}-influx by the loss of RIM1α and accordingly a shift of the threshold of induction.

4.6 The role of RIM1α in activity dependent plasticity and behavior

So far the role of RIM1α in activity-dependent plasticity has only been examined with regard to short-term plasticity in paired and train stimulation and long-term plasticity. As mentioned before, post-tetanic potentiation is another mechanism capable of controlling synaptic strength in an activity-dependent manner (1.3.1). At the granule cell – PC synapse PTP is triggered most efficiently by short high-frequency bursts (e.g. 10 pulses with 50 Hz (Fioravante et al., 2012)) but can also be seen after LTP induction protocols we used. A comparison of PTP between RIM1α wildtype mice and KO littermates revealed a considerable increase in the level of potentiation in RIM1α KO animals (Figure 28A and B). The increase in PTP can not be attributed to a reduced P_r in KO animals alone because experiments with reduced extracellular $[Ca^{2+}]$ in wildtype mice did not resemble the potentiation of PTP in KO animals (Figure 28C). Increased PTP at the granule cell – PC synapse has also been shown (although not quantified) in the initial description of RIM1α KO mice (Castillo et al., 2002) and in RIM1α knockin mice with a single amino acid exchange at serine 413 preventing phosphorylation by PKA (Kaeser et al., 2008b). In wildtype conditions PTP is mediated by PKCα and β but is compensated by a PKA-dependent pathway in PKCα/β dKO mice (Fioravante et al., 2012). How these, at first glance, contradictory mechanisms might function in synapse physiology has to be clarified in further research. But it seems that the loss of RIM1α or a prevention of its phosphorylation is able to unmask an otherwise blocked pathway for post-tetanic potentiation.

Together with the earlier discussed points we can conclude that the loss of RIM1α affects Ca^{2+}-influx, short-term plasticity, post-tetanic potentiation and shifts the threshold of induction but is not an absolute requirement for the expression of long-term plasticity. Having examined the synaptic function of this protein an interesting questions is what is the behavioral phenotype in RIM1α KO mice and how can it be connected to altered synapse function? Of course, there is no exhaustive answer to this question but one can speculate based on the existing results. RIM1α KO mice have been found to have deficits in contextual fear and spatial learning and exhibit increased locomotor activity but have normal basal motor coordination (Powell et al., 2004). Additionally, they display a decreased prepulse inhibition (a paradigm where a startle pulse is preceded by a lighter sensory stimulus which leads to an inhibition of the startle response), reduced social interaction and they respond better to psychotomimetic drugs (Blundell et al., 2010). In view of the current study there are two findings of the above mentioned behavioral tests that are of special interest:

(1) It is remarkable that motor coordination seems to be normal in RIM1α KO mice. As we have shown that synaptic transmission is significantly decreased at the granule cell – PC synapse one might have expected that a cerebellar dependent motor task like coordination is also affected. Instead, a recent study just showed that mice lacking the P/Q-type calcium channel in cerebellar granule cells display normal motor performance. The severe synaptic defect by the reduced Ca^{2+}-influx in these mice, similar to our results, only seems to affect motor behavior during consolidation of specific motor tasks (Galliano et al., 2013a). Thus, it seems that granule cell – PC synaptic transmission is only of special importance in higher order motor tasks. No such tests have been made in RIM1α KO animals so far but it would be interesting to see if the results would resemble those of the latter study. (2) Altered prepulse inhibition in RIM1α KO is of special interest because the intervals of the sensory stimuli that are applied are in the millisecond range and therefore in the same temporal range as short-term plasticity, which has shown to be altered. Additionally, prepulse inhibition probes sensorimotor gating which might involve cerebellar processing (McAlonan et al., 2002) and could therefore reflect the observed synaptic defect.

On the other hand, the loss of RIM1α certainly affects numerous synaptic connections and therefore behavioral changes can hardly be attributed to specific connections. This is especially true for deficits in learning tasks and it is hard to tell if the observed changes are due to the reduced basal synaptic transmission or perhaps stem from the increased threshold of induction for presynaptic LTP. Still, to date the function of presynaptic LTP remains elusive (Le Guen and De Zeeuw, 2010) and it has been speculated that it might serve as an appropriate adaptable frequency filter (i.e. a filter where certain frequencies are better conducted than others) (D'Angelo and Casali, 2012).

In order to reveal further insights into the function of cerebellar synaptic plasticity, work has to focus on one hand on the detailed synaptic mechanisms to be able to discretely manipulate them and on the other hand perform specific tests to link these mechanisms to functional motor output.

4.7 Conclusion and outlook

We could show that in the absence of RIM1α synaptic Ca^{2+}-currents are reduced and accordingly release probability is decreased and short-term potentiation is enhanced. This is line with other studies showing a reduced P_r and altered STP in RIM1α KO animals (Schoch et al., 2002; Fourcaudot et al., 2008). In the light of the double RIM1/2 KO studies (Han et al., 2011; Kaeser et al., 2011) we conclude that the defect in RIM1α KO mice is mainly caused by reduced Ca^{2+}-transients - presumably by a disrupted recruitment of P/Q- and N-type VDCCs to the active zone. Our work could also show that despite the lack of RIM1α and a reduced Ca^{2+}-influx, presynaptic LTP could be readily induced and was expressed normally. Together with the finding that direct phosphorylation of RIM1α is not needed for presynaptic LTP (Kaeser et al., 2008a) but the loss of the protein reduces Ca^{2+}-influx, we argue that RIM1α possibly shifts the threshold of induction at some synapses but is not an absolute requirement of cAMP-dependent, presynaptic LTP.

A central question for future research is the target protein of the cAMP - PKA signaling cascade triggered in presynaptic long-term potentiation. Synaptotagmin-12 seems to be one target but it has been suggested that other proteins might be involved as well (Kaeser-Woo et al., 2013). Still it is unknown by which mechanism Synaptotagmin-12 or other proteins increase release after phosphorylation but it will be a crucial step in order to determine the molecular mechanism of presynaptic LTP and its behavioral relevance.

Furthermore, our results together with others indicate that RIM1α might play a role in activity-dependent regulation of transmitter release during post-tetanic potentiation at the granule cell – PF connection. It would be interesting to further investigate this finding and possibly reveal a to date undescribed function of RIM1α in the regulation of synaptic plasticity.

Finally, this work could add another interesting feature of the properties of the ascending axon and the parallel fiber segment of the granule cell by showing that Ca^{2+}-influx is differentially regulated between both. If this is due to lower number of VDCCs or a distinct pattern of calcium channel subtypes remains unclear. Therefore, future experiments have to clarify the different synaptic characteristics that might reflect differential information processing in the cerebellum.

5 Appendix

5.1 References

Abbott LF, Regehr WG (2004) Synaptic computation. Nature 431:796–803.

Albus JS (1971) A theory of Cerebellar Function. Mathematical Biosciences 10:25-61.

Alle H, Geiger JRP (2006) Combined analog and action potential coding in hippocampal mossy fibers. Science 311:1290–1293.

Anastassiou CA, Perin R, Markram H, Koch C (2011) Ephaptic coupling of cortical neurons. Nat Neurosci 14:217–223.

Apps R, Garwicz M (2005) Anatomical and physiological foundations of cerebellar information processing. Nat Rev Neurosci 6:297–311.

Atluri PP, Regehr WG (1996) Determinants of the time course of facilitation at the granule cell to Purkinje cell synapse. J Neurosci 16:5661–5671.

Atluri PP, Regehr WG (1998) Delayed release of neurotransmitter from cerebellar granule cells. J Neurosci 18:8214–8227.

Barbour B, Häusser M (1997) Intersynaptic diffusion of neurotransmitter. Trends Neurosci 20:377–384.

Basu J, Shen N, Dulubova I, Lu J, Guan R, Guryev O, Grishin NV, Rosenmund C, Rizo J (2005) A minimal domain responsible for Munc13 activity. Nat Struct Mol Biol 12:1017–1018.

Bender VA, Pugh JR, Jahr CE (2009) Presynaptically expressed long-term potentiation increases multivesicular release at parallel fiber synapses. Journal of Neuroscience 29:10974–10978.

Bennett MV, Goodenough DA (1978) Gap junctions, electrotonic coupling, and intercellular communication. Neurosci Res Program Bull 16:1–486.

Blatow M, Caputi A, Burnashev N, Monyer H, Rozov A (2003) Ca^{2+} buffer saturation underlies paired pulse facilitation in calbindin-D28k-containing terminals. Neuron 38:79–88.

Bliss TV, Collingridge GL (1993) A synaptic model of memory: long-term potentiation in the hippocampus. Nature 361:31–39.

Bliss TV, Gardner-Medwin AR (1973) Long-lasting potentiation of synaptic transmission in the dentate area of the unanaestetized rabbit following stimulation of the perforant path. J Physiol (Lond) 232:357–374.

Bliss TV, Lomo T (1973) Long-lasting potentiation of synaptic transmission in the dentate area of the anaesthetized rabbit following stimulation of the perforant path. J Physiol (Lond) 232:331–356.

Blundell J, Kaeser PS, Südhof TC, Powell CM (2010) RIM1alpha and interacting proteins involved in presynaptic plasticity mediate prepulse inhibition and additional behaviors

linked to schizophrenia. Journal of Neuroscience 30:5326–5333.

Bocklisch C, Pascoli V, Wong JCY, House DRC, Yvon C, de Roo M, Tan KR, Luscher C (2013) Cocaine Disinhibits Dopamine Neurons by Potentiation of GABA Transmission in the Ventral Tegmental Area. Science 341:1521–1525.

Bortolotto ZA, Clarke VR, Delany CM, Parry MC, Smolders I, Vignes M, Ho KH, Miu P, Brinton BT, Fantaske R, Ogden A, Gates M, Ornstein PL, Lodge D, Bleakman D, Collingridge GL (1999) Kainate receptors are involved in synaptic plasticity. Nature 402:297–301.

Brenowitz SD, Regehr WG (2007) Reliability and heterogeneity of calcium signaling at single presynaptic boutons of cerebellar granule cells. Journal of Neuroscience 27:7888–7898.

Breustedt J, Gundlfinger A, Varoqueaux F, Reim K, Brose N, Schmitz D (2010) Munc13-2 differentially affects hippocampal synaptic transmission and plasticity. Cereb Cortex 20:1109–1120.

Breustedt J, Vogt KE, Miller RJ, Nicoll RA, Schmitz D (2003) Alpha1E-containing Ca^{2+} channels are involved in synaptic plasticity. Proc Natl Acad Sci USA 100:12450–12455.

Brose N, Hofmann K, Hata Y, Südhof TC (1995) Mammalian homologues of Caenorhabditis elegans unc-13 gene define novel family of C2-domain proteins. J Biol Chem 270:25273–25280.

Bruzzone R, Hormuzdi SG, Barbe MT, Herb A, Monyer H (2003) Pannexins, a family of gap junction proteins expressed in brain. Proc Natl Acad Sci USA 100:13644–13649.

Bucurenciu I, Kulik A, Schwaller B, Frotscher M, Jonas P (2008) Nanodomain coupling between Ca^{2+} channels and Ca^{2+} sensors promotes fast and efficient transmitter release at a cortical GABAergic synapse. Neuron 57:536–545.

Burke RE (2006) Sir Charles Sherrington's The integrative action of the nervous system: a centenary appreciation. Brain 130:887–894.

Carter AG, Regehr WG (2000) Prolonged synaptic currents and glutamate spillover at the parallel fiber to stellate cell synapse. J Neurosci 20:4423–4434.

Castillo PE (2012) Presynaptic LTP and LTD of Excitatory and Inhibitory Synapses. Cold Spring Harbor Perspectives in Biology 4:a005728–a005728.

Castillo PE, Janz R, Südhof TC, Tzounopoulos T, Malenka RC, Nicoll RA (1997a) Rab3A is essential for mossy fibre long-term potentiation in the hippocampus. Nature 388:590–593.

Castillo PE, Malenka RC, Nicoll RA (1997b) Kainate receptors mediate a slow postsynaptic current in hippocampal CA3 neurons. Nature 388:182–186.

Castillo PE, Schoch S, Schmitz F, Südhof TC, Malenka RC (2002) RIM1alpha is required for presynaptic long-term potentiation. Nature 415:327–330.

Castillo PE, Weisskopf MG, Nicoll RA (1994) The role of Ca^{2+} channels in hippocampal mossy fiber synaptic transmission and long-term potentiation. Neuron 12:261–269.

Catterall WA, Few AP (2008) Calcium channel regulation and presynaptic plasticity. Neuron 59:882–901.

Cesana E, Pietrajtis K, Bidoret C, Isope P, D'Angelo E, Dieudonné S, Forti L (2013) Granule cell ascending axon excitatory synapses onto Golgi cells implement a potent feedback circuit in the cerebellar granular layer. Journal of Neuroscience 33:12430–12446.

Chadderton P, Margrie TW, Häusser M (2004) Integration of quanta in cerebellar granule cells during sensory processing. Nature 428:856–860.

Chang W-P, Südhof TC (2009) SV2 renders primed synaptic vesicles competent for Ca^{2+} -induced exocytosis. Journal of Neuroscience 29:883–897.

Chaumonta J, Guyonb N, Valeraa AM, Dugueb GP, Popab D, Marcaggib P, Gautheronc V, Reibel-Foissetd S, Dieudonneb S, Stephane A, Barrota M, Casself J-C, Duponta J-L, Doussaua F, Poulaina B, Fekrije Selimic, Clement Lenab, Isope P (2013) Clusters of cerebellar Purkinje cells control their afferent climbing fiber discharge. Proc Natl Acad Sci USA 110:16223–16228

Chen C, Regehr WG (1997) The mechanism of cAMP-mediated enhancement at a cerebellar synapse. J Neurosci 17:8687–8694.

Chen G, Harata NC, Tsien RW (2004) Paired-pulse depression of unitary quantal amplitude at single hippocampal synapses. Proc Natl Acad Sci USA 101:1063–1068.

Chen L, Bao S, Qiao X, Thompson RF (1999) Impaired cerebellar synapse maturation in waggler, a mutant mouse with a disrupted neuronal calcium channel gamma subunit. Proc Natl Acad Sci USA 96:12132–12137.

Chevaleyre V, Heifets BD, Kaeser PS, Südhof TC, Purpura DP, Castillo PE (2007) Endocannabinoid-mediated long-term plasticity requires cAMP/PKA signaling and RIM1alpha. Neuron 54:801–812.

Chiovini B, Turi GF, Katona G, Kaszás A, Erdélyi F, Szabó G, Monyer H, Csákányi A, Vizi ES, Rózsa B (2010) Enhanced dendritic action potential backpropagation in parvalbumin-positive basket cells during sharp wave activity. Neurochem Res 35:2086–2095.

Christie JM, Chiu DN, Jahr CE (2011) Ca(2+)-dependent enhancement of release by subthreshold somatic depolarization. Nat Neurosci 14:62–68.

Christie JM, Jahr CE (2006) Multivesicular release at Schaffer collateral-CA1 hippocampal synapses. Journal of Neuroscience 26:210–216.

Clements JD, Lester RA, Tong G, Jahr CE, Westbrook GL (1992) The time course of glutamate in the synaptic cleft. Science 258:1498–1501.

Clements JD, Silver RA (2000) Unveiling synaptic plasticity: a new graphical and analytical approach. Trends Neurosci 23:105–113.

Collingridge GL, Kehl SJ, McLennan H (1983) Excitatory amino acids in synaptic transmission in the Schaffer collateral-commissural pathway of the rat hippocampus. J Physiol (Lond) 334:33–46.

Combe G, Combe A (1838) On the functions of the cerebellum by Drs Gall, Vimont and Broussais. Translated from the French by Combe G.

Coppola T, Magnin-Luthi S, Perret-Menoud V, Gattesco S, Schiavo G, Regazzi R (2001) Direct interaction of the Rab3 effector RIM with Ca2+ channels, SNAP-25, and synaptotagmin. J Biol Chem 276:32756–32762.

Custer KL, Austin NS, Sullivan JM, Bajjalieh SM (2006) Synaptic vesicle protein 2 enhances release probability at quiescent synapses. Journal of Neuroscience 26:1303–1313.

D'Angelo E, Casali S (2012) Seeking a unified framework for cerebellar function and dysfunction: from circuit operations to cognition. Front Neural Circuits 6:116.

De Zeeuw CI, Hoebeek FE, Bosman LWJ, Schonewille M, Witter L, Koekkoek SK (2011) Spatiotemporal firing patterns in the cerebellum. Nature Reviews Neuroscience:1–18.

DeFelipe J (2002) Sesquicentenary of the birthday of Santiago Ramón y Cajal, the father of modern neuroscience. Trends in Neurosciences 25: 481-484.

del Castillo J, Katz B (1954a) The effect of magnesium on the activity of motor nerve endings. J Physiol (Lond) 124:553–559.

del Castillo J, Katz B (1954b) Quantal components of the end-plate potential. J Physiol (Lond) 124:560–573.

Deng L, Kaeser PS, Xu W, Südhof TC (2011) RIM proteins activate vesicle priming by reversing autoinhibitory homodimerization of Munc13. Neuron 69:317–331.

Dietrich D, Kirschstein T, Kukley M, Pereverzev A, Brelie von der C, Schneider T, Beck H (2003) Functional specialization of presynaptic Cav2.3 Ca^{2+} channels. Neuron 39:483–496.

Dittman JS, Kreitzer AC, Regehr WG (2000) Interplay between facilitation, depression, and residual calcium at three presynaptic terminals. J Neurosci 20:1374–1385.

Dodge FA, Rahamimoff R (1967) Co-operative action a calcium ions in transmitter release at the neuromuscular junction. J Physiol (Lond) 193:419–432.

Draguhn A, Traub RD, Schmitz D, Jefferys JG (1998) Electrical coupling underlies high-frequency oscillations in the hippocampus in vitro. Nature 394:189–192.

Dulubova I, Lou X, Lu J, Huryeva I, Alam A, Schneggenburger R, Südhof TC, Rizo J (2005) A Munc13/RIM/Rab3 tripartite complex: from priming to plasticity? EMBO J 24:2839–2850.

Dumoulin A, Triller A, Dieudonné S (2001) IPSC kinetics at identified GABAergic and mixed GABAergic and glycinergic synapses onto cerebellar Golgi cells. Journal of Neuroscience 21:6045–6057.

Eccles SJC, Ito M, Szentägothai J (1967) The cerebellum as a neuronal machine. Berlin, Springer-Verlag, 1967

Ekerot C-F, Jörntell H (2008) Synaptic integration in cerebellar granule cells. Cerebellum 7:539–541.

Fatt P, Katz B (1952) Spontaneous subthreshold activity at motor nerve endings. J Physiol (Lond) 117:109–128.

Felmy F, Neher E, Schneggenburger R (2003) Probing the intracellular calcium sensitivity of transmitter release during synaptic facilitation. Neuron 37:801–811.

Fioravante D, Chu Y, Myoga MH, Leitges M, Regehr WG (2011) Calcium-dependent isoforms of protein kinase C mediate posttetanic potentiation at the calyx of Held. Neuron 70:1005–1019.

Fioravante D, Myoga MH, Leitges M, Regehr WG (2012) Adaptive regulation maintains posttetanic potentiation at cerebellar granule cell synapses in the absence of calcium-dependent PKC. Journal of Neuroscience 32:13004–13009.

Fioravante D, Regehr WG (2011) Short-term forms of presynaptic plasticity. Curr Opin Neurobiol 21:269–274.

Foster KA, Crowley JJ, Regehr WG (2005) The influence of multivesicular release and postsynaptic receptor saturation on transmission at granule cell to Purkinje cell synapses. Journal of Neuroscience 25:11655–11665.

Fourcaudot E, Gambino F, Humeau Y, Casassus G, Shaban H, Poulain B, Lüthi A (2008) cAMP/PKA signaling and RIM1alpha mediate presynaptic LTP in the lateral amygdala. Proceedings of the National Academy of Sciences 105:15130–15135.

Fukuda M (2003) Distinct Rab Binding Specificity of Rim1, Rim2, Rabphilin, and Noc2. Journal of Biological Chemistry 278:15373–15380.

Galliano E, Gao Z, Schonewille M, Todorov B, Simons E, Pop AS, D'Angelo E, van den Maagdenberg AMJM, Hoebeek FE, De Zeeuw CI (2013a) Silencing the Majority of Cerebellar Granule Cells Uncovers Their Essential Role in Motor Learning and Consolidation. CellReports 3:1239–1251.

Galliano E, Potters J-W, Ype Elgersma, Wisden W, Kushner SA, Chris I De Zeeuw, Hoebeek FE (2013b) Synaptic Transmission and Plasticity at Inputs to Murine Cerebellar Purkinje Cells Are Largely Dispensable for Standard Nonmotor Tasks. Journal of Neuroscience:1–20.

Garwicz M, Jörntell H, Ekerot CF (1998) Cutaneous receptive fields and topography of mossy fibres and climbing fibres projecting to cat cerebellar C3 zone. J Physiol (Lond) 512 (Pt 1):277–293.

Geppert M, Goda Y, Stevens CF, Südhof TC (1997) The small GTP-binding protein Rab3A regulates a late step in synaptic vesicle fusion. Nature 387:810–814.

Gerber SH, Rah J-C, Min S-W, Liu X, de Wit H, Dulubova I, Meyer AC, Rizo J, Arancillo M, Hammer RE, Verhage M, Rosenmund C, Südhof TC (2008) Conformational switch of syntaxin-1 controls synaptic vesicle fusion. Science 321:1507–1510.

Giaume C, Koulakoff A, Roux L, Holcman D, Rouach N (2010) Astroglial networks: a step further in neuroglial and gliovascular interactions. Nat Rev Neurosci 11:87–99.

Glickstein M, Strata P, Voogd J (2009) Cerebellum: history. Neuroscience 162:549–559.

Golgi C (1873) Sulla struttura della sostanza grigia del cervello. Gazz Med Ital Lombardia:244–246.

Grynkiewicz G, Poenie M, Tsien RY (1985) A new generation of Ca^{2+} indicators with greatly improved fluorescence properties. J Biol Chem 260:3440–3450.

Hallermann S, Kittel RJ, Wichmann C, Weyhersmüller A, Fouquet W, Mertel S, Owald D, Eimer S, Depner H, Schwärzel M, Sigrist SJ, Heckmann M (2010) Naked dense bodies provoke depression. Journal of Neuroscience 30:14340–14345.

Hammond C (2012) Cellular and Molecular Neurobiology. Elsevier.

Han Y, Kaeser PS, Südhof TC, Schneggenburger R (2011) RIM determines Ca^{2+} channel density and vesicle docking at the presynaptic active zone. Neuron 69:304–316.

Harris AL, Spray DC, Bennett MV (1983) Control of intercellular communication by voltage dependence of gap junctional conductance. J Neurosci 3:79–100.

Harris EW, Cotman CW (1986) Long-term potentiation of guinea pig mossy fiber responses is not blocked by N-methyl D-aspartate antagonists. Neurosci Lett 70:132–137.

Hashimoto K, Fukaya M, Qiao X, Sakimura K, Watanabe M, Kano M (1999) Impairment of AMPA receptor function in cerebellar granule cells of ataxic mutant mouse stargazer. Journal of Neuroscience 19:6027–6036.

Heuser JE, Reese TS, Dennis MJ, Jan Y, Jan L, Evans L (1979) Synaptic vesicle exocytosis captured by quick freezing and correlated with quantal transmitter release. J Cell Biol 81:275–300.

Hibino H, Pironkova R, Onwumere O, Vologodskaia M, Hudspeth AJ, Lesage F (2002) RIM binding proteins (RBPs) couple Rab3-interacting molecules (RIMs) to voltage-gated Ca(2+) channels. Neuron 34:411–423.

Ho VM, Lee JA, Martin KC (2011) The Cell Biology of Synaptic Plasticity. Science 334:623–628.

Hosoi N, Holt M, Sakaba T (2009) Calcium dependence of exo- and endocytotic coupling at a glutamatergic synapse. Neuron 63:216–229.

Huang C-M, Wang L, Huang RH (2006) Cerebellar granule cell: ascending axon and parallel fiber. Eur J Neurosci 23:1731–1737.

Huang YH (2004) Climbing Fiber Activation of EAAT4 Transporters and Kainate Receptors in Cerebellar Purkinje Cells. Journal of Neuroscience 24:103–111.

Hull C, Regehr WG (2012) Identification of an Inhibitory Circuit that Regulates Cerebellar Golgi Cell Activity. Neuron 73:149–158.

Ito M (1984) The cerebellum and neural control. Raven Press.

Ito M (2006) Cerebellar circuitry as a neuronal machine. Prog Neurobiol 78:272–303.

Ito M (2011) The Cerebellum: Brain for an Implicit Self. FT Press, USA.

Jackson AC, Nicoll RA (2011) The expanding social network of ionotropic glutamate receptors: TARPs and other transmembrane auxiliary subunits. Neuron 70:178–199.

Jefferys JG (1995) Nonsynaptic modulation of neuronal activity in the brain: electric currents and extracellular ions. Physiol Rev 75:689–723.

Jones MV, Westbrook GL (1996) The impact of receptor desensitization on fast synaptic transmission. Trends Neurosci 19:96–101.

Kaeser PS, Deng L, Fan M, Südhof TC (2012) RIM genes differentially contribute to organizing presynaptic release sites. Proceedings of the National Academy of Sciences.

Kaeser PS, Deng L, Wang Y, Dulubova I, Liu X, Rizo J, Südhof TC (2011) RIM proteins tether Ca2+ channels to presynaptic active zones via a direct PDZ-domain interaction. Cell 144:282–295.

Kaeser PS, Kwon H-B, Blundell J, Chevaleyre V, Morishita W, Malenka RC, Powell CM, Castillo PE, Südhof TC (2008a) RIM1alpha phosphorylation at serine-413 by protein kinase A is not required for presynaptic long-term plasticity or learning. Proceedings of the National Academy of Sciences 105:14680–14685.

Kaeser PS, Kwon H-B, Chiu CQ, Deng L, Castillo PE, Südhof TC (2008b) RIM1alpha and RIM1beta are synthesized from distinct promoters of the RIM1 gene to mediate differential but overlapping synaptic functions. Journal of Neuroscience 28:13435–13447.

Kaeser PS, Südhof TC (2005) RIM function in short- and long-term synaptic plasticity. Biochem Soc Trans 33:1345–1349.

Kaeser-Woo YJ, Younts TJ, Yang X, Zhou P, Wu D, Castillo PE, Südhof TC (2013) Synaptotagmin-12 Phosphorylation by cAMP-Dependent Protein Kinase Is Essential for Hippocampal Mossy Fiber LTP. Journal of Neuroscience 33:9769–9780.

Kandel ER, Schwartz JH (1982) Molecular biology of learning: modulation of transmitter release. Science 218:433–443.

Katz B, Miledi R (1965) The Effect of Calcium on Acetylcholine Release from Motor Nerve Terminals. Proc R Soc Lond, B, Biol Sci 161:496–503.

Katz B, Miledi R (1968) The role of calcium in neuromuscular facilitation. J Physiol (Lond) 195:481–492.

Kawamura Y, Manita S, Nakamura T, Inoue M, Kudo Y, Miyakawa H (2004) Glutamate release increases during mossy-CA3 LTP but not during Schaffer-CA1 LTP. European Journal of Neuroscience 19:1591–1600.

Kiyonaka S, Wakamori M, Miki T, Uriu Y, Nonaka M, Bito H, Beedle AM, Mori E, Hara Y, De Waard M, Kanagawa M, Itakura M, Takahashi M, Campbell KP, Mori Y (2007) RIM1 confers sustained activity and neurotransmitter vesicle anchoring to presynaptic Ca^{2+} channels. Nat Neurosci 10:691–701.

Kochubey O, Han Y, Schneggenburger R (2009) Developmental regulation of the intracellular Ca^{2+} sensitivity of vesicle fusion and Ca^{2+}-secretion coupling at the rat calyx of Held. J

Physiol (Lond) 587:3009–3023.

Kochubey O, Lou X, Schneggenburger R (2011) Regulation of transmitter release by Ca(2+) and synaptotagmin: insights from a large CNS synapse. Trends Neurosci 34:237–246.

Korogod N, Lou X, Schneggenburger R (2007) Posttetanic potentiation critically depends on an enhanced Ca(2+) sensitivity of vesicle fusion mediated by presynaptic PKC. Proc Natl Acad Sci USA 104:15923–15928.

Kreitzer AC, Regehr WG (2001) Retrograde inhibition of presynaptic calcium influx by endogenous cannabinoids at excitatory synapses onto Purkinje cells. Neuron 29:717–727.

Le Guen M-C, De Zeeuw CI (2010) Presynaptic plasticity at cerebellar parallel fiber terminals. Funct Neurol 25:141–151.

Lerma J (2006) Kainate receptor physiology. Current Opinion in Pharmacology 6:89–97.

Linden DJ, Ahn S (1999) Activation of presynaptic cAMP-dependent protein kinase is required for induction of cerebellar long-term potentiation. J Neurosci 19:10221–10227.

Lipstein N, Sakaba T, Cooper BH, Lin K-H, Strenzke N, Ashery U, Rhee J-S, Taschenberger H, Neher E, Brose N (2013) Dynamic control of synaptic vesicle replenishment and short-term plasticity by Ca(2+)-calmodulin-Munc13-1 signaling. Neuron 79:82–96.

Liu KSY, Siebert M, Mertel S, Knoche E, Wegener S, Wichmann C, Matkovic T, Muhammad K, Depner H, Mettke C, Buckers J, Hell SW, Muller M, Davis GW, Schmitz D, Sigrist SJ (2011) RIM-Binding Protein, a Central Part of the Active Zone, Is Essential for Neurotransmitter Release. Science 334:1565–1569.

Lonart G, Schoch S, Kaeser PS, Larkin CJ, Südhof TC, Linden DJ (2003) Phosphorylation of RIM1alpha by PKA triggers presynaptic long-term potentiation at cerebellar parallel fiber synapses. Cell 115:49–60.

Lou X, Scheuss V, Schneggenburger R (2005) Allosteric modulation of the presynaptic Ca^{2+} sensor for vesicle fusion. Nature 435:497–501.

Ma C, Li W, Xu Y, Rizo J (2011) Munc13 mediates the transition from the closed syntaxin-Munc18 complex to the SNARE complex. Nat Struct Mol Biol 18:542–549.

Malenka RC, Bear MF (2004) LTP and LTD: an embarrassment of riches. Neuron 44:5–21.

Marr D (1969) A theory of cerebellar cortex. J Physiol (Lond) 202:437–470.

Martin SJ, Grimwood PD, Morris RG (2000) Synaptic plasticity and memory: an evaluation of the hypothesis. Annu Rev Neurosci 23:649–711.

Martin SJ, Morris RGM (2002) New life in an old idea: the synaptic plasticity and memory hypothesis revisited. Hippocampus 12:609–636.

McAlonan GM, Daly E, Kumari V, Critchley HD, van Amelsvoort T, Suckling J, Simmons A, Sigmundsson T, Greenwood K, Russell A, Schmitz N, Happe F, Howlin P, Murphy DGM (2002) Brain anatomy and sensorimotor gating in Asperger's syndrome. Brain 125:1594–1606.

McNaughton BL, Morris RGM (1987) Hippocampal synaptic enhancement and information storage within a distributed memory system. Trends Neurosci 10:1–8.

Mellor J, Nicoll RA (2001) Hippocampal mossy fiber LTP is independent of postsynaptic calcium. Nat Neurosci 4:125–126.

Miall RC, Christensen LOD, Cain O, Stanley J (2007) Disruption of state estimation in the human lateral cerebellum. PLoS Biol 5:e316.

Mintz IM, Sabatini BL, Regehr WG (1995) Calcium control of transmitter release at a cerebellar synapse. Neuron 15:675–688.

Mittelstaedt T, Alvaréz-Baron E, Schoch S (2010) RIM proteins and their role in synapse function. Biol Chem 391:599–606.

Mochida S, Few AP, Scheuer T, Catterall WA (2008) Regulation of presynaptic Ca(V)2.1 channels by Ca2+ sensor proteins mediates short-term synaptic plasticity. Neuron 57:210–216.

Morris RG (1989) Synaptic plasticity and learning: selective impairment of learning rats and blockade of long-term potentiation in vivo by the N-methyl-D-aspartate receptor antagonist AP5. J Neurosci 9:3040–3057.

Morris RG, Anderson E, Lynch GS, Baudry M (1986) Selective impairment of learning and blockade of long-term potentiation by an N-methyl-D-aspartate receptor antagonist, AP5. Nature 319:774–776.

Myoga MH, Regehr WG (2011) Calcium microdomains near R-type calcium channels control the induction of presynaptic long-term potentiation at parallel fiber to purkinje cell synapses. Journal of Neuroscience 31:5235–5243.

Neher E (1998) Usefulness and limitations of linear approximations to the understanding of Ca2+ signals. Cell Calcium 24:345–357.

Neher E, Sakaba T (2008) Multiple roles of calcium ions in the regulation of neurotransmitter release. Neuron 59:861–872.

Ng D, Pitcher GM, Szilard RK, Sertié A, Kanisek M, Clapcote SJ, Lipina T, Kalia LV, Joo D, McKerlie C, Cortez M, Roder JC, Salter MW, McInnes RR (2009) Neto1 is a novel CUB-domain NMDA receptor-interacting protein required for synaptic plasticity and learning. PLoS Biol 7:e41.

Nicoll RA, Malenka RC (1995) Contrasting properties of two forms of long-term potentiation in the hippocampus. Nature 377:115–118.

Nicoll RA, Roche KW (2013) Long-term potentiation: peeling the onion. Neuropharmacology 74:18–22.

Nicoll RA, Schmitz D (2005) Synaptic plasticity at hippocampal mossy fibre synapses. Nat Rev Neurosci 6:863–876.

Ohno-Shosaku T, Maejima T, Kano M (2001) Endogenous cannabinoids mediate retrograde signals from depolarized postsynaptic neurons to presynaptic terminals. Neuron 29:729–738.

Oláh S, Füle M, Komlósi G, Varga C, Báldi R, Barzó P, Tamás G (2009) Regulation of cortical microcircuits by unitary GABA-mediated volume transmission. Nature 461:1278–1281.

Oliet SH, Piet R, Poulain DA (2001) Control of glutamate clearance and synaptic efficacy by glial coverage of neurons. Science 292:923–926.

Owald D, Khorramshahi O, Gupta VK, Banovic D, Depner H, Fouquet W, Wichmann C, Mertel S, Eimer S, Reynolds E, Holt M, Aberle H, Sigrist SJ (2012) Cooperation of Syd-1 with Neurexin synchronizes pre- with postsynaptic assembly. Nat Neurosci 15:1219–1226.

Pannasch U, Rouach N (2013) Emerging role for astroglial networks in information processing: from synapse to behavior. Trends Neurosci.

Pannasch U, Vargová L, Reingruber J, Ezan P, Holcman D, Giaume C, Syková E, Rouach N (2011) Astroglial networks scale synaptic activity and plasticity. Proceedings of the National Academy of Sciences 108:8467–8472.

Pelkey KA, Topolnik L, Lacaille J-C, McBain CJ (2006) Compartmentalized Ca(2+) channel regulation at divergent mossy-fiber release sites underlies target cell-dependent plasticity. Neuron 52:497–510.

Perkel DJ, Hestrin S, Sah P, Nicoll RA (1990) Excitatory synaptic currents in Purkinje cells. Proc Biol Sci 241:116–121.

Pichitpornchai C, Rawson JA, Rees S (1994) Morphology of parallel fibres in the cerebellar cortex of the rat: an experimental light and electron microscopic study with biocytin. J Comp Neurol 342:206–220.

Pierce KL, Premont RT, Lefkowitz RJ (2002) Seven-transmembrane receptors. Nat Rev Mol Cell Biol 3:639–650.

Pinheiro PS, Mulle C (2008) Presynaptic glutamate receptors: physiological functions and mechanisms of action. Nat Rev Neurosci 9:423–436.

Pouget A, Beck JM, Ma WJ, Latham PE (2013) Probabilistic brains: knowns and unknowns. Nat Neurosci 16:1170–1178.

Powell CM, Schoch S, Monteggia L, Barrot M, Matos MF, Feldmann N, Südhof TC, Nestler EJ (2004) The presynaptic active zone protein RIM1alpha is critical for normal learning and memory. Neuron 42:143–153.

Ramirez S, Liu X, Lin P-A, Suh J, Pignatelli M, Redondo RL, Ryan TJ, Tonegawa S (2013) Creating a false memory in the hippocampus. Science 341:387–391.

Redman S (1990) Quantal analysis of synaptic potentials in neurons of the central nervous system. Physiol Rev 70:165–198.

Reichert H (1992) Introduction to Neurobiology. Oxford University Press.

Reid CA, Bekkers JM, Clements JD (1998) N- and P/Q-type Ca2+ channels mediate transmitter release with a similar cooperativity at rat hippocampal autapses. J Neurosci 18:2849–2855.

Reid CA, Clements JD (1999) Postsynaptic expression of long-term potentiation in the rat

dentate gyrus demonstrated by variance-mean analysis. J Physiol (Lond) 518 (Pt 1):121–130.

Reim K, Mansour M, Varoqueaux F, McMahon HT, Südhof TC, Brose N, Rosenmund C (2001) Complexins regulate a late step in Ca2+-dependent neurotransmitter release. Cell 104:71–81.

Rosenmund C, Sigler A, Augustin I, Reim K, Brose N, Rhee J-S (2002) Differential control of vesicle priming and short-term plasticity by Munc13 isoforms. Neuron 33:411–424.

Rost BR, Nicholson P, Ahnert-Hilger G, Rummel A, Rosenmund C, Breustedt J, Schmitz D (2011) Activation of metabotropic GABA receptors increases the energy barrier for vesicle fusion. J Cell Sci 124:3066–3073.

Sabatini BL, Regehr WG (1997) Control of neurotransmitter release by presynaptic waveform at the granule cell to Purkinje cell synapse. J Neurosci 17:3425–3435.

Salin PA, Malenka RC, Nicoll RA (1996) Cyclic AMP mediates a presynaptic form of LTP at cerebellar parallel fiber synapses. Neuron 16:797–803.

Sasaki T, Matsuki N, Ikegaya Y (2011) Action-potential modulation during axonal conduction. Science 331:599–601.

Scanziani M, Salin PA, Vogt KE, Malenka RC, Nicoll RA (1997) Use-dependent increases in glutamate concentration activate presynaptic metabotropic glutamate receptors. Nature 385:630–634.

Schmahmann JD (2010) The role of the cerebellum in cognition and emotion: personal reflections since 1982 on the dysmetria of thought hypothesis, and its historical evolution from theory to therapy. Neuropsychol Rev 20:236–260.

Schmidt H, Brachtendorf S, Arendt O, Hallermann S, Ishiyama S, Bornschein G, Gall D, Schiffmann SN, Heckmann M, Eilers J (2012) Nanodomain Coupling at an Excitatory Cortical Synapse. Curr Biol.

Schmitz D, Schuchmann S, Fisahn A, Draguhn A, Buhl EH, Petrasch-Parwez E, Dermietzel R, Heinemann U, Traub RD (2001) Axo-axonal coupling. a novel mechanism for ultrafast neuronal communication. Neuron 31:831–840.

Schneggenburger R, Han Y, Kochubey O (2012) Ca2+ channels and transmitter release at the active zone. Cell Calcium:1–9.

Schoch S, Castillo PE, Jo T, Mukherjee K, Geppert M, Wang Y, Schmitz F, Malenka RC, Südhof TC (2002) RIM1alpha forms a protein scaffold for regulating neurotransmitter release at the active zone. Nature 415:321–326.

Schoch S, Mittelstaedt T, Kaeser PS, Padgett D, Feldmann N, Chevaleyre V, Castillo PE, Hammer RE, Han W, Schmitz F, Lin W, Südhof TC (2006) Redundant functions of RIM1alpha and RIM2alpha in Ca(2+)-triggered neurotransmitter release. EMBO J 25:5852–5863.

Shepherd GM (2003) The Synaptic Organization of the Brain. Oxford University Press, USA.

Shepherd GM (2010) Handbook of Brain Microcircuits. Oxford University Press.

Shin O-H, Lu J, Rhee J-S, Tomchick DR, Pang ZP, Wojcik SM, Camacho-Perez M, Brose N, Machius M, Rizo J, Rosenmund C, Südhof TC (2010) Munc13 C2B domain is an activity-dependent Ca^{2+} regulator of synaptic exocytosis. Nat Struct Mol Biol 17:280–288.

Shu Y, Hasenstaub A, Duque A, Yu Y, McCormick DA (2006) Modulation of intracortical synaptic potentials by presynaptic somatic membrane potential. Nature 441:761–765.

Sims RE, Hartell NA (2005) Differences in transmission properties and susceptibility to long-term depression reveal functional specialization of ascending axon and parallel fiber synapses to Purkinje cells. Journal of Neuroscience 25:3246–3257.

Sims RE, Hartell NA (2006) Differential susceptibility to synaptic plasticity reveals a functional specialization of ascending axon and parallel fiber synapses to cerebellar Purkinje cells. Journal of Neuroscience 26:5153–5159.

Storm DR, Hansel C, Hacker B, Parent A, Linden DJ (1998) Impaired cerebellar long-term potentiation in type I adenylyl cyclase mutant mice. Neuron 20:1199–1210.

Straub C, Hunt DL, Yamasaki M, Kim KS, Watanabe M, Castillo PE, Tomita S (2011) Distinct functions of kainate receptors in the brain are determined by the auxiliary subunit Neto1. Nat Neurosci 14:866–873.

Sun J, Pang ZP, Qin D, Fahim AT, Adachi R, Südhof TC (2007) A dual-Ca^{2+}-sensor model for neurotransmitter release in a central synapse. Nature 450:676–682.

Südhof TC (2012) The Presynaptic Active Zone. Neuron 75:11–25.

Südhof TC, Rizo J (2011) Synaptic vesicle exocytosis. Cold Spring Harbor Perspectives in Biology 3.

Svoboda K, Yasuda R (2006) Principles of two-photon excitation microscopy and its applications to neuroscience. Neuron 50:823–839.

Takahashi T, Kajikawa Y, Tsujimoto T (1998) G-Protein-coupled modulation of presynaptic calcium currents and transmitter release by a GABAB receptor. J Neurosci 18:3138–3146.

Thompson SM, Gähwiler BH (1989) Activity-dependent disinhibition. III. Desensitization and GABAB receptor-mediated presynaptic inhibition in the hippocampus in vitro. J Neurophysiol 61:524–533.

Timmann D, Drepper J, Frings M, Maschke M, Richter S, Gerwig M, Kolb FP (2010) The human cerebellum contributes to motor, emotional and cognitive associative learning. A review. CORTEX 46:845–857.

Tong G, Malenka RC, Nicoll RA (1996) Long-term potentiation in cultures of single hippocampal granule cells: a presynaptic form of plasticity. Neuron 16:1147–1157.

Triller A, Korn H (1982) Transmission at a central inhibitory synapse. III. Ultrastructure of physiologically identified and stained terminals. J Neurophysiol 48:708–736.

Tsai PT, Hull C, Chu Y, Greene-Colozzi E, Sadowski AR, Leech JM, Steinberg J, Crawley JN, Regehr WG, Sahin M (2012) Autistic-like behaviour and cerebellar dysfunction in Purkinje cell Tsc1 mutant mice. Nature:1–6.

Ventura R, Harris KM (1999) Three-dimensional relationships between hippocampal synapses and astrocytes. Journal of Neuroscience 19:6897–6906.

Vervaeke K, Lorincz A, Nusser Z, Silver RA (2012) Gap Junctions Compensate for Sublinear Dendritic Integration in an Inhibitory Network. Science.

Vignes M, Collingridge GL (1997) The synaptic activation of kainate receptors. Nature 388:179–182.

Wadiche JI, Jahr CE (2001) Multivesicular release at climbing fiber-Purkinje cell synapses. Neuron 32:301–313.

Wang H, Pineda VV, Chan GCK, Wong ST, Muglia LJ, Storm DR (2003) Type 8 adenylyl cyclase is targeted to excitatory synapses and required for mossy fiber long-term potentiation. Journal of Neuroscience 23:9710–9718.

Wang Y, Okamoto M, Schmitz F, Hofmann K, Südhof TC (1997) Rim is a putative Rab3 effector in regulating synaptic-vesicle fusion. Nature 388:593–598.

Weisskopf MG, Castillo PE, Zalutsky RA, Nicoll RA (1994) Mediation of hippocampal mossy fiber long-term potentiation by cyclic AMP. Science 265:1878–1882.

Williams S, Johnston D (1989) Long-term potentiation of hippocampal mossy fiber synapses is blocked by postsynaptic injection of calcium chelators. Neuron 3:583–588.

Wilson RI, Nicoll RA (2001) Endogenous cannabinoids mediate retrograde signalling at hippocampal synapses. Nature 410:588–592.

Wolpert DM, Flanagan JR (2001) Motor prediction. Current Biology 11:R729–R732.

Wolpert DM, Ghahramani Z, Jordan MI (1995) An internal model for sensorimotor integration. Science 269:1880–1882.

Wozny C, Maier N, Fidzinski P, Breustedt J, Behr J, Schmitz D (2008) Differential cAMP signaling at hippocampal output synapses. Journal of Neuroscience 28:14358–14362.

Xu J, Mashimo T, Südhof TC (2007) Synaptotagmin-1, -2, and -9: Ca(2+) sensors for fast release that specify distinct presynaptic properties in subsets of neurons. Neuron 54:567–581.

Xu-Friedman MA, Harris KM, Regehr WG (2001) Three-dimensional comparison of ultrastructural characteristics at depressing and facilitating synapses onto cerebellar Purkinje cells. Journal of Neuroscience 21:6666–6672.

Xue M, Stradomska A, Chen H, Brose N, Zhang W, Rosenmund C, Reim K (2008) Complexins facilitate neurotransmitter release at excitatory and inhibitory synapses in mammalian central nervous system. Proceedings of the National Academy of Sciences 105:7875–7880.

Yang Y, Calakos N (2010) Acute in vivo genetic rescue demonstrates that phosphorylation of RIM1alpha serine 413 is not required for mossy fiber long-term potentiation. Journal of Neuroscience 30:2542–2546.

Yang Y, Calakos N (2013) Presynaptic long-term plasticity. Front Synaptic Neurosci 5:8.

Yasuda R, Nimchinsky EA, Scheuss V, Pologruto TA, Oertner TG, Sabatini BL, Svoboda K (2004) Imaging calcium concentration dynamics in small neuronal compartments. Sci STKE 2004:pl5.

Yeckel MF, Kapur A, Johnston D (1999) Multiple forms of LTP in hippocampal CA3 neurons use a common postsynaptic mechanism. Nat Neurosci 2:625–633.

Zalutsky RA, Nicoll RA (1990) Comparison of two forms of long-term potentiation in single hippocampal neurons. Science 248:1619–1624.

Zalutsky RA, Nicoll RA (1992) Mossy fiber long-term potentiation shows specificity but no apparent cooperativity. Neurosci Lett 138:193–197.

Zhang W, Linden DJ (2009) Neuromodulation at single presynaptic boutons of cerebellar parallel fibers is determined by bouton size and basal action potential-evoked Ca transient amplitude. Journal of Neuroscience 29:15586–15594.

Ziv NE, Garner CC (2004) Cellular and molecular mechanisms of presynaptic assembly. Nat Rev Neurosci 5:385–399.

Zucker RS, Regehr WG (2002) Short-term synaptic plasticity. Annu Rev Physiol 64:355–405.

5.2 Abbreviations

$[Ca^{2+}]$	Ca^{2+}-concentration
2PLSM	2-photon laser scanning microscopy
γDGG	gamma-D-glutamylglycine
A	
AA	ascending axon
AMPAR	α-amino-3-hydroxy-5-methyl-4-isoxazole propionic acid receptor
AP	action potential
C	
Ca^{2+}	calcium ions
cAMP	cyclic adenosine monophophate
CNS	central nervous system
CF	climbing fiber
E	
EPSC	excitatory postsynaptic current
G	
GDP	guanosine diphosphate
GTP	Guanosine triphosphate
K	
KAR	kainate receptor
KO	(genetic) knockout
L	
LTD	long-term depression
LTP	long-term potentiation
M	
Mg^{2+}	magnesium ions
N	
NMDAR	N-methyl-D-aspartate receptors
P	
PC	Purkinje cell
PF	parallel fiber
PKA	protein kinase A
PPR	paired-pulse ratio
P_r	release probability
PTP	post-tetanic potentiation
R	
RIM	Rab-interacting molecule
S	
STP	short-term plasticity
TARP	transmembrane AMPAR regulatory protein
V	
VDCC	voltage-dependent Ca^{2+}-channel
W	
wt	wildtype

5.3 Curriculum Vitae

Mein Lebenslauf wird aus datenschutzrechtlichen Gründen in der elektronischen Version meiner Arbeit nicht veröffentlicht.

5.4 Publications

Kintscher M, Wozny C, Johenning FW, Schmitz D*, Breustedt J*. Role of RIM1α in short- and long-term synaptic plasticity at cerebellar parallel fibres. Nature Communications. 2013 Sep 3;4:2392.

Kononenko NL, Diril MK, Puchkov D, Kintscher M, Koo SJ, Pfuhl G, et al. Compromised fidelity of endocytic synaptic vesicle protein sorting in the absence of stonin 2. Proceedings of the National Academy of Sciences. 2013 Jan 23.

Kintscher M, Breustedt J, Miceli S, Schmitz D, Wozny C. Group II Metabotropic Glutamate Receptors Depress Synaptic Transmission onto Subicular Burst Firing Neurons. PLoS ONE. 2012;7(9):e45039.

Trimbuch T*, Beed P*, Vogt J*, Schuchmann S, Maier N, Kintscher M, et al. Synaptic PRG-1 modulates excitatory transmission via lipid phosphate-mediated signaling. Cell. 2009 Sep 18;138(6):1222–35.

Sawallisch C, Berhörster K, Disanza A, Mantoani S, Kintscher M, Stoenica L, et al. The insulin receptor substrate of 53 kDa (IRSp53) limits hippocampal synaptic plasticity. J Biol Chem. 2009 Apr 3;284(14):9225–36.

5.5 Erklärung an Eides statt

Ich, Michael Kintscher, versichere an Eides statt durch meine eigenhändige Unterschrift, dass ich die vorgelegte Dissertation mit dem Thema: „The Role of RIM1α in Synaptic Plasticity at the Cerebellar Parallel Fiber“ selbstständig und ohne nicht offengelegte Hilfe Dritter verfasst und keine anderen als die angegebenen Quellen und Hilfsmittel genutzt habe.
Meine Anteile an etwaigen Publikationen zu dieser Dissertation entsprechen denen, die in der untenstehenden gemeinsamen Erklärung mit dem/der Betreuer/in, angegeben sind.
Die vorliegenden Dissertation basiert auf der von mir mitverfassten Publikation „Role of RIM1α in short- and long-term synaptic plasticity at cerebellar parallel fibers” (Kintscher et al. 2013).
Die Bedeutung dieser eidesstattlichen Versicherung und die strafrechtlichen Folgen einer unwahren eidesstattlichen Versicherung (§156,161 des Strafgesetzbuches) sind mir bekannt und bewusst.

Datum, 11.02.2014 Unterschrift

5.6 Anteilserklärung

Michael Kintscher hatte folgenden Anteil an der folgenden Publikation:

Kintscher M, Wozny C, Johenning FW, Schmitz D, Breustedt J. Role of RIM1α in short- and long-term synaptic plasticity at cerebellar parallel fibres. Nature Communications. 2013 Sep 3;4:2392.

M.K., C.W., F.J., D.S. und J.B. konzipierten die Experimente; M.K. führte die Experimente durch; M.K. und J.B. analysierten die Daten; M.K., D.S. und J.B. fertigten die Publikation an.

Für die vorliegende Arbeit führte Michael Kintscher alle Experimente durch und analysierte die Daten.

Unterschrift, Datum und Stempel der betreuenden Hochschullehrer

Unterschrift des Doktoranden

5.7 Acknowledgments

The present work would not have been possible without the support and encouragement of a large number of people to whom I would like to express my gratitude.

First of all I would like to sincerely thank my supervisors Dietmar Schmitz and Jörg Breustedt for providing an excellent mentoring and scientific guidance throughout my thesis.
I further have to thank Dietmar for being part of his group and his constant financial support as well as scientific enthusiasm.
I owe my thanks to Jörg for introducing me to the setup in all its facets, a fruitful collaboration and endless and delightful discussions.

I would like to thank Susanne Rieckmann, Anke Schönherr and Karin Bloch for the perfect technical assistance and for keeping the lab running. I owe my special thanks to Susanne for tirelessly taking care of the mice breeding and ongoing support.

I want to thank Benjamin Rost for giving me a smooth start in the lab and his inspiring attitude.

Thanks to Friedrich Johenning for introducing me to 2P Ca^{2+}-imaging and always stimulating discussions.

I have to thank Vanessa Stempel for critically reading and correcting this thesis.

I am grateful to the whole Schmitzlab for providing such a warm and friendly atmosphere, which makes it feel like working with friends.

And last but not least I want to thank my family for supporting me all the way and just being there and Inge for making the last one and a half years a wonderful time.